

Virginia wetlands in the Anthropocene:  
Tracking wetland photosynthesis for blue carbon budgets  
and environmental policy

Hannah M. Mast  
Menomonee Falls, WI

B.A. Biochemistry, University of Wisconsin-Madison, 2017

A Dissertation presented to the Graduate Faculty of the University of Virginia  
in Candidacy for the Degree of Doctor of Philosophy

Department of Environmental Sciences

University of Virginia  
January 2025

Committee Members:  
Xi Yang  
Sally Pusede  
Scott Doney  
Julianne Quinn

# Table of Contents

Abstract	4
Acknowledgments	5
List of Figures	6
List of Tables	8
Introduction	9
Chapter 1: Midday depression of photosynthesis in <i>Spartina alterniflora</i> in a Virginia salt marsh	12
1.1 Introduction	12
1.1.1 Salt marsh photosynthesis and climate change	12
1.1.2 Midday depression of photosynthesis	13
1.1.3 Chapter 1 Aims	15
1.2 Methods	15
1.2.1 Site description	15
1.2.2 Eddy covariance and other environmental data	16
1.2.3 Photosynthesis-irradiance curves and quantifying midday depression of GPP	17
1.2.4 Random Forest	18
1.3 Results	19
1.4 Discussion	25
1.5 Chapter Conclusions	29
Chapter 2: Remote sensing proxies of salt marsh photosynthesis	31
2.1 Introduction	31
2.1.1 Salt marsh carbon cycle	31
2.1.2 Remote sensing as a tool to improve estimates of salt marsh GPP	32
2.1.2.1 Solar-induced chlorophyll fluorescence	32
2.1.2.2 Near-infrared radiation of vegetation	33
2.1.3 Chapter 2 Aims	35
2.2 Methods	35
2.2.1 Site Description	35
2.2.2 Remote Sensing Observations	36
2.2.3 Eddy CO <sub>2</sub> Flux Measurements	37
2.2.4 Ancillary data	37
2.2.5 Data analysis	38
2.3 Results	39
2.3.1 Relationships between GPP and remote sensing proxies across temporal scales	39
2.3.2 Relationships between GPP and remote sensing proxies across tidal conditions	42
2.4 Discussion	45
2.4.1 Relationships between GPP and remote sensing proxies across temporal scales	45
2.4.2 Relationships between GPP and remote sensing proxies across tidal conditions	46
2.5 Chapter Conclusions	47
Chapter 3: Assessing no net loss of wetland area and function through mitigation banking in Virginia	48
3.1 Introduction	48

3.1.1 Wetland policy and mitigation banking	48
3.1.2 Evaluating no net loss policy	51
3.1.3 Chapter 3 Aims	52
3.2 Methods	53
3.2.1 Wetland Mitigation Bank Permit Data and Analysis	53
3.2.2 Remote Sensing Data Analysis	54
3.3 Results and Discussion	55
3.3.1 How well has mitigation banking achieved no net loss of wetland area and function in Virginia?	55
3.3.2 How may mitigation banking have rearranged wetland distributions and associated ecosystem services in Virginia?	57
3.3.3 How does vegetation function vary over time at mitigation banks?	63
3.4 Chapter Conclusions	76
Conclusions and Future Work	77
Appendix	80
References	83

## Abstract

Wetlands are an invaluable ecosystem that provide many ecosystem services and play an outsized role in the global carbon cycle. Photosynthesis is one of the largest fluxes in the carbon cycle and is a foundational wetland function that underlies many wetland ecosystem services. However, salt marsh wetland gross primary production (GPP), the ecosystem-scale photosynthetic CO<sub>2</sub> flux, is highly uncertain. Increased and improved monitoring of salt marsh GPP is needed to increase its certainty and constrain its sensitivity to climate change. To address this need, I first collect over four years of marsh-atmosphere CO<sub>2</sub> flux measurements to examine patterns of salt marsh GPP and its sensitivity to various environmental conditions. I observe ubiquitous midday depression of GPP at daily and seasonal scales that is primarily driven by salinity and water stress during periods of reduced tidal flooding and warmer air temperatures. To my knowledge, this is the first documentation and analysis of chronic midday depression of photosynthesis in a salt marsh. I then couple the CO<sub>2</sub> flux data with ground-based remote sensing observations to determine which remote sensing proxies best track GPP. I identify the near-infrared radiation of vegetation (NIR<sub>v</sub>) index as a strong proxy for salt marsh photosynthesis, especially at longer temporal scales. In my final chapter, I analyze 30 years of wetland permit data and use satellite-based NIR<sub>v</sub> to track vegetation function in wetland mitigation banks that were restored to offset permitted wetland impact activity. I find most mitigation banks have maintained vegetation function for at least 20 years after their restoration and that mitigation banking has likely upheld the ‘no net loss’ of wetland area and function required by the Clean Water Act. However, the few mitigation banks with negative long-term trends in vegetation function tended to be in coastal areas prone to sea level rise and saltwater intrusion, suggesting that further climate change may challenge ‘no net loss’ in the coming decades. Together, this dissertation furthers our understanding of the climate sensitivity of salt marsh photosynthesis and provides improved remote sensing approaches to monitor wetland vegetation function for scientific, management, and policy applications.

## Acknowledgments

I would like to thank my advisors and committee members for their insightful feedback and support during my dissertation. Xi Yang has been an outstanding advisor and adaptive mentor. His optimism and enthusiasm for science have kept my spirits up during periods of burnout, and I appreciate his support in pursuing my interest in science policy. Working closely with Sally Pusede has been a pleasure, and her feedback on my research and grant writing has significantly enhanced my dissertation and overall writing. I am grateful to Dave Davis for teaching me a great deal about wetland mitigation banking and how to build bridges between academia, government, and management.

I would also like to thank Yang and Pusede lab members for their support and companionship throughout my time at UVA. Andrew Jablonski has spent many brutal days in the field with me and helped me keep my head up when things were hard. Koong Yi also endured some challenging fieldwork with me and gave a great deal of his time to help get my remote sensing instruments up and running. Elliott White has always provided thought-provoking feedback on my research. I am also grateful to Laura Barry, Rong Li, Carmen Petras, and Henry Yeung for their assistance with fieldwork.

I owe an enormous thank you to John Porter and the VCR-LTER staff. John and Buck Doughty patiently helped me with many radio and electrical issues at the flux tower. I'm grateful to David Lee, Jonah Morreale, Tom Burkett, Sophia Hoffman, Buck Doughty, Cora Johnston, and Donna Fauber for many boat trips and fieldwork support.

Working with the Virginia Scientist-Community Interface has been a highlight of my graduate school experience and has shown me how to use science for good. V-SCI has made me a better scientist, strongly influenced my personal and professional development, and inspired much of my third chapter.

I am grateful to the Virginia Sea Grant, Jefferson Scholars Foundation, Virginia Space Grant Consortium, and NSF for their generous financial support throughout my PhD. I would also like to acknowledge Christie Campla (NIH), Aaron Hoskins (UW), and Susan Maroney and Alan Mast (BRI) for their mentorship during my undergraduate and postbac years, which provided me with a strong foundation to succeed in graduate school.

Finally, thank you to Warren & Lenny, my family, and my friends for your love and support during this journey.

## List of Figures

<b>Figure 1.1</b> Diurnal patterns of gross primary production (GPP), respiration, and net ecosystem exchange (NEE) of CO <sub>2</sub>	19
<b>Figure 1.2</b> Morning and afternoon photosynthesis-irradiance curves for each study year's growing season	20
<b>Figure 1.3</b> Time series of daily percent depression of GPP averaged over 10-day moving averages and the distribution of daily percent depression of GPP	22
<b>Figure 1.4</b> The normalized predictor importance of each random forest input parameter used to model GPP's daily depression	23
<b>Figure 1.5</b> Sensitivity of daily depression of GPP to environmental variables in random forest model	24
<b>Figure 1.6</b> Daily depression of GPP by the hour of high tide	25
<b>Figure 2.1</b> Time series of daily NEE, GPP, NIR <sub>v,Rad</sub> , NIR <sub>v,P</sub> , and SIF	39
<b>Figure 2.2</b> Diurnal patterns of GPP, NIR <sub>v,Rad</sub> , NIR <sub>v,P</sub> , and SIF	40
<b>Figure 2.3</b> GPP-NIR <sub>v,Rad</sub> , NIR <sub>v,P</sub> , and SIF linear regressions at the half-hourly, daily, and 5-day scales	41
<b>Figure 2.4</b> Example vegetation radiance spectra collected at midday on two sunny days in July 2021 at low tide and high tide	42
<b>Figure 2.5</b> Tidal attenuation of GPP and remote sensing proxies	43
<b>Figure 2.6</b> GPP-NIR <sub>v,Rad</sub> , NIR <sub>v,P</sub> , and SIF linear regressions at the half-hourly scale during low and high tide conditions	44
<b>Figure 3.1</b> The size of wetland mitigation banks established 1995-2024, and the area of permitted wetland impact was compensated during the same period	49
<b>Figure 3.2</b> Locations of 11 wetland mitigation banks selected for vegetation function remote sensing analysis	54
<b>Figure 3.3</b> Acres and credits of wetland released and purchased from wetland mitigation banks in Virginia 1995-2024	56
<b>Figure 3.4</b> Spatial distributions of wetland mitigation banks and permitted wetland impact activity, and the transaction lines and distances between wetland mitigation bank and permitted wetland impact sites	58

**Figure 3.5** Net gains or losses of wetland acreage and compensation credits by HUC8 code in Virginia \_\_\_\_\_ 61

**Figure 3.6** Time series and the long-term trends of NDVI and NIR<sub>v</sub> at 11 selected mitigation banks \_\_\_\_\_ 65-75

## List of Tables

**Table 1.1** Summary of environmental variables and midday depression of GPP during the 2019 to 2022 growing seasons \_\_\_\_\_ 21

**Table 3.1** Net wetland compensation credits and acreage gains by HUC8 Code \_\_\_\_\_ 62

# Introduction

Wetlands provide numerous ecosystem services, including carbon sequestration, flood protection, water filtration, storm surge mitigation, erosion control, and natural beauty (Mitsch et al., 2015). Further, the large amounts of 'blue carbon' sequestered in the soils of salt marshes and mangroves are a potential nature-based solution to help mitigate climate change (Macreadie et al., 2021). Many of these ecosystem services depend on photosynthesis and the overall health of the wetland vegetation. However, due to a lack of wetland-specific measurements and high spatial variability, the wetland photosynthetic carbon flux and its sensitivity to various environmental stressors remain uncertain in the Anthropocene (Holmquist et al., 2018; US Global Change Research Program, 2018).

Improving the constraints of wetland carbon budgets and their climate sensitivity is critical to meeting the United Nations Paris Agreement's carbon neutrality goals (Seddon et al., 2020). Research is needed to understand environmental tipping points that may flip a wetland from a carbon sink to a carbon source, affecting carbon accounting and markets (Barnard et al., 2021; Wang et al., 2023). U.S. policy has historically protected wetlands, but the jurisdiction of federal wetland protections has been in flux in recent years (Sulliván & Gardner, 2023). Combined with the >50% historical loss of wetlands in the contiguous U.S., developing and communicating the best wetland conservation and restoration practices that maximize wetland protection and ecosystem services is more critical than ever (Dahl, 1990).

To address the above challenges, this dissertation aims to improve our understanding of wetland photosynthesis in the context of climate change and environmental policy. The following questions guide my three dissertation chapters:

1. What are the patterns and environmental drivers of wetland photosynthesis, and how may climate change alter them?
2. What remote sensing approaches can improve estimates of wetland photosynthesis?
3. What are the ecological outcomes of wetland management and policy?

In my first chapter, I use the eddy covariance method to measure ecosystem-scale CO<sub>2</sub> fluxes of a *Spartina alterniflora* salt marsh on the Eastern Shore of Virginia. I find the diurnal pattern of the gross primary production (GPP) flux to skew towards the morning, indicating greater photosynthesis in the morning than in the afternoon for a given amount of sunlight. This phenomenon is called midday depression of photosynthesis and has been reported in multiple ecosystems as a response to drought and other severe environmental stress (Xu & Shen, 1996). However, midday depression of photosynthesis has not been previously reported in a salt marsh and is uncommon in C<sub>4</sub> vegetation like *S. alterniflora*. During the summers of 2019-2022, 76% of days showed some degree of midday depression. Higher tides were associated with less severe depression, while warmer temperatures were related to more severe depression. The midday depression is likely driven by vegetation closing stomata or increased photorespiration in response to low soil moisture and high salinity that builds up during relatively low tides and warm temperatures. My results highlight the potential of an altered salt marsh carbon sink due to climate change and the need to better understand species-specific responses to environmental stressors at sub-daily timescales.

In my second chapter, I test the potential of three remote sensing proxies to track salt marsh GPP across temporal scales and during different tidal conditions. The first two proxies, radiance-based near-infrared reflectance of vegetation (NIR<sub>v,Rad</sub>) and its product with photosynthetically active radiation (NIR<sub>v,P</sub>), are part of a new class of vegetation indices that have recently shown promising results as photosynthesis proxies in multiple ecosystem types but have not been extensively studied in salt marshes (Badgley et al., 2017). The third proxy, solar-induced chlorophyll fluorescence (SIF), is empirically linked to the electron transport chain of photosynthesis and has been shown to correlate with canopy-scale photosynthesis but has also received limited study in salt marshes (Porcar-Castell et al., 2014; Yang et al., 2015). I collected half-hourly ground-based observations of the three remote sensing proxies and compared them to concurrent GPP flux measurements at various temporal scales and tidal conditions. Overall, I find NIR<sub>v,Rad</sub> and NIR<sub>v,P</sub> to be strong proxies for GPP, especially at longer temporal scales and during low tide conditions. My results indicate that both NIR<sub>v</sub> indices are strong candidates for tracking salt marsh GPP from satellite observations and with relatively affordable ground-based sensors.

In my third chapter, I analyze U.S. Army Corps of Engineers wetland permit data and remote sensing observations to determine if no net loss of wetland area and function has been achieved through mitigation banking in Virginia. The Clean Water Act aims to protect U.S. waterways and ensure there is ‘no net loss’ of wetland area and function due to permitted wetland impact activity (33 USC §1251 et seq., 1972; US Army Corps of Engineers & Environmental Protection Agency, 2008; US Environmental Protection Agency, 1990). Wetland mitigation banks are large restoration projects constructed in anticipation of a developer’s need to offset wetland impacts and maintain ‘no net loss.’ I first compiled 5100 wetland mitigation bank transactions from 1995-2024 and determined mitigation banking has led to a net increase of over 15,000 acres of wetland. Over 50% of the net gains of wetland areas are concentrated in two HUC8 codes on the outskirts of major urban areas that contain multiple large mitigation banks. However, no HUC8 code lost more than a few hundred acres of wetland. To examine the conservation of wetland function, I use satellite-based  $NIR_v$  and the normalized difference vegetation index (NDVI) as proxies of photosynthesis and vegetation greenness to monitor 11 of the largest mitigation banks in Virginia. Most mitigation banks maintain vegetation function for 10-20 years after restoration. Although a few mitigation banks have slight negative long-term trends in photosynthesis and vegetation greenness, most banks show positive long-term trends. These results suggest mitigation banking has achieved no net loss of wetland area and function in Virginia. However, the few mitigation banks showing negative trends in vegetation function are in areas vulnerable to sea level rise and saltwater intrusion, suggesting that climate change may lead to further declines in vegetation function in the coming decades.

I conclude this dissertation by synthesizing my chapters’ results and providing recommendations for future work.

# Chapter 1: Midday depression of photosynthesis in *Spartina alterniflora* in a Virginia salt marsh

A slightly modified version of this chapter is currently under revision to be published in the *Journal of Geophysical Research: Biogeosciences*

## 1.1 Introduction

Despite their small global spatial coverage, salt marshes play an outsized role in the global carbon cycle. High rates of photosynthesis and carbon storage per unit area make salt marshes one of the most powerful natural carbon sinks, removing  $49.6 \pm 9.4$  Tg CO<sub>2</sub> year<sup>-1</sup> from the atmosphere and storing carbon at densities up to 10 times greater than terrestrial ecosystems (Duarte et al., 2013; Lovelock & Reef, 2020; Mcleod et al., 2011; Rosentreter et al., 2023). The conservation and restoration of salt marshes could potentially help mitigate the impacts of climate change by sequestering atmospheric CO<sub>2</sub> on millennial time scales and serve as a nature-based solution (Duarte et al., 2013; Griscom et al., 2017; Nellemann & Corcoran, 2009; Rosentreter et al., 2023).

### 1.1.1 Salt marsh photosynthesis and climate change

However, the salt marsh carbon cycle and its potential as a nature-based solution are threatened by a wide range of climate change stressors. Photosynthesis under future climate change scenarios is particularly uncertain, with numerous vegetation stressors likely to increase in the coming decades. Although the effects of rising temperatures on vegetation productivity are well studied in general, it is unclear how temperature affects *Spartina alterniflora* (*S. alterniflora*), a C<sub>4</sub> salt marsh cordgrass, at the ecosystem scale. From warming experiments and leaf-level studies, *S. alterniflora* is known to increase photosynthesis with rising temperature up to its optimum temperature range of 30–35 °C, beyond which assimilation decreases (Charles & Dukes, 2009; Ge et al., 2014; Giurgevich & Dunn, 1979; Kathilankal et al., 2011; Shea, 1977). Ecosystem scale studies utilizing eddy covariance flux towers have associated greater marsh CO<sub>2</sub> uptake with warmer temperatures and longer growing seasons at the seasonal scale, but cooler temperatures may enhance gross primary production at short time scales (Forbrich et al., 2018; Knox et al., 2018). Kirwan et al. (2009) attributed a latitudinal gradient in *S. alterniflora* productivity to temperature and length of the growing season and modeled a

marsh productivity increase of 10–40% with 2–4 °C of warming over the next century. However, despite being a C<sub>4</sub> plant, there is evidence *S. alterniflora* has significant photorespiration at temperatures greater than 30 °C, within the range of its typical summertime climate (Giurgevich & Dunn, 1979; Shea, 1977). Climate change-driven temperature increases may exacerbate this phenomenon and offset gains in photosynthetic CO<sub>2</sub> uptake due to the CO<sub>2</sub> fertilization effect (Dusenage et al., 2019). Rising temperatures will also increase vapor pressure deficit (VPD), which can induce stomata closure and reduce photosynthesis (Grossiord et al., 2020; Knox et al., 2018).

Altered precipitation patterns, increased frequency of drought, and longer tidal flooding duration due to sea level rise are also expected to impact marsh productivity in the coming decades by altering marsh soil moisture and salinity (O'Donnell et al., 2024; Poppe & Rybczyk, 2021). Precipitation is an important variable regulating marsh productivity because it can reduce soil salinity (De Leeuw et al., 1990; Dunton et al., 2001; Forbrich et al., 2018). In situ precipitation enhances vegetation productivity, especially in the marsh interior (Hawman et al., 2024). The productivity of taller vegetation found along creekbanks is more sensitive to increased river discharge driven by in-land precipitation (Biçe et al., 2023; Hawman et al., 2024; Więski & Pennings, 2014). However, extreme precipitation events have been linked to marsh dieback events due to sediment waterlogging (Rolando et al., 2023; Stagg et al., 2021). Marsh soil desiccation and hypersalinity due to drought have also been attributed to numerous marsh dieback events in the Southeastern United States and reduced photosynthesis (Alber et al., 2008; Hughes et al., 2012; Li et al., 2022; McKee et al., 2004; Rolando et al., 2023; Russell et al., 2023). Longer tidal flooding duration due to sea level rise can provide nutrients and help alleviate hypersaline soils that build up during drought or low tide periods, but too much flooding can limit oxygen availability and lead to sulfide build-up (Lamers et al., 2013).

### 1.1.2 Midday depression of photosynthesis

While many studies have examined the response of *S. alterniflora* productivity to environmental stress, gaps remain in our understanding of the sub-daily responses in the natural environment. Vegetation is known to respond to stress at different timescales,

and diurnal patterns of gross primary production (GPP), or photosynthesis at the ecosystem scale, can be highly variable throughout the day (Li et al., 2021; Lin et al., 2019; Paul-Limoges et al., 2018). Understanding the diurnal variations in GPP can disentangle photosynthesis controls that may be obscured at longer temporal scales. Thus, higher frequency measurements that can continuously measure the diurnal pattern of photosynthesis are needed to fully capture how climate change impacts salt marsh vegetation.

Midday depression of photosynthesis, when plants have a lower photosynthetic rate in the afternoon at the same light intensity relative to the morning, is a sub-daily response of vegetation to environmental stress that can only be captured with higher frequency measurements (Xu & Shen, 1996). Multiple mechanisms can lead to midday depression, either by decreasing true photosynthesis (carboxylation), increasing photorespiration (oxygenation), or both. Afternoon stomata closure in response to high temperature, high VPD, or low soil moisture is one common mechanism that reduces photosynthesis by limiting the internal leaf CO<sub>2</sub> concentration (Pathre et al., 1998; Raschke & Resemann, 1986; Turner & Burch, 1983; Wilson et al., 2003). Light saturation from high irradiance can also decrease the quantum yield of photosystem II in the afternoon (Tenhunen et al., 1984). Photorespiration is largely a function of temperature and cellular CO<sub>2</sub>:O<sub>2</sub> ratios around Rubisco and can increase in response to heat waves, droughts, and other environmental stressors (Voss et al., 2013). Stomata closure can also increase the leaf temperature and promote photorespiration, leading to a lower observed net photosynthesis (Franco & Lüttge, 2002; Pathre et al., 1998; Pons & Welschen, 2003; Valentini et al., 1995). Midday depression has been reported in C<sub>3</sub>, C<sub>4</sub>, and CAM plants, but it is considered less common in C<sub>4</sub> and CAM because they are generally more adaptive to temperature and water stress and evolved to minimize photorespiration (Bräutigam & Gowik, 2016; Lara & Andreo, 2011; Lin et al., 2019; Pardo & VanBuren, 2021; Xu et al., 2020). Thus, to what extent a *S. alterniflora* salt marsh shows midday depression is unclear.

### 1.1.3 Chapter 1 Aims

In this chapter, I examine the diurnal patterns of photosynthesis in a *S. alterniflora* salt marsh in Virginia. My primary research questions include:

How often and to what extent does midday depression of photosynthesis occur?

What environmental factors may be driving the severity of the depression?

To quantify the frequency and severity of midday depression, I fit photosynthesis-irradiance curves to GPP flux data and calculate a percent depression as the reduction in afternoon photosynthesis relative to the morning for a given amount of incoming sunlight. This quantitative approach allowed me to examine the daily variability of midday depression and model potential environmental drivers more closely. I then use a random forest model to examine the environmental drivers of the midday depression. To my knowledge, this is the first study to report and investigate midday depression of photosynthesis in a C<sub>4</sub> salt marsh grass at the ecosystem scale.

## 1.2 Methods

### 1.2.1 Site description

The study site was in an intertidal salt marsh dominated by *Spartina alterniflora* (salt marsh cordgrass; also referred to as *Sporobolus alterniflorus* (Peterson et al., 2014a, 2014b)) within the Virginia Coast Reserve Long Term Ecological Research site (VCR-LTER) on the Eastern Shore of Virginia (AmeriFlux ID US-VFP; 37° 24' N, 75° 50' W). The marsh is on the Atlantic Ocean side of the Delmarva Peninsula and faces shallow coastal lagoons backed by barrier islands. No major rivers drain into the area, and the site's hydrology is primarily driven by in situ precipitation and the nearby coastal bays. The flux tower is located 2 km from the shoreline and 85 m from a major creek edge. The marsh is dominated by the intermediate form of *S. alterniflora*, with an average height of 0.6 m. The area has a semidiurnal tidal cycle with two daily high and low tides and a tidal amplitude of ~1.3 meters. Tidal flooding duration, when the tide is above the marsh platform, averages ~2 hours for a single high tide event, but it can be longer during spring or shorter during neap tides.

### *1.2.2 Eddy covariance and other environmental data*

I collected eddy covariance (EC) measurements of the net ecosystem exchange (NEE) flux of CO<sub>2</sub> during the growing seasons (May to September) of 2019 to 2022. A sonic anemometer (Gill Windmaster) and open-path infrared gas analyzer (LI-COR 7500DS) were mounted on the tower 3 m above the marsh canopy to measure 3-dimensional windspeed and CO<sub>2</sub> mixing ratios at 10 Hz. The EC data was processed in EddyPro (version 7.0.9, LI-COR (2020)) and custom MATLAB scripts to align with FLUXNET protocols (Pastorello et al., 2020). NEE fluxes were calculated as the mean covariance between deviations of vertical windspeed and gas molar density over a 30-minute block average. Prior to the flux calculation, a double wind rotation was performed to account for any sonic anemometer misalignment (Wilczak et al., 2001). Molar densities were processed with a spike removal (Vickers & Mahrt, 1997). Fluxes were filtered with a u-star threshold estimation based on a moving point test and by season (Papale et al., 2006). Air density fluctuations were compensated with Webb, Pearman, and Leuning correction terms added to the fluxes (Webb et al., 1980). High- and low-pass frequency corrections were applied to the flux as described in Moncrieff et al. (1997) and Moncrieff et al. (2005), respectively.

Stationarity and turbulence tests were used to flag fluxes with a 0-1-2 quality control score, with 0 being the highest quality flux (Foken et al., 2005). Only fluxes with a quality flag of 0 were used in subsequent analysis. To account for precipitation, high humidity, and sediment obstructing the sensor light paths, NEE fluxes with a CO<sub>2</sub> signal strength of less than 80% were filtered from the dataset. Gross primary production (GPP) was partitioned from the NEE flux using a nighttime approach in the REddyProc software package (Lasslop et al., 2010; Wutzler et al., 2018). I did not use any gap-filled flux data in the analysis presented in this chapter. All fluxes measured when the tide was above the marsh mud platform were removed from the dataset to avoid the effects of water limiting marsh-air gas exchange on the observed diurnal pattern. The tidal filtering removed 16% of fluxes from the total dataset.

Air temperature was measured at 3.4 m above the marsh canopy and averaged over 30 minutes. Vapor pressure deficit (VPD) was calculated as the difference between the actual water vapor pressure and its saturation pressure for a given air temperature, as described in the EddyPro Software Instruction Manual (LI-COR, 2020).

Photosynthetically active radiation (PAR, PQS1, Kipp & Zonen) and tidal depth (CTD Diver, Van Essen) were collected at one-minute intervals and averaged over the 30-minute flux interval. Data collected by the VCR-LTER, the U.S. Climate Reference Network in Cape Charles, VA, and NOAA’s nearby Wachapreague tidal station filled gaps when onsite instruments were not operational (Porter et al., 2023).

### 1.2.3 Photosynthesis-irradiance curves and quantifying midday depression of GPP

To quantify the severity of midday depression of photosynthesis, I fit daily and seasonal morning and afternoon photosynthesis-irradiance (PI) curves with GPP and PAR observations. The difference in area under corresponding morning and afternoon PI curves represents midday depression as a percent depression of GPP in the afternoon relative to the morning. In contrast to the centroid method to examine midday depression, I choose this approach because it accounts for changes in PAR and allows me to calculate a percent depression in GPP at the daily scale, even on days when multiple time points were filtered during high tide conditions (Li et al., 2023; Wilson et al., 2003). I fit PI curves to morning (6:00–10:00 LST) and afternoon (14:00–18:00 LST) data using Equation 1:

$$P = \frac{P_{max} \times I}{KI + I} \quad (1)$$

where P is the measured half-hour GPP flux,  $P_{max}$  is the modeled maximum rate of photosynthesis, I is solar irradiance represented as measured PAR, and KI is the modeled half-saturation constant (the irradiance at which  $1/2$  of  $P_{max}$  is reached). PI curves with less than five fitting data points, a root mean square error  $> 2.5 \mu\text{mol m}^{-2} \text{s}^{-1}$ , or an  $R^2 < 0.5$  were removed from subsequent analysis. I then calculated midday depression as the normalized percent difference in the area under the PI curves for corresponding daily and seasonal fitting windows using Equation 2:

$$\text{Depression of GPP (\%)} = \frac{\text{Area}_{\text{afternoon}} - \text{Area}_{\text{morning}}}{\text{Area}_{\text{morning}}} \times 100 \quad (2)$$

where a negative percent depression indicates GPP is suppressed in the afternoon compared to the morning for a given amount of PAR.

Of the 612 days during the study period, 54 days had an instrument malfunction or a site power outage. Of the remaining days with data and after tidal filtering, 439 mornings and 424 had at least 5 GPP and PAR data pairs to fit a PI curve. The  $R^2 < 0.5$  filter flagged 49 (11%) of the morning and 39 (9%) of the afternoon PI curves. The  $RMSE > 2.5 \mu\text{mol m}^{-2} \text{s}^{-1}$  filter flagged 18 (4%) of the morning and 18 (4%) of the afternoon PI curves. Together, the  $R^2$  and RMSE filters removed 75 days of data from subsequent analysis. The distribution of the  $R^2$  and RMSE of the daily-scale morning and afternoon PI curves can be found in Appendix Figure A1. In total, 283 days had high-quality PI curves for both the morning and afternoon that could be used to calculate a daily-scale depression of GPP and input into the random forest model

#### *1.2.4 Random Forest*

To examine potential environmental drivers of midday depression, I trained a random forest model to predict a percent depression of GPP at the daily scale with daily total PAR, average air temperature between 6:00 and 18:00 LST, maximum VPD, total precipitation on the previous day, and maximum and minimum tidal height as model predictors. The model was trained using MATLAB's TreeBagger package with 1000 regression trees and sampled with a replacement on a 0.7 in-bag training fraction (MATLAB, n.d.). The model's  $R^2$  was calculated as Pearson's correlation between the model's predicted percent depression of GPP and the out-of-bag depression. The out-of-bag permuted predictor delta error was used to represent predictor importance. To visualize the marginal impact of each predictor on the predicted depression, partial dependence plots were generated using MATLAB's partial dependence function.

### 1.3 Results

I observed midday depression of photosynthesis at daily and seasonal time scales. The growing season averaged diurnal pattern of GPP was skewed towards morning hours in all study years (Figure 1.1a). The diurnal patterns in 2019, 2021, and 2022 were markedly skewed to the morning hours, with peaks in GPP at 10 am, two hours before PAR peaked at noon. GPP was the largest in 2020 and was the only year that peaked at the same time as PAR. However, GPP in 2020 was depressed in afternoon hours compared to morning hours, i.e., 12:00–14:00 GPP was lower compared to 10:00–12:00 GPP. Respiration and net ecosystem exchange (NEE) also had asymmetrical diurnal patterns (Figure 1.1b and c). NEE showed a similar diurnal shape to GPP, with the largest CO<sub>2</sub> uptake (most negative NEE) occurring around 10 am in 2019, 2021, and 2022. The gradual increase in respiration from the midmorning to midafternoon indicates the midday depression is not entirely an artifact of the NEE flux partitioning into GPP and respiration component fluxes.

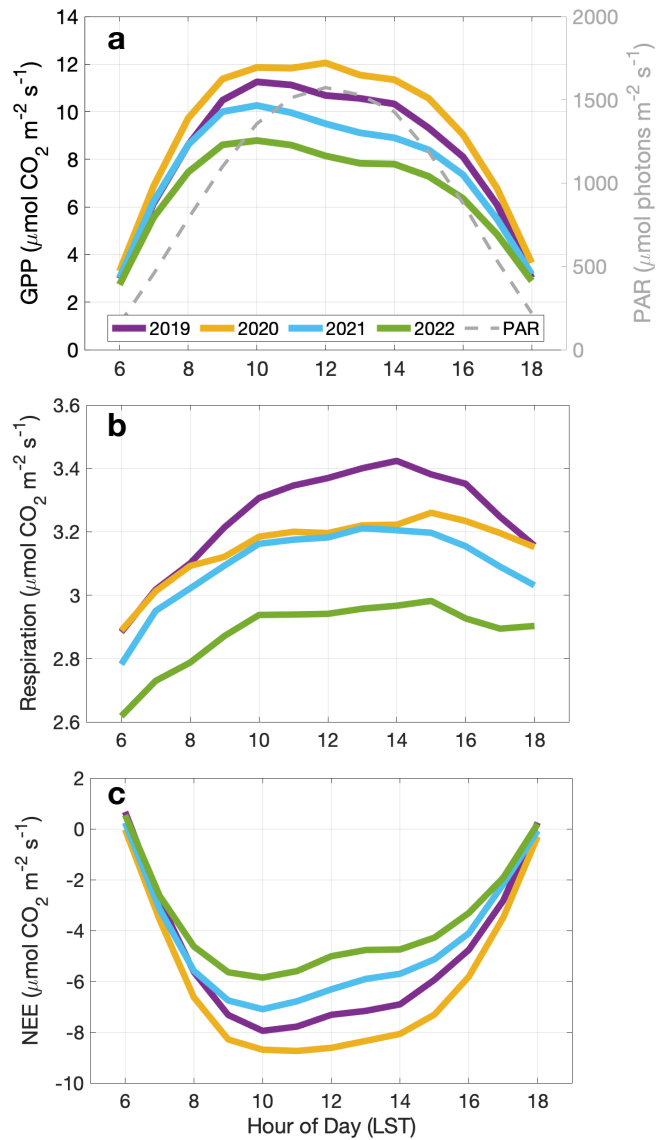


**Figure 1.1** Diurnal patterns of (a) gross primary production (GPP), (b) respiration, and (c) net ecosystem exchange (NEE) of CO<sub>2</sub>. The fluxes were averaged by hour of day from May to September for each study year. The dashed grey line in the first panel is the diurnal pattern of PAR (May to September) averaged across all study years.

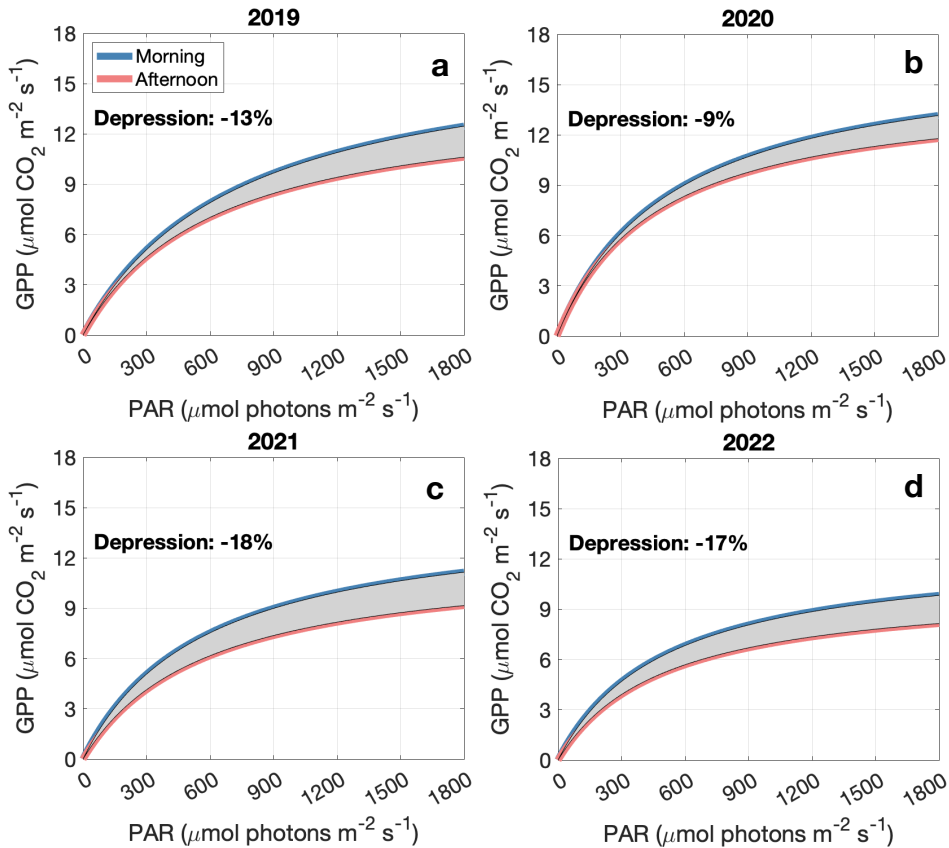


**Figure 1.2** Morning (blue) and afternoon (pink) photosynthesis-irradiance curves for each study year's growing season. The curves were fitted with half-hourly GPP and PAR data for each study year. The shaded area represents the difference in the area under each paired morning and afternoon curve. The depression percentage was calculated with Equation 2, where a negative percentage indicates a reduced GPP for a given PAR level in the afternoon relative to the morning.

The seasonal PI curves and calculated percent depression of GPP for each growing season suggested chronic midday depression at the seasonal scale (Figure 1.2). Depressions of GPP were  $-18\%$  and  $-17\%$  across the 2021 and 2022 growing seasons, respectively. 2019 and 2020 had milder seasonal depressions of  $-13\%$  and  $-9\%$ . Table 1.1 provides a summary of the average environmental conditions for each of the study years. 2019 and 2020 had higher peak tides of 0.23 and 0.21 m, while 2021 had much lower peak tides of 0.15 m on average. 2019 was particularly warm, with an average air temperature of  $25.32\text{ }^{\circ}\text{C}$  and a relatively high average maximum VPD. 2020 was the coolest, with an average air temperature of  $23.74\text{ }^{\circ}\text{C}$ .

**Table 1.1** Summary of environmental variables and midday depression of GPP during the 2019 to 2022 growing seasons. Tidal heights are the average daily peak and minimum tidal height. Air temperature is the average daily temperature from 6:00 to 18:00 LST. PAR is the average daily cumulative incoming photosynthetically active radiation. Max VPD is the average daily maximum vapor pressure deficit. Precipitation is the total precipitation during the growing season.

	<b>2019</b>	<b>2020</b>	<b>2021</b>	<b>2022</b>
<b>Midday Depression of GPP (%)</b>	-13	-9	-18	-17
<b>Peak tidal height (m)</b>	0.23 ± 0.16	0.21 ± 0.17	0.15 ± 0.17	0.19 ± 0.18
<b>Air Temperature (°C)</b>	25.32 ± 3.40	23.74 ± 5.09	24.21 ± 4.08	24.11 ± 4.38
<b>PAR (μmol m<sup>-2</sup> d<sup>-1</sup>)</b>	2.04e4 ± 1.10e4	2.28e4 ± 7.70e3	2.40e4 ± 7.76e3	2.35e4 ± 7.27e3
<b>Max VPD (kPa)</b>	1.70 ± 0.64	1.30 ± 0.64	1.37 ± 0.54	1.40 ± 0.62
<b>Min tidal height (m)</b>	-1.13 ± 0.16	-1.13 ± 0.17	-1.17 ± 0.16	-1.11 ± 0.23
<b>Precipitation (mm)</b>	108	80	132	55

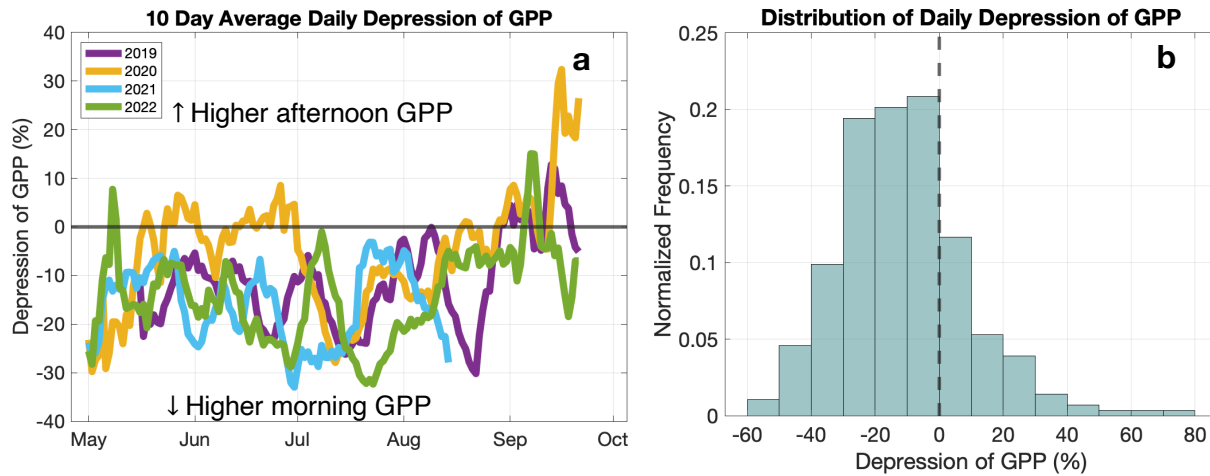


**Figure 1.3** (a) Time series of daily percent depression of GPP averaged over 10-day moving averages. (b) The distribution of daily percent depression of GPP. Any values below the 0 line in panel A or to the left of the dashed 0 line in panel B indicate observations where midday depression of GPP occurs.

An example PI curve fitting for the daily scale is shown for July 12, 2021, in the Appendix (Appendix Figure A2). The  $P_{\max}$  coefficients from the daily scale PI curves also illustrate the midday depression, with  $P_{\max}$  values from the afternoon curves shifted to smaller maximum photosynthesis rates than the morning curves (Appendix Figure A3a). The distribution of KI from the daily scale PI curves did not show a marked difference between the morning and afternoons, indicating no difference in the point at which the vegetation reached light saturation (Appendix Figure A3b).

The midday depression of GPP calculated at the daily scale ranged from  $-55\%$  to  $+79\%$  throughout the summer and approached more positive percent depressions (i.e., higher afternoon GPP) at the tail end of the growing season in September (Figure 1.3). Across all study years, 76% of days showed a negative percent depression of GPP and averaged  $-11\%$ . When averaged by 10-day moving windows, only 2020 showed any periods of positive depression between June and August.

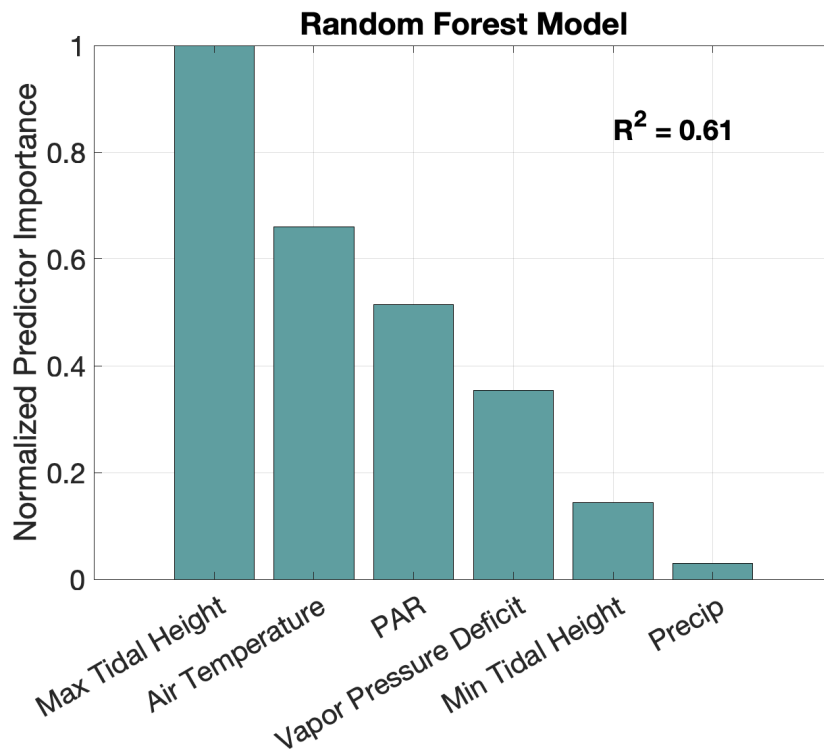


**Figure 1.4** The normalized predictor importance of each random forest input parameter used to model GPP's daily depression. The model's  $R^2$  was calculated as Pearson's correlation between out-of-bag depression data and the model's predicted depression.

Maximum daily tidal depth and average daily temperature were identified as the most important predictors of the severity of daily midday depression by the random forest model (Figure 1.4). Daily total PAR and maximum VPD were also identified as moderate predictors, while daily minimum tidal height and precipitation were minimally important. Partial dependence plots in Figure 1.5 illustrate the marginal relationships between the model sensitivity and each input predictor. Generally, daily maximum and minimum tidal height showed a positive relationship with the model sensitivity—as these predictors increased, the depression sensitivity became less negative, which would lead to a less severe midday depression (Figure 1.5a and e). In contrast, the model sensitivity and predicted depression became more negative as air temperature, PAR, or VPD increased (Figure 1.5b, c, d). The depression severity was insensitive to precipitation on the previous day (Figure 1.5f).

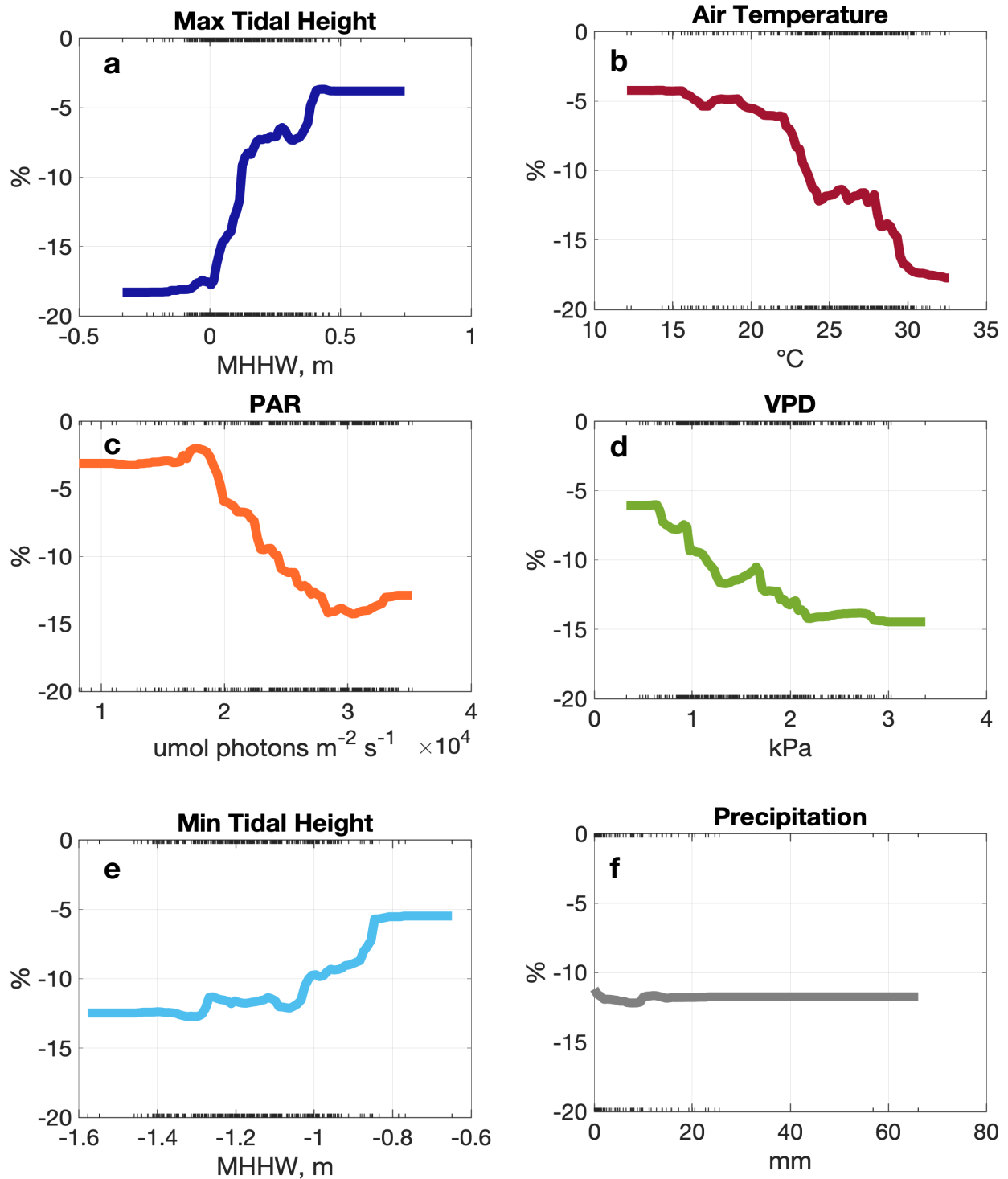


**Figure 1.5** Sensitivity of daily depression of GPP to environmental variables in random forest model. Each panel is a partial dependence plot of the depression's sensitivity to an environmental variable on the x-axis. The whiskers on the x-axis mark the daily scale observations of each environmental variable.

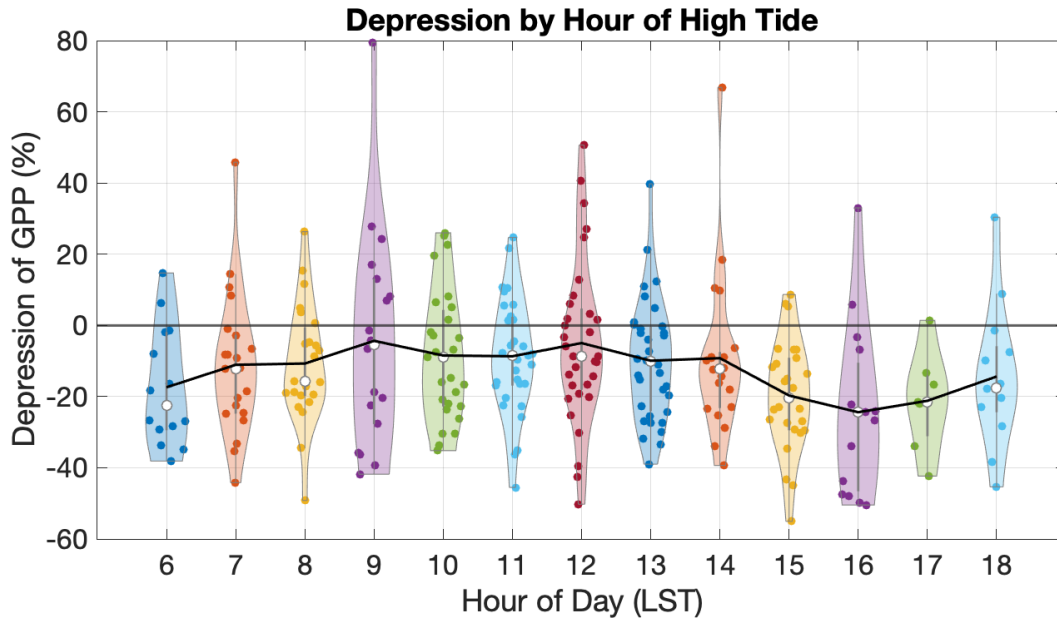


**Figure 1.6** Daily depression of GPP by the hour of high tide. The colored points within each violin mark individual daily percent depressions on days with a high tide event during the corresponding hour of the day. The white circles are the median depression for each hour of the day. The black line connects the mean depression for each hour of the day. Any points below the horizontal 0% line indicate observations where midday depression of GPP occurs.

When binned by the hour of daytime high tide, the percent depression of GPP was more severe (more negative) on days when the high tide occurred in the late afternoon (Figure 1.6). Decreasing water availability throughout the day, leading to decreased photosynthesis in the afternoon, may explain this result. Combined with the maximum tidal height being the strongest predictor in the random forest model, water availability and soil salinity are likely important controls of the severity of the depression of GPP.

#### 1.4 Discussion

Understanding the responses of vegetation to climate change-driven stressors at sub-daily timescales is critical to forecasting photosynthetic CO<sub>2</sub> uptake under future climate scenarios. Further, sub-daily observations are necessary to constrain larger-scale models that often rely on single-overpass satellite observations. In this study, I examine the diurnal patterns of photosynthesis in an *S. alterniflora* salt marsh and observe the ubiquitous midday depression of GPP across four growing seasons. The severity of the depression varied between years and within seasons in response to environmental

drivers, predominantly tidal height and air temperature. It is important to note that GPP is a canopy-scale integrated measurement of apparent photosynthesis—the difference between true photosynthesis (carboxylation) and photorespiration (oxygenation) (Wohlfahrt & Gu, 2015). Thus, the midday depression observed in this study suggests the marsh grass either decreases true photosynthesis, increases photorespiration, or a combination of both after the midmorning peak in GPP. Below, I discuss these two potential mechanisms for the midday depression observed in this study.

I suspect that the midday depression is at least partially a result of a decrease in afternoon photosynthesis due to increasing salinity and decreasing water availability during periods of lower tides and warmer temperatures. Despite being a salt-tolerant species, the optimal range of salinity for specific salt marsh species can be narrow (Odum, 1988; Poppe & Rybczyk, 2021). Hypersaline and dry soils can build up beyond a stress threshold when warm temperatures enhance evaporation from the marsh surface and during neap tide conditions when tidal flooding depth is reduced and shorter in duration (Shen et al., 2018; Xin et al., 2013, 2017; Xu et al., 2024). Further, the marsh in this study is not near a significant river mouth that could provide a freshwater input to relieve low soil moisture and high salinity. Although I did not have frequent enough soil moisture and salinity observations to use it as a random forest model predictor, I measured salinities over 40 parts per thousand during periods of low tidal flooding and warm temperatures (data not shown), which exceeded the salinity stress threshold of 30–35 parts per thousand identified in previous work (Kathilankal et al., 2011; Maricle et al., 2007; Pearcy & Ustin, 1984).

High salinity and low soil moisture can reduce photosynthesis through multiple mechanisms. Hypersalinity can decrease the photosynthetic capacity by increasing plant tissue ion concentrations (DeLaune & Pezeshki, 1994; Maricle et al., 2007; Poppe & Rybczyk, 2021). Salinity and soil moisture are also important controls of salt marsh stomatal conductance (Hessini et al., 2021; Hwang & Morris, 1994; Maricle et al., 2007; Maricle & Lee, 2006). Both raise the osmotic potential of porewater, making it harder for the plant to pull water up through its roots (Betzen et al., 2019). In response, stomata may close to prevent further water loss, which reduces internal CO<sub>2</sub> concentrations and limits photosynthesis. This mechanism may be exacerbated by higher VPD and warmer

afternoon temperatures, leading to the observed midday depression of GPP. Higher spring tides can relieve vegetation stress and lead to an increase in photosynthesis, which can explain why midday depression was less severe during periods with higher tides (Jones et al., 2018; Knox et al., 2018; Liu et al., 2020; Nahrawi et al., 2020; Teal, 2001).

Vegetation stress caused by lower high tides and warmer temperatures may shift *S. alterniflora* to downregulate its C<sub>4</sub> photosynthetic pathway and utilize photorespiration as a damage control mechanism in the afternoon. Various abiotic stressors can trigger the generation of reactive oxygen species (ROS) that harm vegetation (Choudhury et al., 2017). Photorespiration is a critical 'release valve' protective mechanism to prevent ROS accumulation and photoinhibition (Voss et al., 2013). Although C<sub>4</sub> plants evolved to minimize photorespiration, multiple studies have suggested that *S. alterniflora* can modify its C<sub>4</sub> photosynthetic pathway and have significant photorespiration under stress (Sage et al., 2012). For instance, *S. alterniflora* has multiple height ecophenes, or phenotypes from the same genotype, with different photosynthetic characteristics that arise from microclimate variations in soil salinity (Giurgevich & Dunn, 1979; Shea et al., 1975). The tall ecophene stands at one to two meters in height and grows in the intertidal zone of low marshes along creek edges, where the soil is relatively less saline. The short ecophene measures 0.3 to 0.5 meters in height and occupies higher marsh elevations with higher soil salinities. An intermediate height form, ranging from 0.5 to 1 meter, is found in relatively moderate soil salinities and is the predominant ecophene present at this study's field site. Comparisons of ecophenes have found the short and intermediate height forms to have larger CO<sub>2</sub> compensation points within the range of C<sub>3</sub>-C<sub>4</sub> intermediate plants, lower enzymatic activity of C<sub>4</sub>-specific photosynthetic pathway proteins, lower light saturation, significant photorespiration, and overall lower photosynthetic capacity than the tall form, which has values in the typical C<sub>4</sub> range (Giurgevich & Dunn, 1979; Shea et al., 1975). The ecophenes are dynamic and can change type within their lifetime when transplanted to a different salinity microclimate (Shea et al., 1975). Further, Kathilankal et al. (2011) observed increased CO<sub>2</sub> compensation points of *S. alterniflora* throughout the day at this study's field site. In contrast to the tall ecophene, the short and intermediate ecophenes may be more susceptible to midday depression because they experience higher salinity and lower soil

moisture conditions in the marsh interior and generally have a lower photosynthetic capacity.

The dynamic nature of *S. alterniflora*'s CO<sub>2</sub> compensation points and other photosynthetic properties raises the possibility that the midday depression observed in this study results from an increase in afternoon photorespiration. Both salinity and drought stress are known to increase ROS production and induce oxidative stress in *S. alterniflora* (Hessini et al., 2021; Maricle et al., 2007). An increase in photorespiration in the afternoon would help relieve ROS accumulation during the warmer hours when the salinity or drought stress may be more acute. Further, photorespiration is highly temperature-dependent and naturally increases during warmer afternoons (Jordan & Ogren, 1984; Ku & Edwards, 1977b, 1977a). Stomata closure in the afternoon would also lead to a decrease in intracellular CO<sub>2</sub> and an increase in leaf temperature, both of which could increase photorespiration.

At longer temporal scales, the persistent midday depression of photosynthesis observed in this study has significant implications for the total salt marsh carbon uptake. I estimated up to an 18% decrease in afternoon photosynthesis compared to the morning across the growing season. Goulden et al. (2004) quantified a similar midday depression of NEE in a tropical rainforest of up to ~40%, which the authors attributed to a combination of high evaporative demand, high temperature, and intrinsic circadian rhythm. During the 2020 southwest US drought, (Zhang et al., 2023) found grasslands had an average 33% decrease in afternoon light use efficiency compared to the morning. The magnitude of midday depression of GPP is thus not inconsequential and must be carefully interpreted when extrapolating coarser temporal measurements. Polar satellite observations that provide a single snapshot of a landscape could lead to an underestimation or overestimation of the total GPP depending on the time of the satellite overpass. However, recent advances in geostationary satellites have made it possible to measure the midday depression of GPP at larger scales with greater accuracy (Khan et al., 2022; Li et al., 2021; Li et al., 2023; Zhang et al., 2023).

To determine the exact mechanism of midday depression observed in this study, future work must collect concurrent leaf-level gas exchange measurements within the flux footprint. These measurements can be used to isolate if afternoon photosynthesis decreases due to stomatal closure or biochemical mechanisms and if photorespiration is

a significant component of the GPP flux and increases in the afternoon. These studies can also help improve salt marsh photosynthesis modeling parameterization. In addition, comparisons of GPP estimated with geostationary and polar satellite observations can determine if the midday depression can be tracked at larger scales and what may be missed with multiday satellite return times.

In the context of climate change, my results highlight the complexity of multiple changing environmental conditions impacting the photosynthesis of salt marshes. Both temperature and sea level will continue to rise in the coming decades. Higher tidal levels may attenuate the severity of midday depression associated with warmer temperatures, but only up to a threshold when additional flooding becomes a stressor. Higher tides may also lead to shifts in distributions from short to tall ecophenes that are more productive and likely have less midday depression than the short ecophene. My results also raise questions about the photosynthetic responses of *S. alterniflora* to climate change. If *S. alterniflora* behaves more like a C<sub>3</sub>-C<sub>4</sub> intermediate plant when under heat and salinity stress, it may show CO<sub>2</sub> fertilization effects and be more sensitive to temperature in the future (Boretti & Florentine, 2019; Haverd et al., 2020; Yamori et al., 2014).

## **1.5 Chapter Conclusions**

This study used EC flux observations to measure daily midday depression of photosynthesis and explore the environmental factors influencing the phenomenon in an intertidal salt marsh. I observed ubiquitous midday depression throughout the 2019–2022 growing seasons, which, to my knowledge, has not been reported in other *S. alterniflora*-dominated marshes. Maximum daily tidal height was the strongest environmental control and attenuated the severity of depression, with higher tide days having less severe depression. Warmer air temperature was also a strong control and contributed to a more severe depression. I suspect that tidal height and air temperature modulate the severity of depression by impacting soil salinity and water availability to plant roots, which ultimately causes stomata to close and reduce CO<sub>2</sub> uptake to minimize water loss. The abiotic stress may also trigger dynamic biochemical changes that lead to changes in the CO<sub>2</sub> compensation point and increased photorespiration. Ultimately, my results highlight a previously unreported diurnal pattern in a C<sub>4</sub> salt marsh grass that will

likely be further exacerbated by climate change and have significant implications for carbon uptake.

## Chapter 2: Remote sensing proxies of salt marsh photosynthesis

### 2.1 Introduction

#### 2.1.1 Salt marsh carbon cycle

Blue carbon ecosystems play an outsized role in the global carbon cycle. Despite covering only ~0.2% of the ocean's surface, they account for up to 10% of ocean net primary production and up to a third of marine CO<sub>2</sub> uptake (Duarte, 2017). Blue carbon, defined as organic carbon buried in the soils of salt marshes, seagrass meadows, and mangrove forests, accumulates because of the high rates of photosynthesis, efficient trapping of suspended particles, and hypoxic conditions that slow the decomposition rate (Lovelock et al., 2017; Mcleod et al., 2011). In contrast to terrestrial forests that sequester carbon on decadal scales, an estimated 50% of detritus (carbon originally assimilated through photosynthesis and then stored as plant biomass) in blue carbon ecosystems is buried in vertically accumulating sediments for millennia and accounts for 0.9–2.6% of mitigated anthropogenic CO<sub>2</sub> emissions globally (Lo Iacono et al., 2008; McKee et al., 2007; Murray et al., 2011).

The combination of high rates of photosynthesis and storage per unit area makes salt marshes one of the largest natural carbon sinks (Howard et al., 2014). Marshes sequester 57–218 gC m<sup>-2</sup> year<sup>-1</sup> and hold an average carbon stock of 593 Mg ha<sup>-1</sup> globally (Alongi, 2014; Chmura et al., 2003; Hopkinson et al., 2012). However, the variety of local and global drivers makes salt marsh carbon sequestration highly variable across space. This leads to uncertainty as one moves to larger spatial and temporal scales that cannot be captured with *in situ* measurements. Furthermore, the global extent of salt marshes is poorly constrained, especially in tropical regions (Mcowen et al., 2017; Ouyang & Lee, 2014). Thus, significant uncertainties remain in current inventories of global blue carbon sinks (Windham-Myers et al., 2018).

Accurate estimates of salt marsh gross primary production (GPP), the amount of carbon taken up by vegetation through photosynthesis at the ecosystem scale, is a crucial challenge to producing a more certain inventory of the global blue carbon stocks and improving global carbon models (Feagin et al., 2020). Eddy covariance (EC) is a powerful tool to address this challenge at the ecosystem-scale and ground-truth satellite observations of GPP. EC measures the net ecosystem exchange flux of CO<sub>2</sub> by correlating

deviations in the vertical wind speed and CO<sub>2</sub> mixing ratios from their means (Baldocchi et al., 1988). Although empirical modeling is commonly used to partition the net flux into photosynthetic and respiration components in terrestrial ecosystems, these approaches are highly uncertain when applied in intertidal landscapes during high tides because inundation physically impacts gas exchange by slowing diffusion, reduces the surface area of leaves exposed to the atmosphere, and adds an environmental control of GPP that is not in current flux partitioning models. This uncertainty warrants additional, independent approaches to complement EC and improve GPP estimates across all tidal conditions.

### *2.1.2 Remote sensing as a tool to improve estimates of salt marsh GPP*

Remote sensing is a promising approach to improving estimates of salt marsh GPP at multiple scales (Campbell et al., 2022). Ground-based strategies can continuously and autonomously monitor surface spectral properties linked to plant health and function, complement EC and local meteorological data, and validate larger-scale satellite observations. Below, I describe approaches to estimating GPP with proximal (i.e., ground-based) remote sensing, which was used in this study.

#### *2.1.2.1 Solar-induced chlorophyll fluorescence*

Recently, it has become possible to measure solar-induced chlorophyll fluorescence (SIF) with proximal, airborne, and satellite remote sensing. While most of the incident solar radiation absorbed by a plant is partitioned to photosynthesis or dissipated as heat, excited chlorophyll molecules fluoresce 1–2% of absorbed photons as SIF (Frankenberg & Berry, 2018). The SIF intensity has been empirically shown to be proportional to the electron transport rate in photosynthesis and to correlate with photosynthesis at the canopy scale (Porcar-Castell et al., 2014; Yang et al., 2015). In contrast to vegetation indices that only track vegetation structure or chlorophyll content, SIF is more directly linked with GPP through photochemistry and is sensitive to the physiologic responses of plants to stress and structural changes (Baker, 2008; Pinto et al., 2020).

In the past decade, numerous studies have examined the SIF-GPP relationship at various temporal and spatial scales and with multiple retrieval approaches. Satellite and

proximal observations of SIF have found strong correlations with GPP derived from EC flux towers, but it is unclear if a universal slope of the relationship exists or if the slope varies by ecosystem type (Frankenberg et al., 2011; He et al., 2020; Li & Xiao, 2022; Li et al., 2018; Liu et al., 2017; Rossini et al., 2016; Sun et al., 2017). A lack of a clear universal SIF-GPP slope requires ecosystem-specific, proximal observations to increase the accuracy of vegetation carbon fluxes derived from remote sensing across spatial scales.

Only two studies have collected concurrent ground observations of salt marsh SIF and EC fluxes. In a *Phragmites australis* salt marsh, Huang et al. (2022) observed strong correlations between SIF and GPP at half-hourly, weekly, and seasonal scales, but the relationship was weakened during tidal inundation. However, this study was over a relatively tall, dense vegetation canopy and did not need to consider the impact of soil background and water absorption of near-infrared radiation in shorter, sparse canopies that are more frequently partially to fully inundated by the tide. Vázquez-Lule & Vargas, (2023) found SIF to poorly track GPP in a relatively high-elevation salt marsh dominated by *Spartina alterniflora* and *Spartina cynosuroides* that were rarely inundated. Thus, additional studies are needed that examine SIF-GPP relationships across the tidal cycle in low-lying and shorter marsh vegetation canopies.

#### 2.1.2.2 Near-infrared radiation of vegetation

Near-infrared radiation of vegetation ( $\text{NIR}_v$ ) is a new class of vegetation indices that has shown promise in improving estimates of GPP.  $\text{NIR}_v$  is the product of the normalized difference vegetation index (NDVI) and near-infrared (NIR) radiation upwelling from a vegetation canopy. For decades, NIR radiation has been hypothesized as a proxy of GPP because modeling studies have shown it is proportional to absorbed photosynthetically active radiation (APAR) by vegetation (Sellers, 1987; Sellers et al., 1992). NIR radiation is also linked to canopy structure, which determines how light exits a vegetation canopy (Dechant et al., 2020; Zeng et al., 2019). Further, vegetation with a higher photosynthetic capacity displays its leaves at angles to capture a more significant proportion of incoming sunlight and thus reflect more NIR radiation. NIR reflectance is also related to leaf nitrogen content, the primary determinant of leaf photosynthetic capacity, and the ratio of sun-exposed leaf area (Knyazikhin et al., 2013; Ollinger et al., 2008). Thus, NIR radiation integrates components of leaf light capture and canopy

structure related to GPP at short and long-time scales, respectively. The NDVI term in  $NIR_v$  represents the fraction of vegetation within the field of view and effectively isolates the proportion of the observed NIR signal that arises from vegetation.

Multiple ground-based and satellite studies have found near-infrared reflectance of vegetation ( $NIR_{v,Ref}$ ), the product of NDVI and NIR reflectance, and near-infrared radiance of vegetation ( $NIR_{v,Rad}$ ), the product of NDVI and NIR radiance, to be strong proxies of GPP in multiple ecosystem types and on short and long time scales (Badgley et al., 2019, 2017; Baldocchi et al., 2020; Chen et al., 2023; Liu et al., 2020; Merrick et al., 2021; Wang et al., 2021; Wu et al., 2020; Zhao et al., 2022). The  $NIR_{v,Rad}$ -GPP relationship has been empirically explained by strong correlations between  $NIR_{v,Rad}$  and APAR by green leaves, which is a dominant driver of GPP at short time scales (Wu et al., 2020).  $NIR_{v,P}$ , the product of  $NIR_{v,Ref}$  and photosynthetically active radiation, is another member of the  $NIR_v$  class that is a strong proxy for GPP (Chen et al., 2023; Dechant et al., 2022; Jeong et al., 2023; Kong et al., 2022; Liu et al., 2023).  $NIR_{v,P}$  adds information about incoming solar radiation, an important driver of GPP, not embedded in  $NIR_{v,Ref}$ .

$NIR_v$  has multiple advantages over other remote sensing approaches to track GPP.  $NIR_v$  is a simple vegetation index that does not require a complex retrieval algorithm like SIF.  $NIR_v$  also addresses the ‘mixed pixel problem’ because the NDVI term represents the fraction of the field of view that is vegetation (Badgley et al., 2017). This makes  $NIR_v$  particularly appealing for studying salt marshes, which can have patches of marsh dieback, sparse canopies, and dead vegetation wrack cover. In contrast to SIF,  $NIR_v$  does not require a high signal-to-noise ratio and can be measured with relatively inexpensive instrumentation on the ground or from many moderate spectral resolution satellite products.  $NIR_v$  is readily available from multiple satellites spanning decades of data and can upscale GPP from flux towers without additional meteorological datasets to constrain photosynthesis (Badgley et al., 2019). Further,  $NIR_v$  may be insensitive to soil background and dead legacy vegetation in some ecosystems, though this is still an area of active research (Baldocchi et al., 2020; Zeng et al., 2021).

However, questions remain about ecosystem-specific  $NIR_v$ -GPP relationships and which  $NIR_v$  index to use in salt marsh studies. The mixed pixel problem and soil background are particularly challenging when studying salt marshes with sparse vegetation canopies and a heterogeneous landscape of vegetation, mud flats, and water

that changes throughout the tidal cycle. One study found  $\text{NIR}_{v,\text{Ref}}$  improved estimates of salt marsh net ecosystem productivity, but the marsh was rarely flooded, and additional studies are needed in low-lying marshes (Hill et al., 2021). Another study assessed the potential of several vegetation indices from Landsat and MODIS to predict salt marsh GPP and found  $\text{NIR}_{v,\text{P}}$  to be a good proxy for GPP, but a combination of other indices that incorporate the tidal conditions outperformed  $\text{NIR}_{v,\text{P}}$  (Yang et al., 2023). MODIS  $\text{NIR}_{v,\text{Ref}}$  has also been shown to improve salt marsh air-exposed leaf area estimates during different tidal conditions (Hawman et al., 2023). The applicability of  $\text{NIR}_v$  to salt marsh GPP remains uncertain, as studies have shown the  $\text{NIR}_v$ -GPP relationship was weaker over more heterogeneous, less dense vegetation canopies (Badgley et al., 2017; Baldocchi et al., 2020).

### 2.1.3 Chapter 2 Aims

In this chapter, I couple proximal remote sensing observations and GPP flux measurements to test the potential of  $\text{NIR}_{v,\text{Rad}}$ ,  $\text{NIR}_{v,\text{P}}$ , and SIF to track salt marsh photosynthesis. The continuous measurements allow me to examine  $\text{NIR}_{v,\text{Rad}}$ ,  $\text{NIR}_{v,\text{P}}$ , and SIF trends and relationships with GPP at multiple temporal scales and across different tidal conditions. I hypothesize that  $\text{NIR}_{v,\text{Rad}}$  and  $\text{NIR}_{v,\text{P}}$  will outperform SIF because they better capture components of canopy structure, are less sensitive to soil background, and have lower signal-to-noise requirements. I also hypothesize that the tidal cycle will decouple GPP- $\text{NIR}_v$  and GPP-SIF relationships by differentially impacting  $\text{CO}_2$  gas exchange and remote sensing observations in the NIR wavelengths.

## 2.2 Methods

### 2.2.1 Site Description

The study site was in an intertidal salt marsh dominated by *Spartina alterniflora* (salt marsh cordgrass, also referred to as *Sporobolus alterniflorus* (Peterson et al., 2014a, 2014b)) within the Virginia Coast Reserve Long Term Ecological Research site (VCR-LTER) on the Eastern Shore of Virginia (AmeriFlux ID US-VFP; 37°24'39.8"N 75°49'59.6"W). The marsh is on the Atlantic Ocean side of the Delmarva Peninsula and faces shallow coastal lagoons backed by barrier islands. The tower is located 2 km from the shoreline and 85 m from a major creek edge. The marsh is dominated by the

intermediate form of *S. alterniflora*, with an average height of 0.6 m. The semidiurnal tidal cycle inundates the marsh platform twice daily, with ~15% of time points having water above the mud platform.

### 2.2.2 Remote Sensing Observations

Remote sensing observations were collected in the 2021, 2022, and 2023 growing seasons. Two hyperspectral spectrometers (QE Pro, Ocean Optics Inc.) measured five scans of vegetation radiance and sky irradiance over red (650–742 nm) and far-red (730–784 nm) wavelengths with a spectral resolution of 0.1 nm every 15 minutes. Spectrometer digital numbers were converted to vegetation radiance or sky irradiance, filtered, and corrected for dark current as described (Yang et al., 2018).

In the summer of 2021, observations were collected from the top of the flux tower at 7 m with the vegetation-viewing optic fiber placed at a 35° zenith viewing angle. The sky-viewing fiber pointed directly upwards and was capped with a cosine corrector (CC-3, Ocean Optics Inc.) to integrate light over a 180° viewing angle. In 2022, the optic fibers were lowered to a height of 1.5 m due to poor SIF retrieval quality and rusting of the cosine corrector in 2021. The vegetation fiber was also adjusted to a 60° zenith viewing angle to reduce soil background effects, and the sky fiber’s cosine corrector was replaced with a hardier plastic cosine corrector (JB COS, JB Hyperspectral) that is more resistant to rust from salty and humid conditions.

The spectral fitting method was used to retrieve SIF in the far-red wavelengths (Meroni et al., 2009). In this approach, the following equation is used to describe the relationship between radiance upwelling from vegetation ( $L$ ), reflectance ( $r$ ), downwelling sky irradiance ( $E$ ), model error ( $\varepsilon$ ), and fluorescence emission ( $F$ ) at a given wavelength ( $\lambda$ ):

$$L(\lambda) = \frac{r(\lambda)E(\lambda)}{\pi} + F(\lambda) + \varepsilon(\lambda)$$

$F$  and  $L$  are assumed to be linear functions over the wavelengths of the O<sub>2</sub>A oxygen absorption band (759.3–767.5 nm), allowing SIF to be best estimated as  $F$  for a chosen wavelength. The method is applied to the oxygen absorption feature because fluorescence

accounts for a more significant portion of the total radiance observed upwelling from vegetation in those wavelengths.

Near-infrared radiance of vegetation ( $NIR_{v, Rad}$ ) was calculated as:

$$NIR_{v, Rad} = \frac{NIR - Red}{NIR + Red} \times NIR_{Rad}$$

NIR is the reflectance at 780 nm, Red is the reflectance at 670 nm, and  $NIR_{Rad}$  is vegetation radiance at 780 nm.  $NIR_{v,P}$  was calculated with a slightly modified equation that multiplies NDVI by NIR reflectance and photosynthetically active radiation (PAR):

$$NIR_{v,P} = \frac{NIR - Red}{NIR + Red} \times NIR \times PAR$$

### *2.2.3 Eddy CO<sub>2</sub> Flux Measurements*

Eddy covariance (EC) CO<sub>2</sub> flux measurements were collected and processed as described in Chapter 1 with a few changes. Fluxes measured when the tide was above the marsh mud platform were included in the dataset to investigate how CO<sub>2</sub> fluxes and remote sensing observations compare across the entire tidal cycle. Gap-filled NEE and GPP fluxes were used to plot seasonal time series in Figure 2.1 but were not included in correlation plots to compare GPP and remote sensing observations.

### *2.2.4 Ancillary data*

Photosynthetically active radiation (PQS1, Kipp & Zonen), long and shortwave radiation (CNR4, Kipp & Zonen), and tidal depth (CTD Diver, Van Essen) were collected at one-minute intervals and averaged over 30 minutes to align with flux and remote sensing observations. Data collected by the Virginia Coast Reserve LTER and NOAA's Wachapreague tidal station were used to fill in gaps when onsite instruments were not operational.

### *2.2.5 Data analysis*

To examine the relationships between photosynthesis and the three remote sensing proxies, GPP was compared with  $\text{NIR}_{\text{v, Rad}}$ ,  $\text{NIR}_{\text{v, Ref}}$ , and SIF at multiple temporal scales and tidal conditions. Only remote sensing data collected from 8:30 to 15:30 LST were used due to uncertainties from the bidirectional reflectance distribution function effect under high sun angles. High tide conditions were defined as time points with greater than 0 cm of water depth on the marsh platform. Linear regressions of GPP and remote sensing data were forced to y-intercepts of 0. The coefficients of determination ( $R^2$ ) were used to quantify the strength of GPP and remote sensing proxy relationships.

## 2.3 Results

### 2.3.1 Relationships between GPP and remote sensing proxies across temporal scales

At the seasonal scale,  $\text{NIR}_{v,\text{Rad}}$  and  $\text{NIR}_{v,\text{P}}$  tracked trends in GPP across the growing season (Figure 2.1). Seasonal peaks in  $\text{NIR}_{v,\text{Rad}}$  and  $\text{NIR}_{v,\text{P}}$  aligned with GPP, and both captured within-season peaks and troughs. Daily total NEE and GPP reached up to  $-2.14$  (a negative NEE flux indicates the marsh was a  $\text{CO}_2$  sink) and  $5.35 \text{ g C m}^{-2} \text{ d}^{-1}$ , respectively.  $\text{NIR}_{v,\text{Rad}}$ ,  $\text{NIR}_{v,\text{P}}$ , and SIF reached daily averages of up to  $22.23 \text{ mW m}^{-2} \text{ nm}^{-1} \text{ sr}^{-1}$ ,  $150 \mu\text{mol photons m}^{-2} \text{ s}^{-1}$ , and  $0.32 \text{ mW m}^{-2} \text{ nm}^{-1} \text{ sr}^{-1}$ , respectively. SIF also followed trends in GPP, but limited high-quality data hindered successful SIF retrieval for much of the study period.

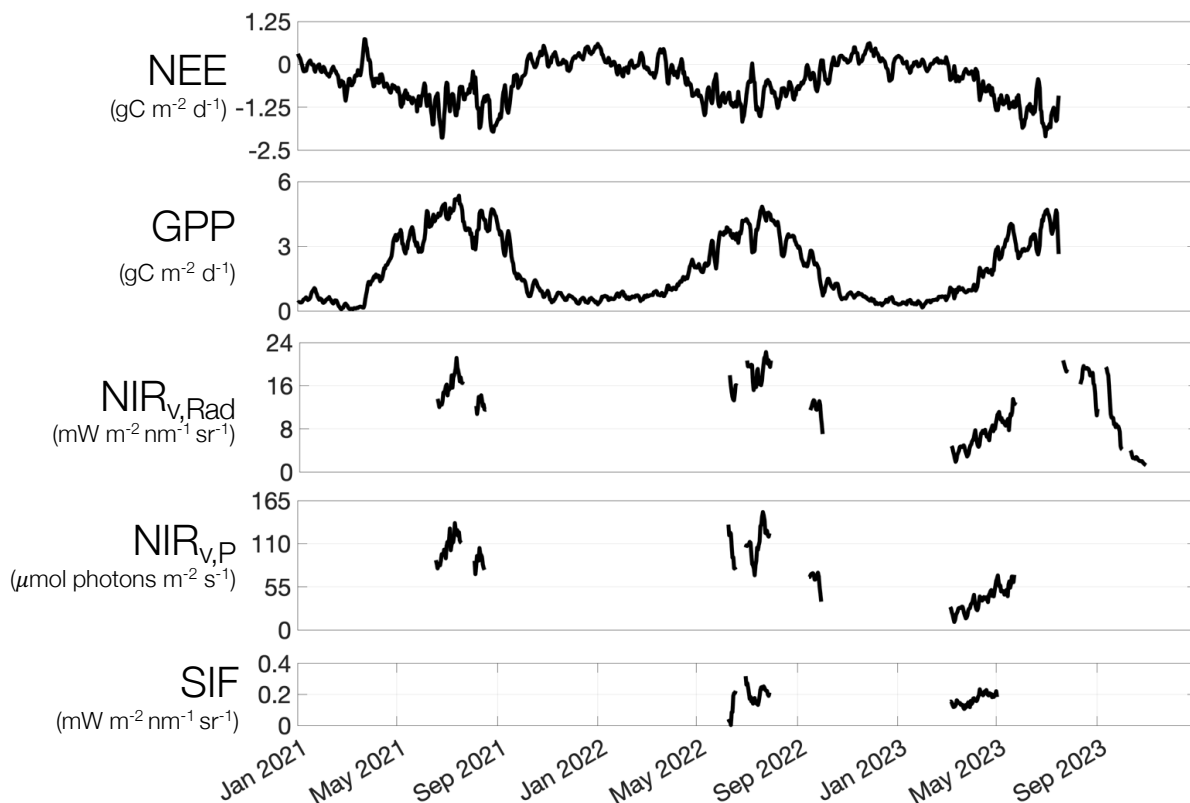


**Figure 2.1** Time series of daily net ecosystem exchange (NEE), GPP,  $\text{NIR}_{v,\text{Rad}}$ ,  $\text{NIR}_{v,\text{P}}$ , and SIF. NEE and GPP are plotted as the 5-day moving average of daily total grams of carbon. Remote sensing data are plotted as the 5-day moving average of observations collected from 8:30 to 15:30 LST.

When excluding data collected during high tide conditions, the diurnal patterns of the remote sensing proxies showed similarities and differences from GPP (Figure 2.2). Within the 8:30 to 15:30 time frame, all peaked at 10:00 and showed varying degrees of midday depression. The diurnal pattern of  $\text{NIR}_{v,\text{Rad}}$  most closely aligned with the diurnal pattern of GPP, though  $\text{NIR}_{v,\text{Rad}}$  plateaued in the afternoon while GPP steadily declined after its midmorning peak.  $\text{NIR}_{v,\text{P}}$  sharply declined by  $\sim 33\%$  after its mid-morning peak, then plateaued for the afternoon. SIF had a relatively similar decline as GPP but showed substantial recovery in the afternoon hours that nearly reached the level of its midmorning peak.

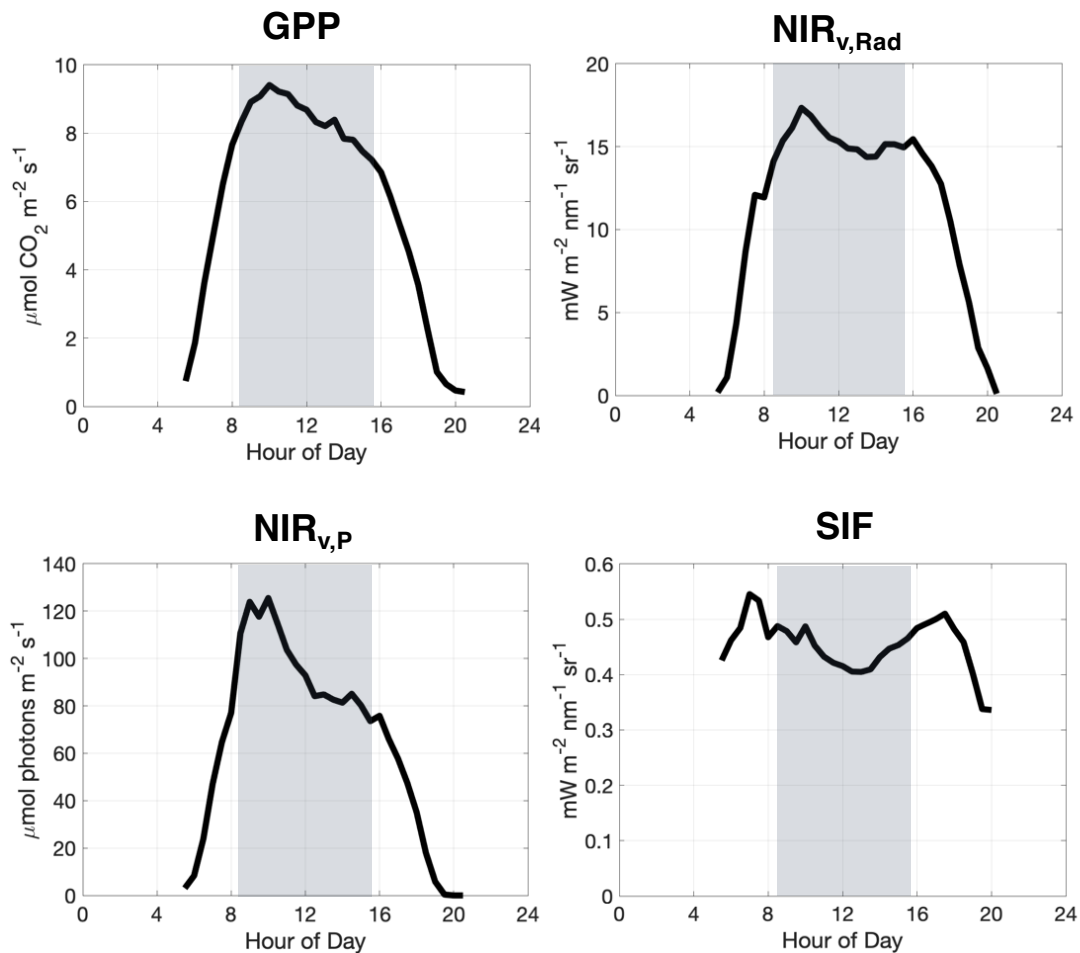


**Figure 2.2** Diurnal patterns of GPP,  $\text{NIR}_{v,\text{Rad}}$ ,  $\text{NIR}_{v,\text{P}}$ , and SIF. Data was averaged at half-hourly time points during low tide conditions from the 2021, 2022, and 2023 growing seasons. The shaded areas cover hours 8:30 to 15:30 LST, when bidirectional reflectance viewing effects minimally impact the remote sensing observations.

The correlation strength between GPP and the remote sensing proxies varied with temporal scale and generally increased when data was averaged over more extended periods (Figure 2.3).  $\text{NIR}_{v,\text{Rad}}$  had the strong correlations with GPP and displayed a linear relationship with minimal saturation effects. From half-hourly to 5-day aggregation, the  $R^2$  of  $\text{NIR}_{v,\text{Rad}}$ -GPP increased from 0.45 to 0.72.  $\text{NIR}_{v,\text{P}}$  had a similar correlation with GPP, increasing from 0.43 to 0.73 when aggregated over 5-day windows. Although  $\text{NIR}_{v,\text{P}}$  had a slightly stronger correlation with GPP than  $\text{NIR}_{v,\text{Rad}}$  at the 5-day scale, it showed saturation at high light intensities. SIF had the weakest relationship with GPP and did not show increased correlations over longer temporal windows.

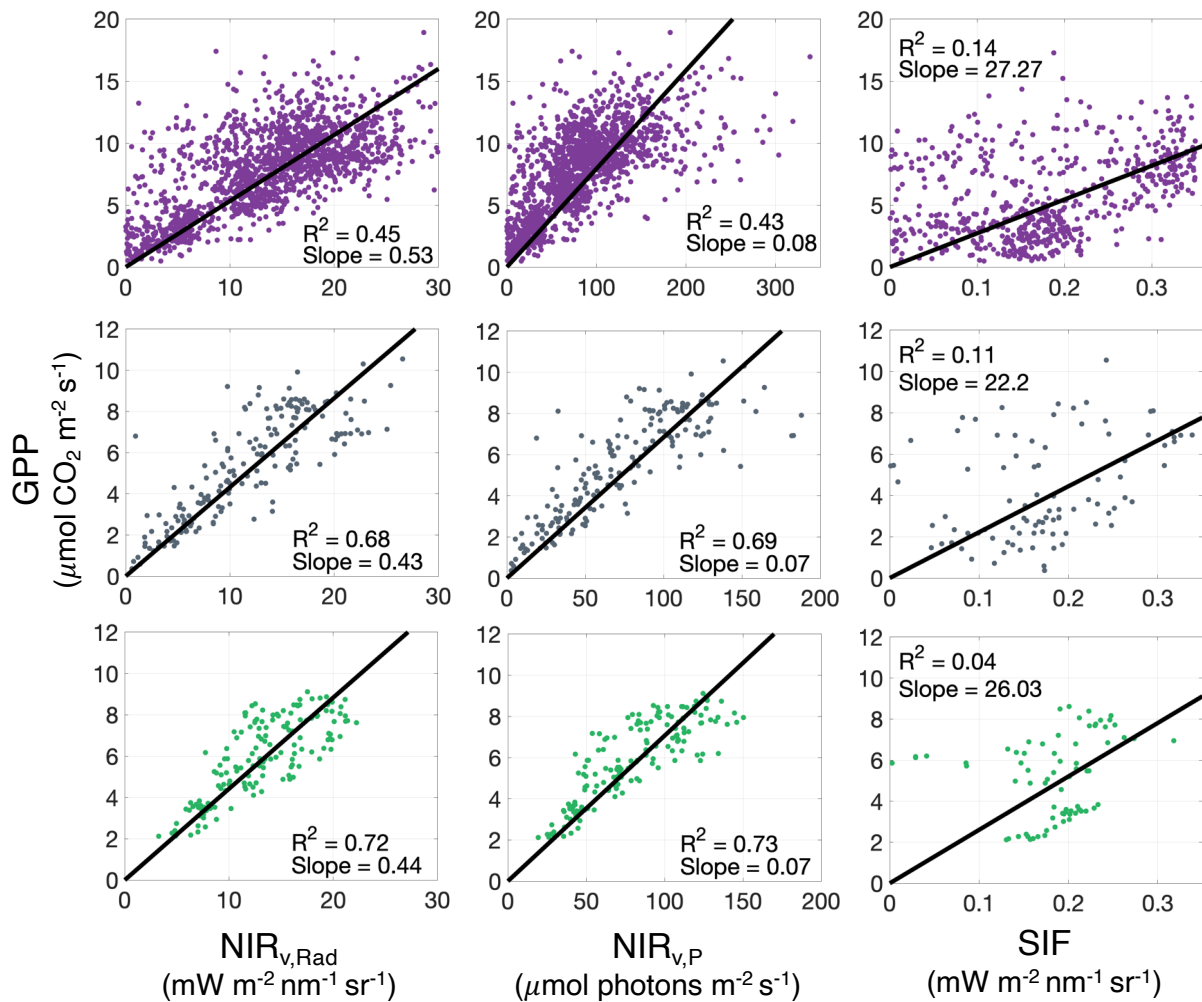


**Figure 2.3** GPP- $\text{NIR}_{v,\text{Rad}}$ ,  $\text{NIR}_{v,\text{P}}$ , and SIF linear regressions at the half-hourly (purple), daily (grey), and 5-day (green) scale.

### 2.3.2 Relationships between GPP and remote sensing proxies across tidal conditions

Examining how the tidal cycle at my field site impacts proximal remote sensing observations in the red and NIR wavelengths is essential to understanding how the tide may attenuate  $\text{NIR}_{v,\text{Rad}}$ ,  $\text{NIR}_{v,\text{P}}$ , and SIF. When comparing spectra collected during high and low tides on two days with nearly identical meteorological conditions, the tide strongly absorbed wavelengths greater than 700 nm but did not affect the red wavelengths. This effect was seen for even moderately high tides of 10 cm of water on the marsh platform (Figure 2.4).

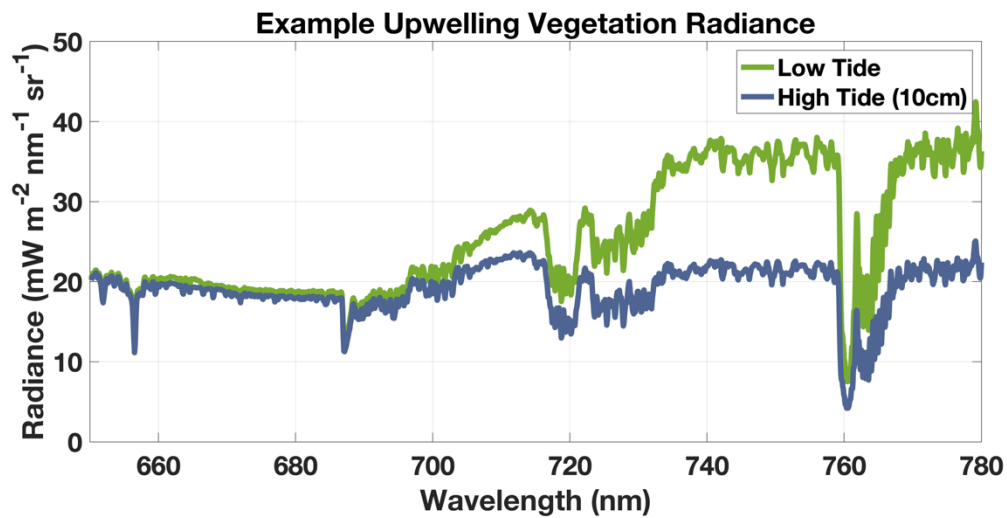


**Figure 2.4** Example vegetation radiance spectra collected at midday on two sunny days in July 2021 at low tide (green) and high tide (blue).

The tide attenuated both GPP and the remote sensing proxies (Figure 2.5). On two days when the tide reached 15 and 10 cm, GPP decreased by ~40% from its mid-morning peak to a trough during the high tide events at noon and 1 pm but recovered in the afternoon hours. The tide also attenuated the remote sensing proxies, but to a much greater degree.  $\text{NIR}_{\text{v,Rad}}$  and  $\text{NIR}_{\text{v,P}}$  decreased by ~80% during the 15 cm tide and ~70% during the 10 cm tide. SIF declined by ~75% during the 15 cm tide and ~40% during the 10 cm tide.

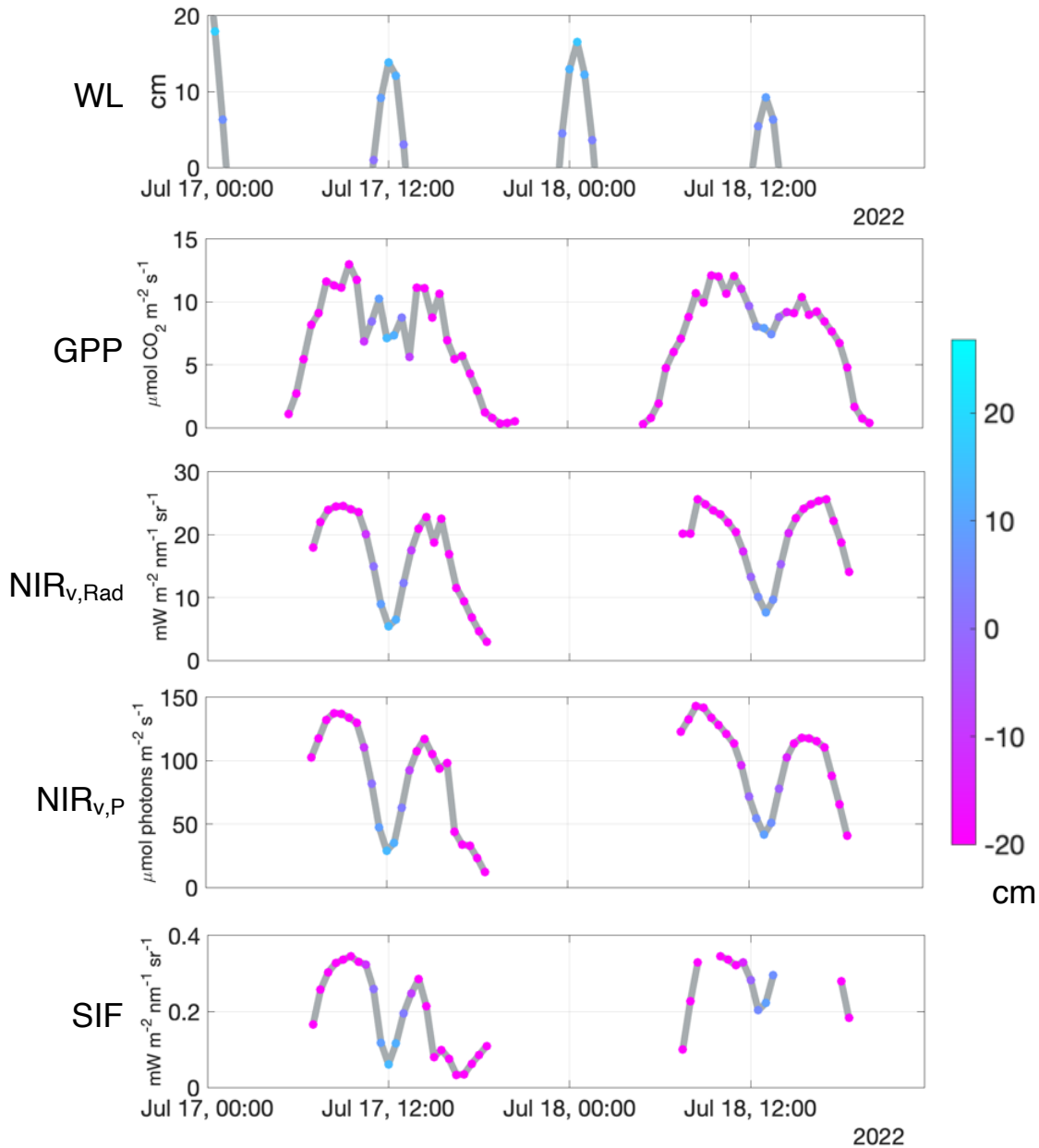


**Figure 2.5** Tidal attenuation of GPP and remote sensing proxies. The color bar indicates the water level (WL) on the marsh platform.

The correlation strength between half-hourly GPP and the remote sensing proxies decreased during high-tide events compared to low tide conditions (Figure 2.6). The  $R^2$  of  $\text{NIR}_{v,\text{Rad}}$ -GPP and  $\text{NIR}_{v,\text{P}}$ -GPP decreased from 0.47 to 0.32 and 0.43 to 0.38, respectively, during high tide events. The SIF-GPP relationship dropped from an  $R^2$  of 0.14 to 0.03.

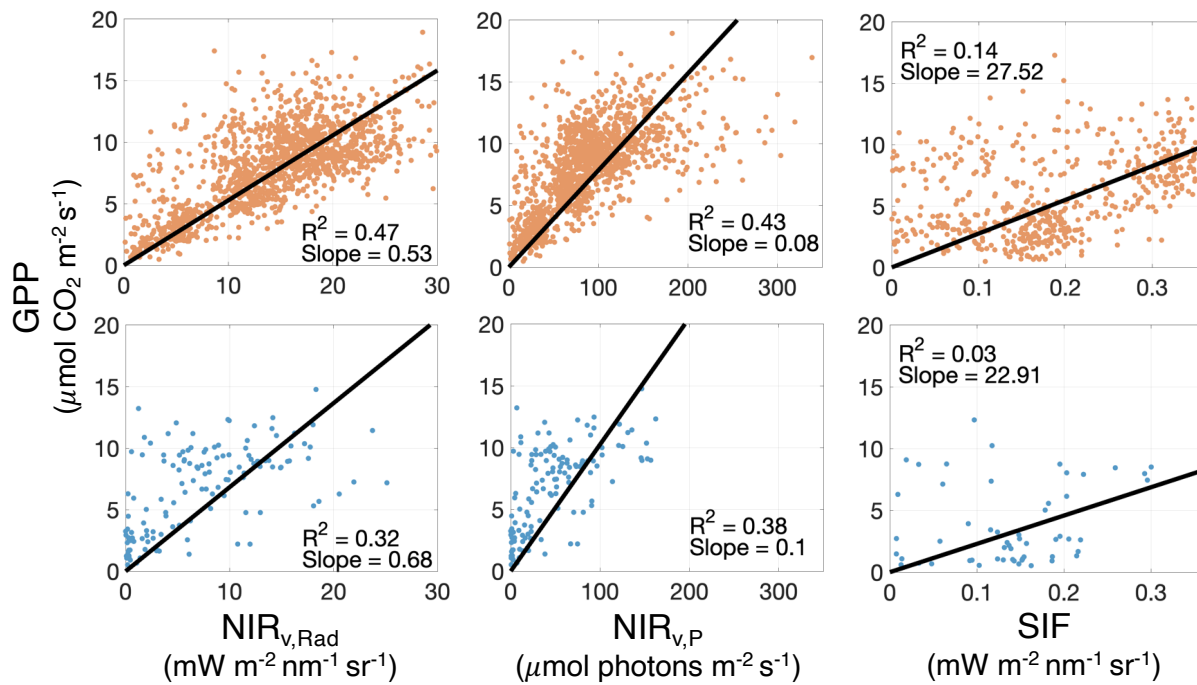


**Figure 2.6** GPP-  $\text{NIR}_{v,\text{Rad}}$ ,  $\text{NIR}_{v,\text{P}}$ , and SIF linear regressions at the half-hourly scale during low (orange) and high (blue) tide conditions.

## 2.4 Discussion

Significant uncertainties remain in the carbon budgets of salt marshes. Improving estimates of salt marsh GPP is essential to constrain its overall carbon budget and understand how the carbon cycle will be impacted by climate change. Remote sensing is a promising approach to constrain salt marsh photosynthesis at various spatial and temporal scales. However, proximal observations are needed to validate satellite observations. In this chapter, I examined the potential of three proximal remote sensing proxies to track salt marsh GPP across a range of temporal scales and tidal conditions. I found  $\text{NIR}_{v,\text{Rad}}$  to be the best proxy for GPP at short and long time scales. Although the tide differentially impacted  $\text{CO}_2$  fluxes and remote sensing observations, the relationship between  $\text{NIR}_{v,\text{Rad}}$  and GPP was not completely decoupled at high tides.

### *2.4.1 Relationships between GPP and remote sensing proxies across temporal scales*

At sub-daily time scales, both  $\text{NIR}_{v,\text{Rad}}$  and  $\text{NIR}_{v,\text{P}}$  were strong proxies for tracking salt marsh GPP. The strong relationship between the  $\text{NIR}_v$  proxies and GPP is likely due to their ability to capture sub-daily variability in sunlight conditions.  $\text{NIR}_{v,\text{P}}$  has PAR embedded in its equation. The NIR radiance term in  $\text{NIR}_{v,\text{Rad}}$ , can be represented as NIR reflectance  $\times$  NIR irradiance, which is also strongly linked to PAR. Previous studies have also found  $\text{NIR}_v$  to outperform SIF and identified strong links between  $\text{NIR}_{v,\text{Rad}}$  and absorbed PAR that explained much of the  $\text{NIR}_{v,\text{Rad}}$ -GPP relationship (Wu et al., 2020). In the late morning and afternoon, water, salinity, or heat stress may cause the marsh grass to close stomata or increase photorespiration, leading to an observed midday depression of GPP. The  $\text{NIR}_v$  proxies partially captured the midday depression of GPP, which suggests that PAR does not entirely drive the  $\text{NIR}_v$ -GPP relationships. However, both  $\text{NIR}_v$  proxies showed afternoon plateaus, while GPP steadily declined after its mid-morning peak. Thus, the  $\text{NIR}_v$  proxies cannot fully capture the impact of sub-daily stress on GPP. The divergence of  $\text{NIR}_v$  and GPP may be explained in future work with leaf-level measurements to understand the mechanism of the midday depression of photosynthesis.

The strength of the  $\text{NIR}_{v,\text{Rad}}$  and  $\text{NIR}_{v,\text{P}}$  correlations with GPP improved when the data was averaged over single and five-day periods. Reflectance-based metrics like  $\text{NIR}_v$  better capture longer-term variability in GPP because plant function and structure are

more coordinated over longer temporal scales (Yang et al., 2023). Differences in the large EC flux footprint and small optic fiber field of view may also average over longer temporal scales. However, future work incorporating satellite data should match the flux footprint with the satellite pixel to address this uncertainty (Kong et al., 2022). Although  $\text{NIR}_{v,P}$  correlated slightly more strongly with GPP at the daily and 5-day scale,  $\text{NIR}_{v,\text{Rad}}$  is overall a better proxy for GPP because it does not saturate at high light tendencies like  $\text{NIR}_{v,P}$  does at shorter time scales. Further, for proximal remote sensing studies,  $\text{NIR}_{v,\text{Rad}}$  does not require an additional PAR measurement, unlike  $\text{NIR}_{v,P}$ .

While SIF has shown promising results in previous studies, it was a weak proxy for salt marsh GPP at short or long-term scales in this study. SIF observations have much higher uncertainty than radiance, irradiance, and reflectance measurements used to calculate  $\text{NIR}_v$  (Meroni et al., 2009). Challenges related to the complexity of retrieval algorithms, the humid and salty marsh environment, signal-to-noise requirements, and soil background likely led to SIF poorly tracking GPP in this study.

#### *2.4.2 Relationships between GPP and remote sensing proxies across tidal conditions*

High tide events attenuated both GPP and the remote sensing proxies. However, the tide had a much stronger effect on remote sensing proxies than GPP. Differences in the mechanism by which the tide attenuates GPP and the remote sensing proxies can explain the differences in the severity of the attenuation. The tide attenuated the remote sensing proxies because water strongly absorbs wavelengths in the NIR wavelength region (Trabjerg & Højerslev, 1996). Previous work has documented how water physically slows the rate of gas exchange, leading to a decrease in the net  $\text{CO}_2$  flux and GPP (Forbrich & Giblin, 2015; Kathilankal et al., 2008). Partial to complete inundation of the marsh grass will also decrease photosynthesis by decreasing the availability of  $\text{CO}_2$  substrate, and *S. alterniflora* photosynthesizes at a reduced rate when submerged (Mao et al., 2023). The tide also increases the lateral flow of carbon within the water column, adding more uncertainty to the  $\text{CO}_2$  flux partitioning. Slight variations in marsh elevation could also lead to varying degrees of tidal inundation within the mismatched flux and remote sensing footprints.

Tidal attenuation and midday depression likely contributed to the midday declines in GPP and the remote sensing observations presented in Figure 2.5. However, the shifts

in the GPP and remote sensing observation troughs from 12 to 1 pm correspond to the timing of the peak tide, indicating the tide significantly contributes to the declines. Further, the recovery in GPP and the remote sensing proxies after the tide receded was not seen in the low tide only diurnal patterns (Figure 2.2).

Despite varying degrees of the impact of tidal attenuation, including all tidal conditions did not substantially reduce the half-hourly correlations between GPP and the  $\text{NIR}_v$  proxies, and longer-term correlations were robust. Thus, care should be taken when using  $\text{NIR}_v$  measured during high tide events for short-term analysis, but longer-term analysis likely does not need to account for the tide.

## **2.5 Chapter Conclusions**

This chapter used EC flux and proximal remote sensing observations to examine the potential of  $\text{NIR}_{v,\text{Rad}}$ ,  $\text{NIR}_{v,\text{P}}$ , and SIF to track salt marsh photosynthesis. I found both  $\text{NIR}_v$  indices to be strong proxies for GPP, while SIF poorly tracked GPP.  $\text{NIR}_{v,\text{Rad}}$  is likely the best proxy because it did not saturate at high sunlight intensities like  $\text{NIR}_{v,\text{P}}$  at short timescales. Although the tidal cycle more strongly attenuated the remote sensing proxies, the effect averaged out on longer temporal scales. The robust correlations with GPP at longer temporal scales indicate  $\text{NIR}_{v,\text{Rad}}$  and  $\text{NIR}_{v,\text{P}}$  are strong candidates for tracking salt marsh photosynthesis with satellite observations and improving the certainty of the salt marsh carbon cycle.

## Chapter 3: Assessing no net loss of wetland area and function through mitigation banking in Virginia

### 3.1 Introduction

Wetlands are an invaluable ecosystem that mitigates flooding, improves local and downstream water quality through nutrient cycling and sediment capture, and provides storm surge protection, shoreline stabilization, fishery and wildlife habitat, and recreation area (Friess et al., 2021; Mitsch & Gosselink, 2015). Wetlands are estimated to provide \$447 billion/year in storm protection and save over 4,000 lives per year globally (Costanza et al., 2021). Despite these ecosystem services to humans, development and conversion to agricultural land have driven the loss of over 50% of wetlands in the United States and 20% globally in the past 300 years (Dahl, 1990; Fluet-Chouinard et al., 2023). Urbanization and land use changes, such as the conversion of wetlands to hardened surfaces, have worsened flooding and property damage from storms (Brody et al., 2013, 2007; Vázquez-González et al., 2019; Zhang et al., 2018). Development continues encroaching on wetlands in many areas, such as Houston, Texas, which has lost over 30% of its wetlands from 1992 to 2012 due to rapid urbanization (Jacob et al., 2014).

#### *3.1.1 Wetland policy and mitigation banking*

Since the 1970s, the Clean Water Act has aimed to address the historical loss of wetlands and “restore and maintain the chemical, physical, and biological integrity of the Nation’s waters” (33 USC §1251 et seq., 1972). Section 404 of the Clean Water Act requires projects that discharge dredge or fill material into all waters of the United States, including wetlands, to receive a permit from the US Army Corps of Engineers (33 USC §1344, 1972). Permittees must first avoid and minimize any impacts to wetlands and then are required to compensate for unavoidable impacts. The wetland compensation process aims to restore, create, or enhance wetlands to ensure ‘no net loss’ of wetland area or function (US Environmental Protection Agency, 1990). Purchasing compensation credits from a wetland mitigation bank is the most common approach for permittees to compensate for their wetland impacts (Hough & Harrington, 2019; US Army Corps of Engineers & Environmental Protection Agency, 2008). Some states have extended wetland protections beyond federal jurisdiction, such as Virginia, which requires wetland

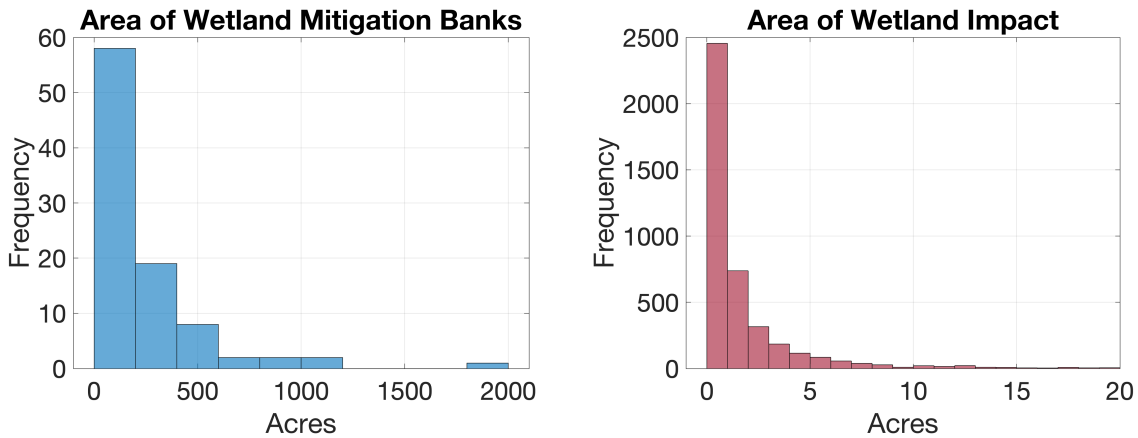


**Figure 3.1.** The size of wetland mitigation banks established in Virginia during 1995-2024 (left), and the area of permitted wetland impact activity during the same period (right).

compensation for all surface water impacts through its Virginia Water Protection Permit and is the study area in this chapter (Va Code § 62.1-44.15:20, 2001).

Mitigation banks are large wetland restoration, enhancement, creation, and preservation projects managed by a third party and constructed in anticipation of developers’ needs to offset wetland impacts (US Army Corps of Engineers & Environmental Protection Agency, 2008). In contrast to other forms of compensation, wetland mitigation banks have a higher chance of restoration success than multiple smaller compensation projects constructed on an impact-by-impact basis (Levrel et al., 2017; Moreno-Mateos et al., 2012). In Virginia, wetland mitigation banks average 220 acres in size and pool credits from many much smaller impact sites (Figure 3.1). Most mitigation banks restore agricultural land that was historically wetland and supplement credits by preserving and enhancing neighboring wetlands or upland buffers. The restoration process usually involves removing drain tiles and filling ditches used to drain the agricultural land to restore wetland hydrology, planting native facultative or wetland species of trees, and planting a seed mix of common wetland shrubs and grasses.

Permittees must purchase bank compensation credits based on the area and type of wetland their project impacts (US Army Corps of Engineers & Environmental Protection Agency, 2008; Va Code § 62.1-44.15:20, 2001). For instance, a project impacting one acre of an emergent wetland requires the permittee to purchase one compensation credit (one credit per acre impact ratio). Impacts to shrub-shrub and

forested wetlands have higher compensation ratios of 1.5 and 2 credits per acre impacted, respectively. Permittees must buy credits from a bank in the same U.S. Geological Survey 8-digit Hydrological Unit Code (HUC8) subbasin or an adjacent HUC8 in the same river watershed. Although permittees are not required to purchase credits of the same wetland type (i.e., purchase credits from forested wetland restoration for impacts to another forested wetland), most of Virginia's mitigation banks, impact wetlands, and historical wetlands have been forested (Bauer & Campbell, 2022).

Mitigation banks are assigned credits representing the wetland acreage and function of the bank. In Virginia, an Interagency Review Team (IRT) of federal and state agency representatives assigns credits to banks using the following ratios (VA Dept. of Environmental Quality, n.d.):

Restoration = 1:1 (one credit per acre)

Creation = A range of 1:1 to 1:2 (one credit per acre to two acres)

Enhancement = A range of 1:3 to 1:9, depending on functions enhanced

Preservation = 1:10

Upland Buffer Restoration = 1:15

Upland Buffer Preservation = A range of 1:20 to 1:40

At least 50% of a bank's credits must be from wetland restoration or creation to ensure new wetlands are being produced and no net loss of wetland area is achieved (US Army Corps of Engineers & Environmental Protection Agency, 2008). The low credit-to-acre ratios for enhancement and preservation also ensure the compensation process does not rely heavily on strategies that don't produce new wetlands.

Bank credits are posted for sale in phases as the bank reaches a series of performance criteria. Hydrological, soil, and vegetation performance standards are specific to each bank and wetland type and can be found in detail in the Virginia Department of Environmental Quality's Mitigation Bank Instrument on their compensatory mitigation webpage (VA Dept. of Environmental Quality, n.d.). Hydrologically, restoration and creation sites must have a water table depth less than 12 inches below the surface for at least 14 consecutive days during the growing season. Soils must be hydric, have bulk density for specific target wetland types, and meet required

redox chemistry standards. Vegetation performance standards require specific native plant species canopy coverages and stem heights. Wetland enhancement standards depend on the function the bank explicitly tries to enhance. In Virginia, most wetland enhancements aim to restore an existing wetland's historical hydrology by filling ditches and removing drain tiles.

### *3.1.2 Evaluating no net loss policy*

Although the Clean Water Act aims to conserve wetland area and function, assessing how well this is achieved in practice is challenging. While quantitative metrics of no net loss of wetland areas are straightforward, characterizing ecosystem function is not. Ecosystem function is a multifaceted concept composed of many ecological processes, such as carbon and nutrient cycling, which are generally uncorrelated with wetland size (Barbier, 2012; Barbier et al., 2008). Moreover, wetland function varies with environmental factors and climate change stressors, and thus, evaluations must be site-specific (Koch et al., 2009).

Studies examining the success of mitigation banks have typically relied on floristic metrics, such as floristic quality assessments that measure species richness and the density of native vs. non-native vegetation species. Some in situ floristic studies have found mitigation banks tend to have significantly different species compositions and be more dominated by non-native species than natural wetlands (Stefanik & Mitsch, 2012; Tillman & Matthews, 2023). Others found no difference in floristic quality and suggested mitigation banks are higher quality than degraded natural wetlands typically impacted by permitted activity (Gutrich et al., 2009; Hopple & Craft, 2013; Spieles et al., 2006; Tillman et al., 2022; Van den Bosch & Matthews, 2017). However, floristic metrics are not direct metrics of wetland vegetation function and can vary over a decade after restoration (Matthews, 2015; Matthews et al., 2009; Spieles, 2005; Spieles et al., 2006; Tillman et al., 2022; Wall & Stevens, 2015). One of the few studies directly examining function found mitigation banks to have less aboveground net primary productivity than reference sites (Stefanik & Mitsch, 2012). However, the authors found older mitigation banks (>15 years old) approached the productivity levels of reference wetlands. Other work using aerial photography has found overestimations and inaccuracies in assessments of the

reestablished wetland area and ecological gains from mitigation banks (Griffin & Dahl, 2016; Mack & Micacchion, 2006).

These findings emphasize the variability in wetland mitigation banks regarding restoration success, species composition, and function and the need to improve ecological monitoring approaches to capture wetland dynamics beyond the typical monitoring period of 5 years without intensive in-field sampling. Collecting and synthesizing new and existing data that represent the spatial and temporal variability of wetland function is pivotal to improving management practices and determining whether no net loss is achieved through mitigation banking (Levrel et al., 2017).

Remote sensing of wetland vegetation is a prime candidate for addressing this challenge in wetland management and assessing the efficacy of no net loss of wetland function in mitigation banking. Photosynthesis is a foundational component of ecosystem function; it underlies many foundational vegetation properties, such as aboveground biomass, stem height, and canopy density (Cavender-Bares & Bazzaz, 2004). In the case of wetlands, these vegetation properties ultimately determine the potential of a wetland to attenuate wave energy, mitigate flooding, improve water quality, and remove carbon dioxide from the atmosphere (Coops et al., 1996; Möller, 2006; Rupprecht et al., 2017). Thus, remote sensing of photosynthesis can be a proxy for wetland function and its overall potential to provide ecosystem services. Further, remote sensing can also provide long-term ecological monitoring datasets without time-intensive field sampling.

### *3.1.3 Chapter 3 Aims*

Twenty years ago, the National Research Council published a consensus study that concluded the conservation of wetland function is not being achieved through Section 404 permit mitigation banking and called for improved methods to assess wetland function in mitigation banks (National Research Council et al., 2001). This dissertation chapter reexamines the question of no net loss of wetland function using remote sensing. I build off the approaches optimized in Chapter 2 to quantify vegetation function in wetland mitigation banks in Virginia. I explore the following research questions:

1. How well has mitigation banking achieved no net loss of wetland area and function in Virginia?

2. How may mitigation banking have rearranged wetland distributions and associated ecosystem services in Virginia?
3. How does wetland photosynthesis and vegetation greenness vary over time at mitigation banks?

## **3.2 Methods**

### *3.2.1 Wetland Mitigation Bank Permit Data and Analysis*

Wetland mitigation bank and Section 404/Virginia Water Protection permit data were retrieved from the U.S. Army Corps of Engineers' Regulatory In-lieu Fee and Bank Information Tracking System (*RIBITS*, n.d.). Mitigation bank data included year of establishment, credit release schedule, total acreage, and bank location. Mitigation banks whose status was pending, terminated, or withdrawn were excluded from the analysis. Banks selling only stream credits were also excluded. Tidal wetland banks were excluded from the analysis because their crediting system is regulated by the Virginia Marine Resource Commission, which uses a different system for assigning credits. This filtering left 97 banks located in Virginia for further analysis.

Wetland acreage and credit initiation, release, and withdrawal transactions from 1995 to July 2024 were obtained by downloading the RIBITS transaction ledgers of the 97 selected banks. Stream credit transactions were removed from bank ledgers selling wetland and stream credits, leaving 5,100 transactions for further analysis.

To examine the supply and demand for wetland compensation credits, bank release credits were totaled (supply) and compared against credit withdrawal transactions (demand) across all banks for five-year periods starting in 1995. To examine no net loss of wetland area, newly established bank acreage was totaled and compared to impacted acreage over five-year periods starting in 1995. Bank and impact locations were plotted on a map of Virginia to determine the spatial distribution of compensation and impact sites (note that only 22% of permits listed the latitude and longitude of the impact site). The net gain or loss of wetland area and credits for HUC8 hydrological units was calculated to examine potential redistributions of wetlands and ecosystem services across Virginia.

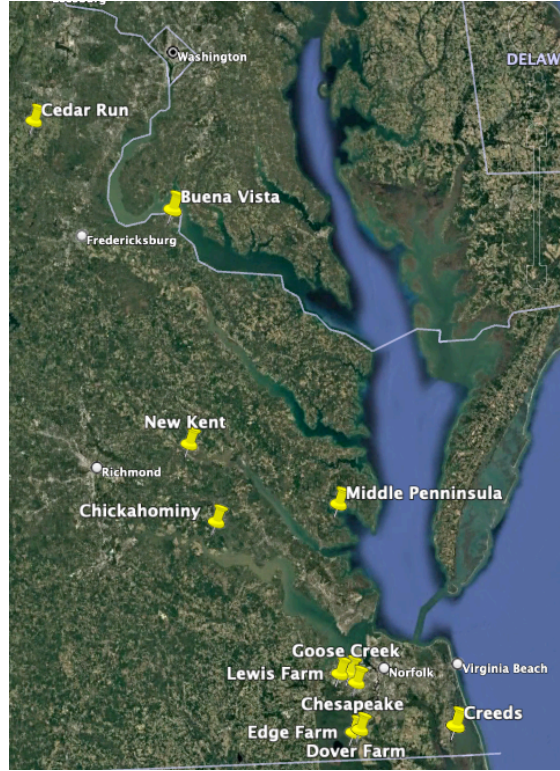


**Figure 3.2** Locations of 11 wetland mitigation banks that were selected for vegetation function remote sensing analysis.

### 3.2.2 Remote Sensing Data Analysis

The MOD13Q1 and MOD09A1 MODIS sensor data products (Terra satellite) were used to examine vegetation greenness and photosynthesis as a proxy of wetland function for 11 selected mitigation banks from 2000-2023 (Figure 3.2). All mitigation banks were non-tidal wetlands except for Goose Creek. The selected banks accounted for 40% of total non-tidal wetland compensation credits released between 1995 and 2024, excluding Goose Creek, which is on a different tidal wetland credit system. All MODIS data products were downloaded from the Oak Ridge National Lab’s Terrestrial Ecology Subsetting & Visualization Services Global Subsets Tool over the locations of selected wetland mitigation banks (“ORNL DAAC,” 2024). The MOD13Q1 data product is a 250 m, 8-day normalized difference vegetation index (NDVI) observation. The MOD09A1 500 m, 8-day product includes a red reflectance band (Band 1, 620-670 nm) and a near-infrared reflectance (NIR) band (Band 2, 841-876 nm) that were used to calculate the near-infrared reflectance of vegetation ( $NIR_v$ ) as:

$$NIR_v = \frac{NIR - Red}{NIR + Red} \times NIR$$

$NIR_v$  has recently been shown to be a strong proxy for canopy photosynthesis in multiple ecosystem types (Badgley et al., 2019, 2017; Baldocchi et al., 2020; Dechant et al., 2022). Banks were selected for remote sensing analysis based on the bank's size and shape to align with the size of the MODIS pixel. Each bank's NDVI and  $NIR_v$  time series were analyzed with a singular spectrum analysis to isolate the long-term trends in vegetation greenness and photosynthesis post-restoration. MATLAB's `trenddecomp` function was used to decompose NDVI and  $NIR_v$  post-restoration into long-term, seasonal, and residual trend components over three-year lag windows. The linear slope of the long-term trend line was used to determine if a mitigation bank maintained vegetation function over time.

### 3.3 Results and Discussion

This dissertation chapter aims to assist regulators and practitioners involved with wetland mitigation banking and management in assessing whether compensation programs meet their goals of no net loss of wetland area and function and provide new ecological monitoring approaches. Below, I present the results and discuss my research questions.

#### *3.3.1 How well has mitigation banking achieved no net loss of wetland area and function in Virginia?*

A comparison of bank supply and permittee demand for wetland areas suggests that mitigation banking has achieved no net loss in the total wetland area in Virginia (Figure 3.3a). In total, 26,679 acres of wetland mitigation bank were established, and 11,024 acres of wetland were impacted by permittee activity during the 30-year study period. The total acres of wetland in mitigation banks exceed the acres of permitted wetland impact activity by 2.42-fold. From 1995 to 2014, wetland acre supply far exceeded

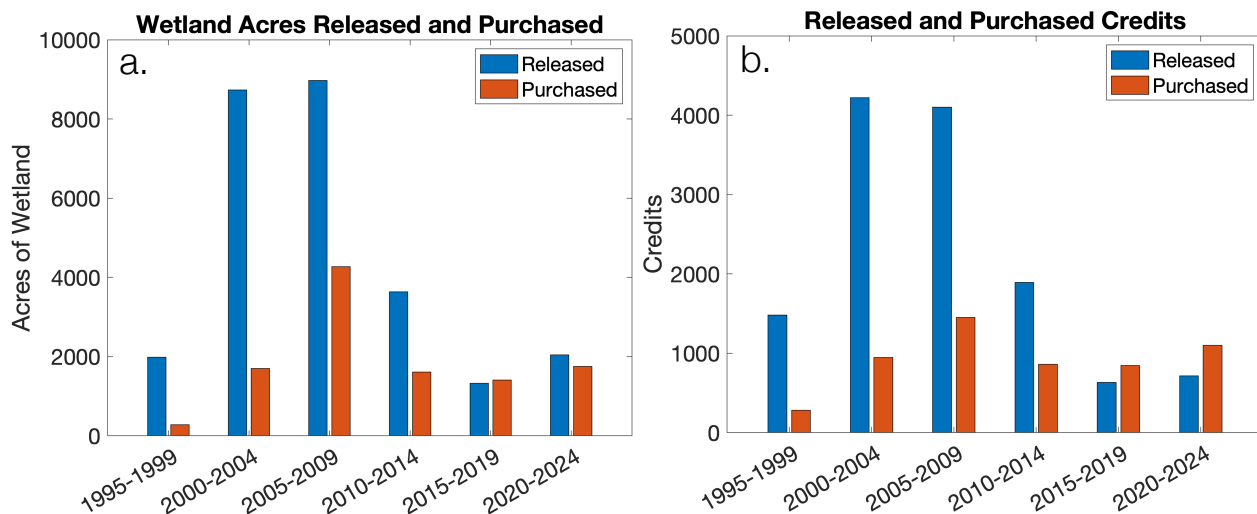


**Figure 3.3** Acres (a) and credits (b) of wetland released (blue) and purchased (orange) from wetland mitigation banks in Virginia 1995-2024.

demand. However, the rate of bank acres produced in the past 15 years has declined while the acres impacted have remained relatively constant. This has led to only a small surplus of bank acres in recent years and a shortage in 2015-2019. Not every acre of wetland in a mitigation bank results from wetland creation or restoration: preservation or enhancement can also count towards a bank’s total acreage. Thus, some of the total wetland acres released should not technically count towards an accounting of no net loss of wetland area because they existed before the bank was established. However, given the significant excess of bank acres and the requirement that at least 50% be from restoration or creation, there has been no net loss of area over the entire 30-year study period.

There is a similar 2.38-fold excess in total bank credits released compared to credits purchased by wetland impact permittees, further suggesting that no net loss of area has been achieved over time (Figure 3.3b). A similar bank-to-impact credit ratio for wetland acres and credits indicates that the excess supply mainly comes from wetland restoration and creation, not wetland preservation or enhancement, which have smaller credit-to-area ratios. This indicates that mitigation banking is upholding the requirement that 50% of bank credits come from wetland creation or restoration compensation strategies.

Although available bank credits vastly exceeded permittee demand from 1995 to 2009, declines in bank supply led to shortages in the past decade. Correspondence with Virginia Department of Environmental Quality staff has confirmed a bank credit shortage that may push permittees to other forms of compensation or a decrease in wetland permits. ‘Rollover’ credits from older mitigation banks established 15-plus years ago are helping to meet the current demand for wetland credits. However, this also means we must ensure older banks maintain function and meet performance criteria after their monitoring period of 5 years has passed. Banks that passed performance criteria decades ago are likely experiencing more significant effects of climate change and thus may not function at the same capacity. Thus, assuming no net loss of area equates to no net loss of function does not hold. Additional analysis is presented in Research Question 3 to more conclusively determine if no net loss of function has been achieved.

### *3.3.2 How may mitigation banking have rearranged wetland distributions and associated ecosystem services in Virginia?*

Most wetland mitigation banks are clustered in the eastern half of Virginia, on the outskirts of Virginia Beach, Richmond, and Washington, D.C. (Figure 3.4a). Permittee impact locations are concentrated in urban areas around Washington, D.C., Richmond, Charlottesville, and Virginia Beach (Figure 3.4b). Although most permittee-bank transaction distances are less than 50 km, mitigation banking has shifted wetlands from urban areas to more rural locations (Figures 3.4c & 3.4d). This shift makes economic sense: permittee impact locations are concentrated in areas of development and urban growth, and mitigation banks need large undeveloped areas and will favor cheaper land in more rural areas. Previous studies have reported similar urban-to-rural shifts when examining wetland mitigation banks and similar biodiversity compensation programs (BenDor et al., 2007; BenDor & Stewart, 2011; Ruhl & Salzman, 2006; van Maasakkers, 2021).

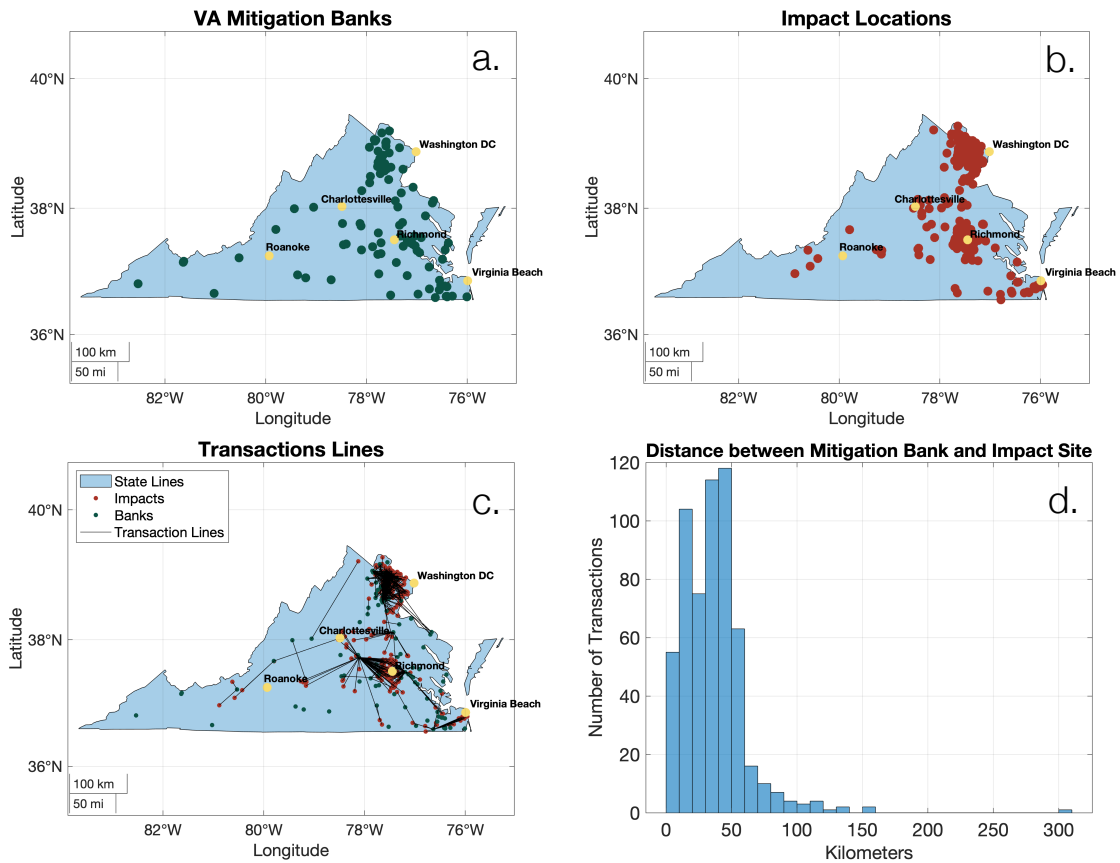


**Figure 3.4** Spatial distributions of wetland mitigation banks (a) and permitted wetland impact activity (b), and the transaction lines (c) and distances (d) between wetland mitigation bank and permitted wetland impact sites.

At the watershed subbasin scale, wetland credits and acreage were generally conserved in individual HUC8 watershed subbasins. Most HUC8 codes had a moderate increase or no net change in wetland area (Figure 3.5a & b). However, there were areas with significant net wetland gain and a few with net wetland loss. Over 50% of net wetland area and credit gains were concentrated in three HUC8 codes south of Virginia Beach (0301005), north of the Richmond-Charlottesville corridor (02080106), and near Washington D.C. (02070010) (Table 3.1). These three HUC8s gained 3,752, 3,142, and 2,405 acres of wetland, respectively. HUC8 codes along the James River and in Northern Virginia also gained significant wetland acreage. Five of the 51 HUC8 codes had a net loss of wetland area, but no area lost more than 150 acres. None of the areas with a net loss had a mitigation bank in the same HUC8, meaning any impacts were compensated by purchasing credits in an adjacent HUC8. Four of the five net loss HUC8 codes lined the bottom of the Chesapeake Bay and contributed to a significant shift of wetlands from the Virginia Beach area to a few large mitigation banks that line the Great Dismal Swamp further inland.

Although wetland area was generally conserved or increased by HUC8 code, the urban-to-rural shift within HUC8 codes may impact the distribution and quality of wetland ecosystem services. Shifting wetlands to a more rural and pristine environment, free from potential sources of degradation in urban areas, could mean wetlands will function at a higher capacity, thus increasing ecosystem services. However, the location of a wetland within the watershed or subbasin significantly affects who may benefit from local ecosystem services, such as flood control, shoreline stabilization, and access to nature and recreation. For instance, wetlands upstream or within an urban area will mitigate flooding events for more people than a wetland located downstream (Tang et al., 2020). Ecosystem service redistributions could also have environmental justice implications, as documented in previous studies examining mitigation banking (BenDor et al., 2007; BenDor & Stewart, 2011; Dernoga et al., 2015; Ruhl & Salzman, 2006). Further, low-income populations, communities of color, and otherwise disadvantaged communities disproportionately live in low-lying coastal areas vulnerable to flooding and are already facing additional challenges to climate mitigation and adaptation (Gourevitch et al., 2022; Hardy et al., 2017; Lu, 2017). Concentrating many smaller urban wetlands into a few large wetlands in rural areas also increases the average distance between

population densities and wetlands. The urban-to-rural shift is particularly concerning for low-lying coastal cities like Norfolk and Virginia Beach, which are experiencing land subsidence, high relative rates of sea level rise, and frequent nuisance flooding and are expected to face increasing flood hazards (Burgos et al., 2018; Shen et al., 2022; Van Coppenolle & Temmerman, 2020).

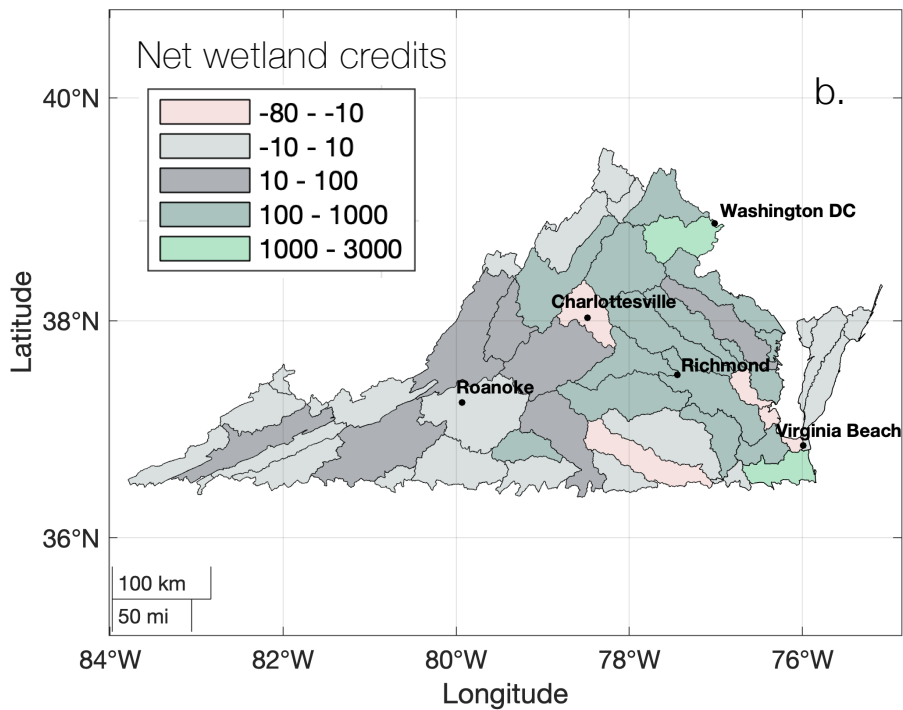
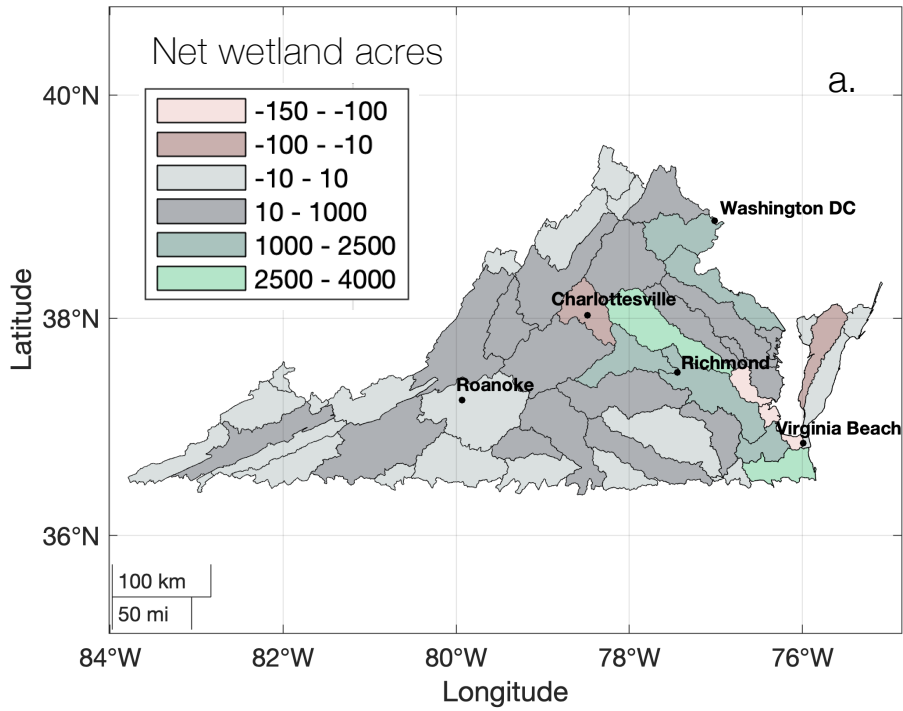


**Figure 3.5.** Net gains or losses of wetland acreage (a) and compensation credits (b) by HUC8 code.

**Table 3.1** Net wetland compensation credits and acreage gains by HUC8 Code

HUC8	Net Acreage	Net Credits
02080108	-131	-76
02080107	-123	-23
02080204	-20	-13
02080111	-11	-5
03010103	-7	-7
03010104	-2	-2
03010203	-1	-1
05050002	-1	0
03010101	-1	-7
02070006	-1	-1
06010102	0	0
05070202	0	0
02070007	0	0
03010106	0	0
02040303	0	0
02040304	0	0
02070001	0	0
02070003	0	0
02070004	0	0
02080110	0	0
03040101	0	0
06010101	0	0
06010104	0	0
06010206	0	0
02080102	0	0
02080108	0	0

HUC8	Net Acreage	Net Credits
03010201	4	7
05070201	10	6
02080203	28	39
03010102	30	29
05050001	33	11
02080202	37	33
06010205	63	37
02080201	82	73
03010204	89	-24
02080104	106	80
02070005	194	101
03010105	292	195
02080103	301	155
02080105	320	140
02070008	321	140
02080102	344	170
02080207	474	236
03010202	596	402
02070011	1114	210
02080205	1237	635
02080206	1401	260
02080208	1649	838
02070010	2405	1490
02080106	3142	644
03010205	3752	2853
<b>Total</b>	<b>17724</b>	<b>8623</b>

### *3.3.3 How does vegetation function vary over time at mitigation banks?*

In Virginia, mitigation bank production boomed in the early 2000s before declining after the 2008 economic recession (Figure 3.1). Ecological monitoring of older wetland banks is essential to determine if wetland function is maintained after the bank passes the final performance criteria and if wetland function is conserved through mitigation banking. This is of particular concern with increasing environmental stressors from climate change that can decrease wetland function. I used MODIS data products of two metrics of wetland vegetation function, NDVI (vegetation greenness) and  $NIR_v$  (photosynthesis), to assess how well 11 Virginia mitigation banks have maintained function for over a decade after restoration and long-term trends in function. Although I only looked at 10% of mitigation banks in Virginia, I chose some of the largest banks that account for 40% of total non-tidal wetland credits. Thus, results from this sample represent a sizeable portion and representative sample of wetland function in Virginia mitigation banks.

NDVI and  $NIR_v$  captured clear shifts in vegetation function before and after restoration. Before restoration at the Dover Mitigation Bank, NDVI and  $NIR_v$  have short growing seasons with high peak vegetation greenness and photosynthesis characteristics of cropland (Figure 3.6.1). After a transition period during the restoration, NDVI and  $NIR_v$  recalibrate to a longer growing season with lower peak vegetation greenness and photosynthesis. Similar seasonal shifts in NDVI and  $NIR_v$  pre- and post-restoration are observed in most mitigation banks (Figure 3.6.2-7).

The long-term trends in NDVI and  $NIR_v$  suggest that Dover and most mitigation banks maintain vegetation function for at least 15 years after restoration. At Dover, NDVI quickly increased after the restoration before approaching a plateau when vegetation communities became established (Figure 3.6.1).  $NIR_v$  shows a similar though more gradual increase after restoration. The increase in  $NIR_v$  should be attributed to increased vegetation density and total photosynthesis within the satellite pixel, not individual trees increasing photosynthesis over time. Buena Vista, Edge Farm, Goose Creek, Lewis Farm, and New Kent followed similar long-term trends as Dover (Figures 3.6.2, 3.6.7, 3.6.8, 3.6.9, & 3.6.11).

A few mitigation banks did not have linear trends and showed different trajectories in vegetation function. Chickahominy declined in NDVI and  $NIR_v$  for a few years after

restoration before quickly increasing and approaching plateaus (Figure 3.6.5). At Cedar Run, vegetation greenness had a slight positive long-term trend for the 20 years after its restoration but had shorter periods of declining NDVI (Figure 3.6.3). Despite small gains in vegetation greenness,  $NIR_v$  gradually declined by 12% during the same period. Chesapeake's and Middle Peninsula's vegetation greenness steadily increased after restoration (Figures 3.6.4 & 3.6.10). However,  $NIR_v$  did not follow the same trend and showed periods of decline for a few years before increasing and approaching a maintenance level. This indicates that vegetation greenness does not fully capture trends in wetland photosynthesis. Although most of these banks eventually established robust vegetation functions, the non-linear trends in reaching a maintenance state suggest there may be a time lag compensating for wetland impacts at permitted activity sites.

Creeds was the only mitigation bank with consistent negative long-term trends in NDVI and  $NIR_v$ , which declined by 2% and 10% in the past 22 years (Figure 3.6.6). Creeds was the most coastal mitigation bank in this study and was only one kilometer from the coastline; the negative trends seen at Creeds are likely due to chronic sea level rise and saltwater intrusion (Campbell et al., 2022; Chen & Kirwan, 2022; Saintilan et al., 2023). Across all banks, most of the observed downward trends were minor and did not indicate a significant net loss of wetland vegetation function. However, slight declines may signal that climate change is exerting low-level stress on the wetlands that, over time, may contribute to a net loss of wetland function.

Though the Clean Water Act aims to achieve no net loss of wetlands, considering the fate of mitigation banks in the Anthropocene is essential to determining if wetland function will be maintained. Although the observed trends in vegetation function suggest mitigation banking has achieved no net loss of wetland function, climate change may exert a tipping point that leads to declines in function in the near future. Warming temperatures and increased precipitation may have aided bank restoration and driven the increases in vegetation greenness in the more upland sites (Chen & Kirwan, 2022). Increased vegetation stress from rising sea levels and saltwater intrusion will likely increase. It may lead to a tipping point or gradual decline in vegetation function, as seen at Creeds in this study (Barnard et al., 2021; Herbert et al., 2015; Wang et al., 2023).

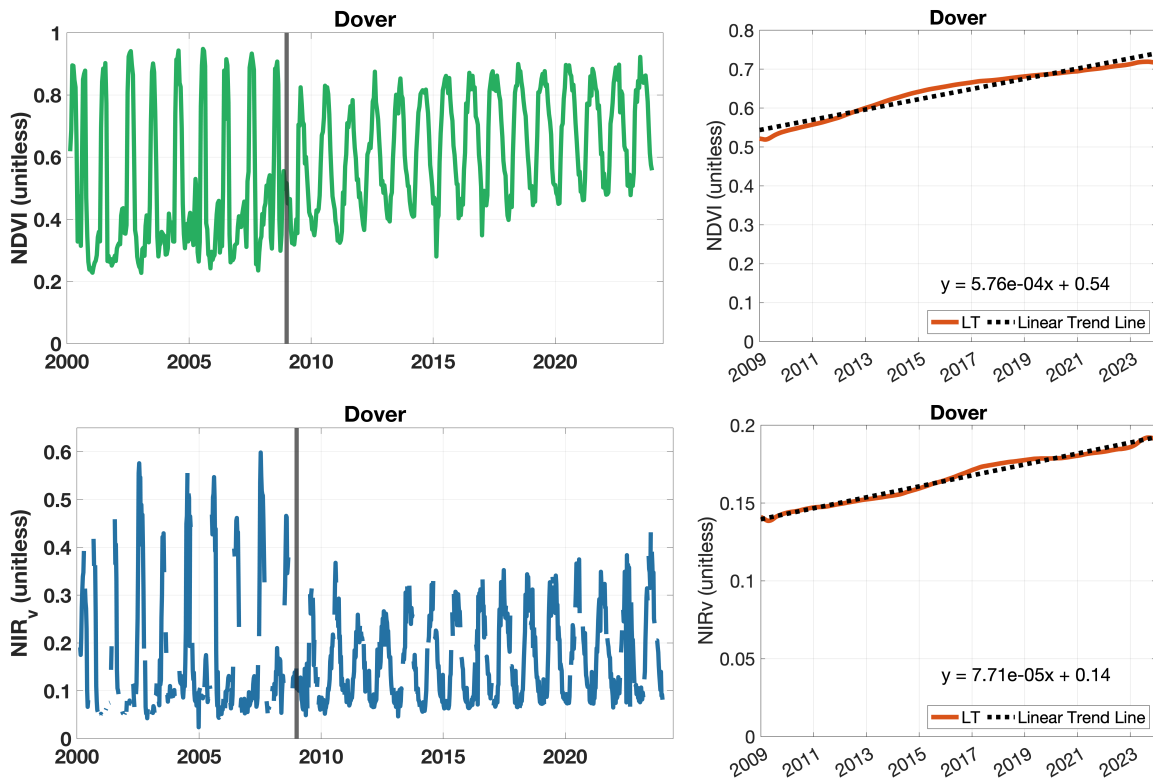


**Figure 3.6.1** Time series (left) and the long-term trends (LT, right) of NDVI (top) and NIR<sub>v</sub> (bottom) at the Dover Mitigation Bank. Note the time series plot data before and after the restoration and the long-term trend plots are only from data after the restoration. The vertical line on the time series marks the year of the bank’s restoration.

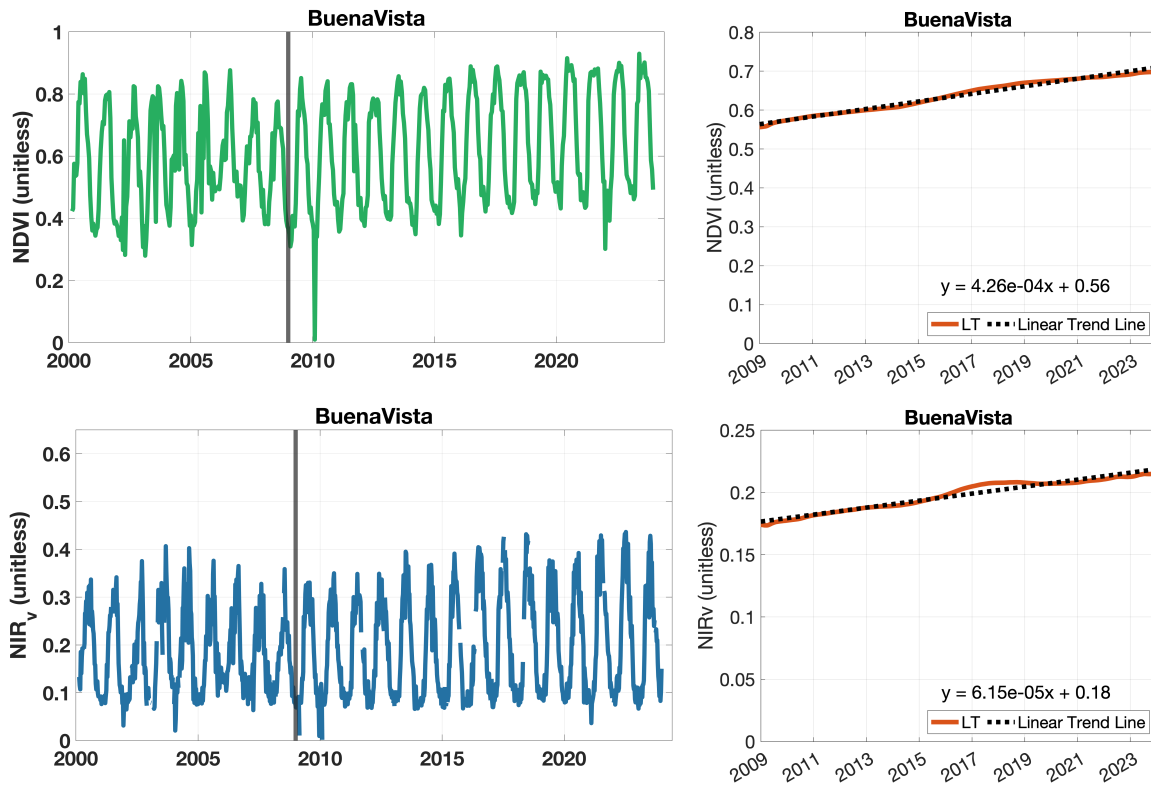


**Figure 3.6.2** Time series (left) and the long-term trends (LT, right) of NDVI (top) and NIR<sub>v</sub> (bottom) at the Buena Vista Mitigation Bank. Note the time series plot data before and after the restoration and the long-term trend plots are only from data after the restoration. The vertical line on the time series marks the year of the bank’s restoration.

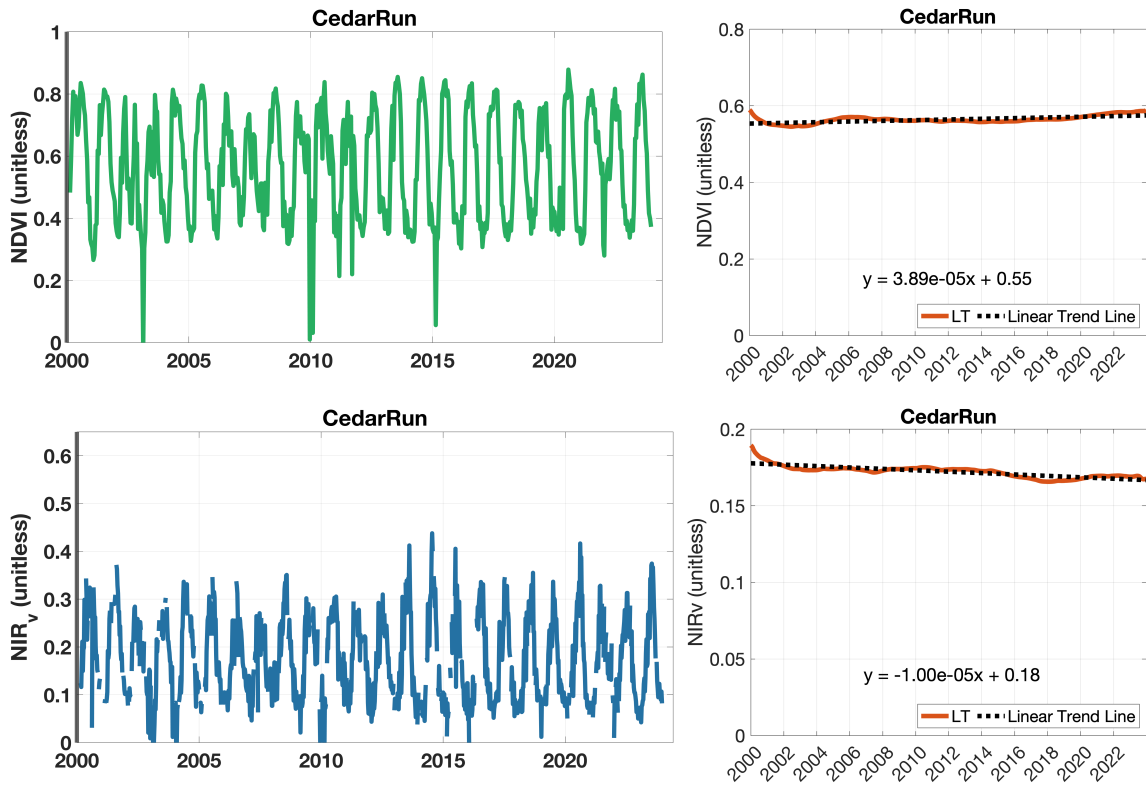


**Figure 3.6.3** Time series (left) and the long-term trends (LT, right) of NDVI (top) and NIR<sub>v</sub> (bottom) at the Cedar Run Mitigation Bank. The vertical line on the time series marks the year of the bank’s restoration.

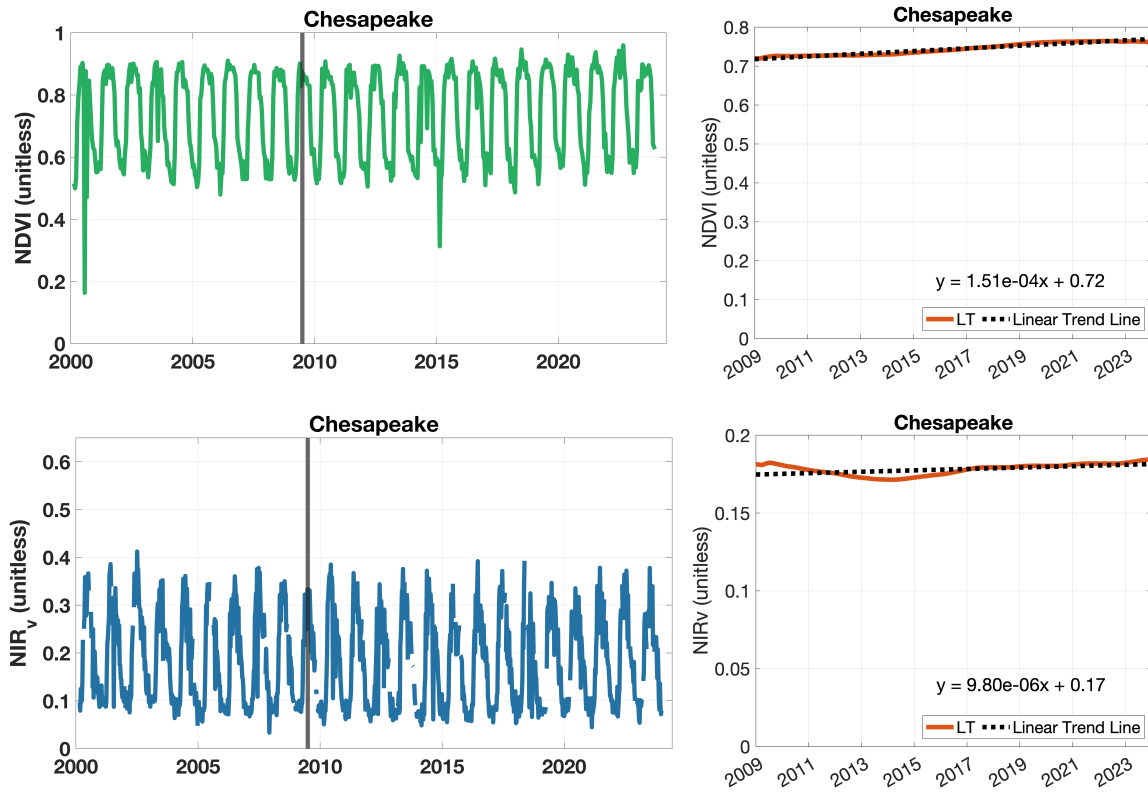


**Figure 3.6.4** Time series (left) and the long-term trends (LT, right) of NDVI (top) and NIR<sub>v</sub> (bottom) at the Chesapeake Mitigation Bank. Note the time series plot data before and after the restoration and the long-term trend plots are only from data after the restoration. The vertical line on the time series marks the year of the bank's restoration.

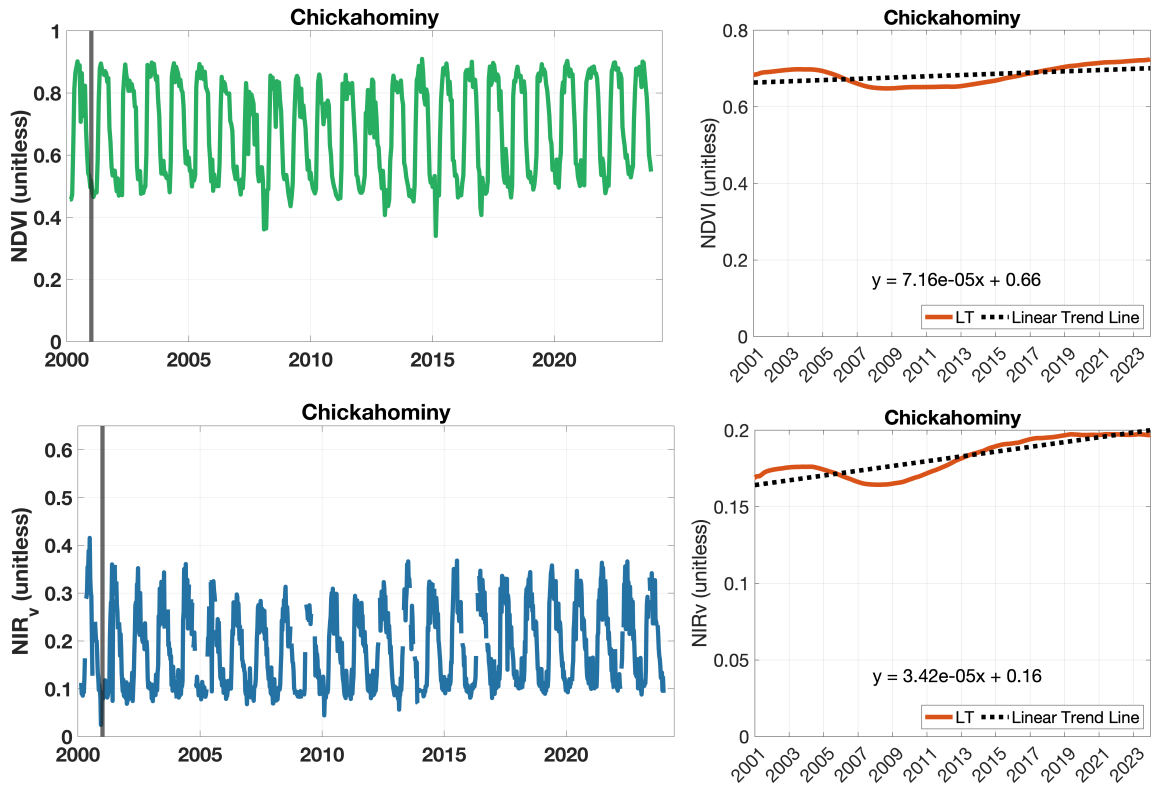


**Figure 3.6.5** Time series (left) and the long-term trends (LT, right) of NDVI (top) and NIR<sub>v</sub> (bottom) at the Chickahominy Mitigation Bank. Note the time series plot data before and after the restoration and the long-term trend plots are only from data after the restoration. The vertical line on the time series marks the year of the bank’s restoration.

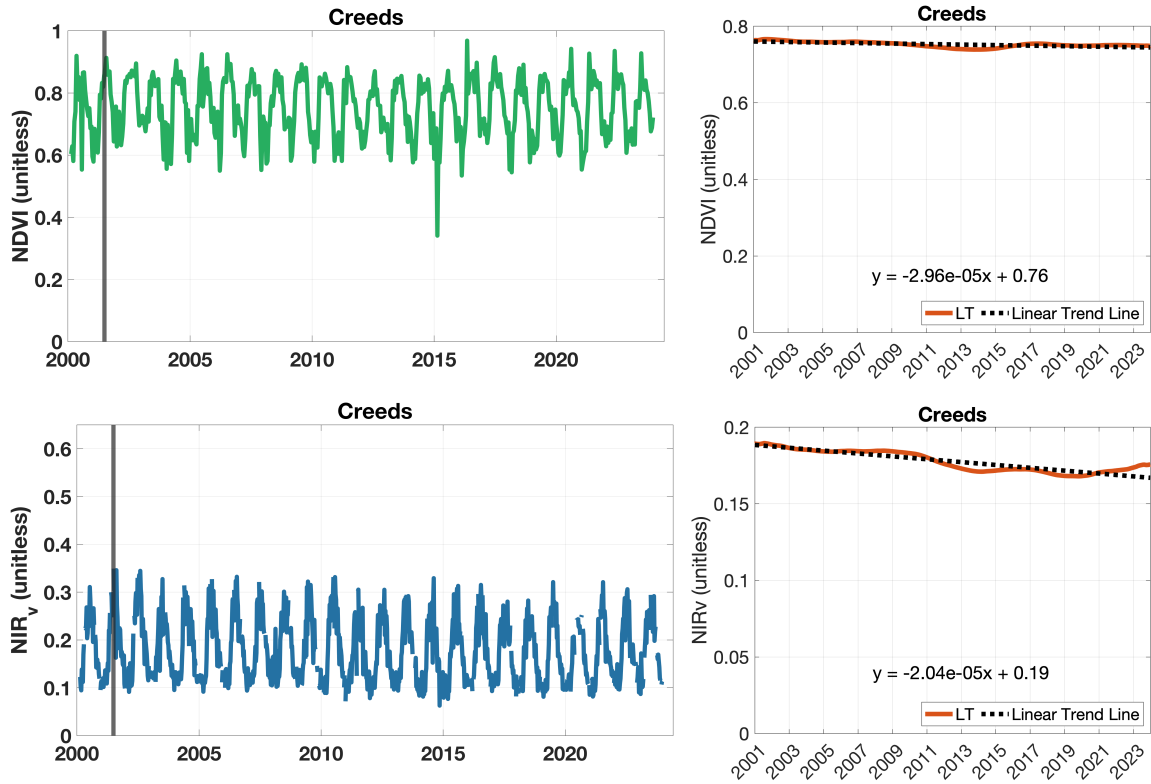


**Figure 3.6.6** Time series (left) and the long-term trends (LT, right) of NDVI (top) and NIR<sub>v</sub> (bottom) at the Creeds Mitigation Bank. Note the time series plot data before and after the restoration and the long-term trend plots are only from data after the restoration. The vertical line on the time series marks the year of the bank’s restoration.

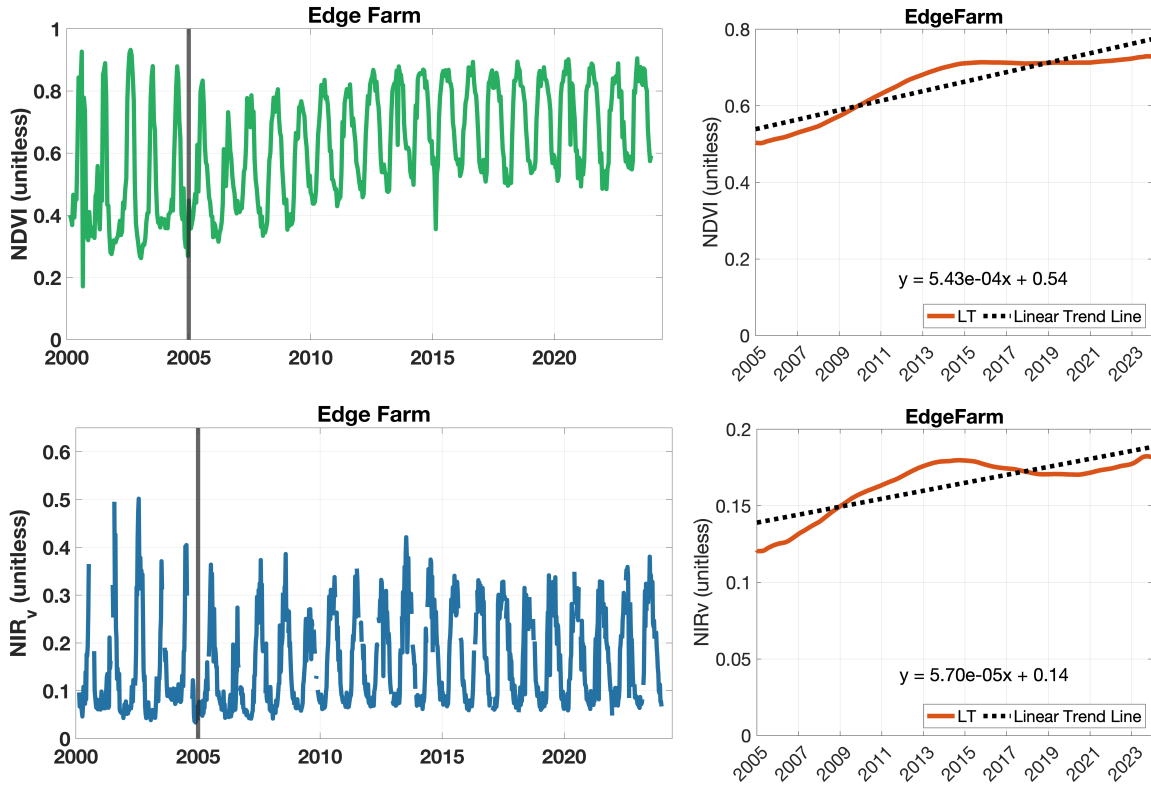


**Figure 3.6.7** Time series (left) and the long-term trends (LT, right) of NDVI (top) and NIR<sub>v</sub> (bottom) at the Edge Farm Mitigation Bank. Note the time series plot data before and after the restoration and the long-term trend plots are only from data after the restoration. The vertical line on the time series marks the year of the bank’s restoration.

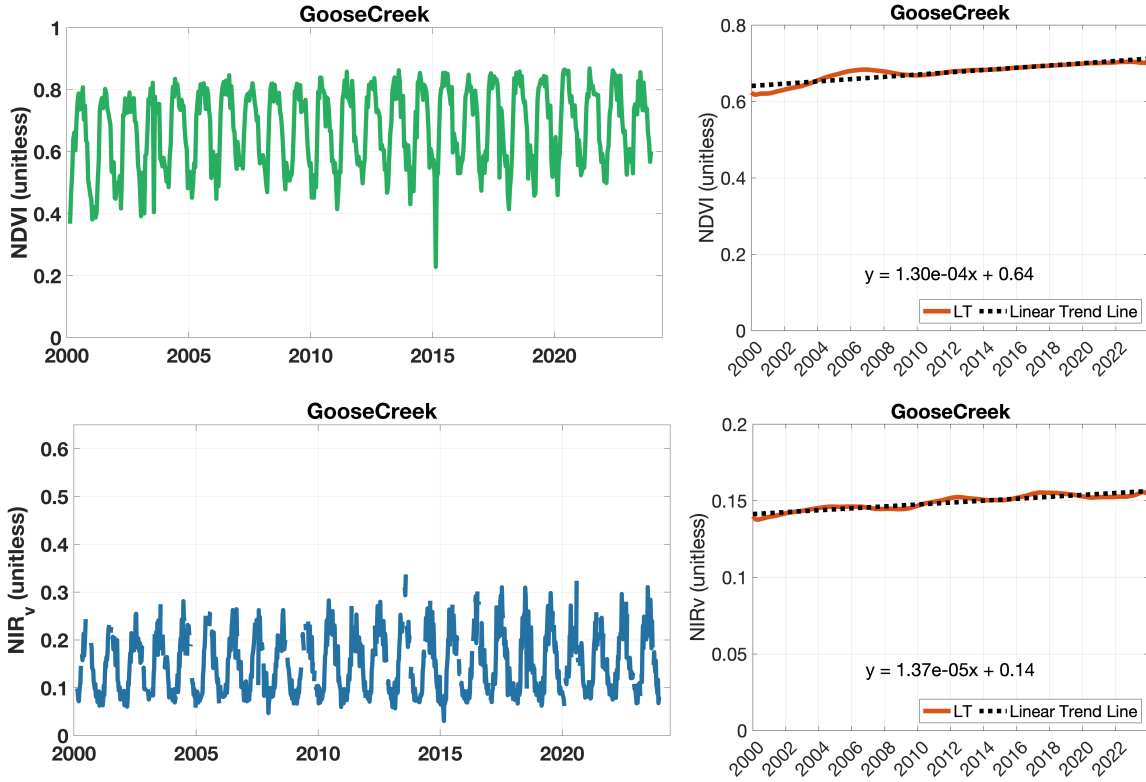


**Figure 3.6.8** Time series (left) and the long-term trends (LT, right) of NDVI (top) and NIR<sub>v</sub> (bottom) at the Goose Creek Mitigation Bank. This bank was established in 1982, before the Terra satellite was launched. The long-term trend analysis begins in 2000 when MODIS data is first available.

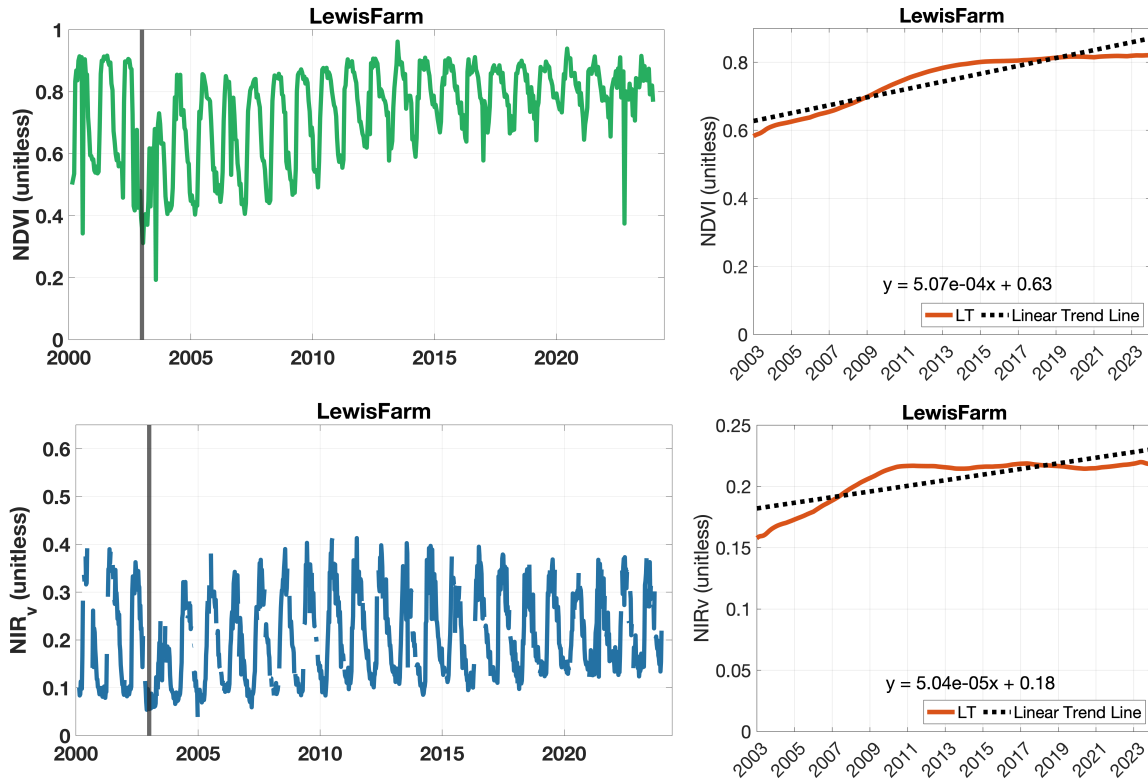


**Figure 3.6.9** Time series (left) and the long-term trends (LT, right) of NDVI (top) and NIR<sub>v</sub> (bottom) at the Lewis Farm Mitigation Bank. Note the time series plot data before and after the restoration and the long-term trend plots are only from data after the restoration. The vertical line on the time series marks the year of the bank’s restoration.

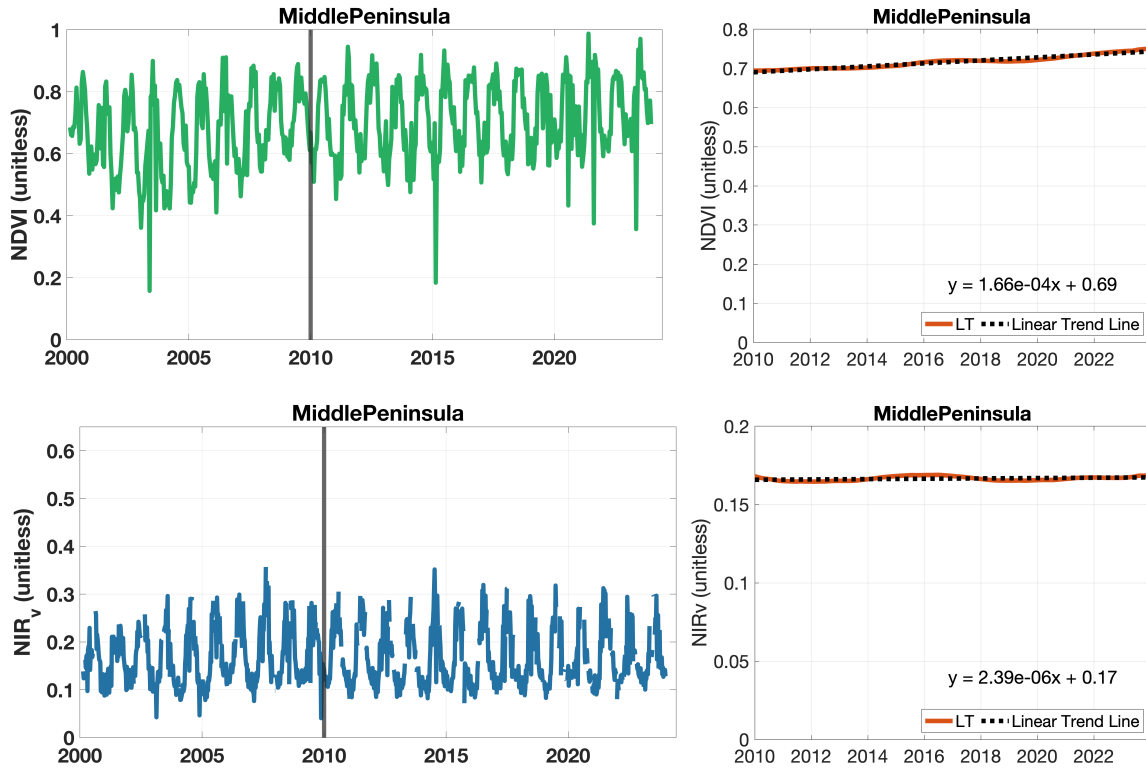


**Figure 3.6.10** Time series (left) and the long-term trends (LT, right) of NDVI (top) and NIR<sub>v</sub> (bottom) at the Middle Peninsula Mitigation Bank. Note the time series plot data before and after the restoration and the long-term trend plots are only from data after the restoration. The vertical line on the time series marks the year of the bank’s restoration.

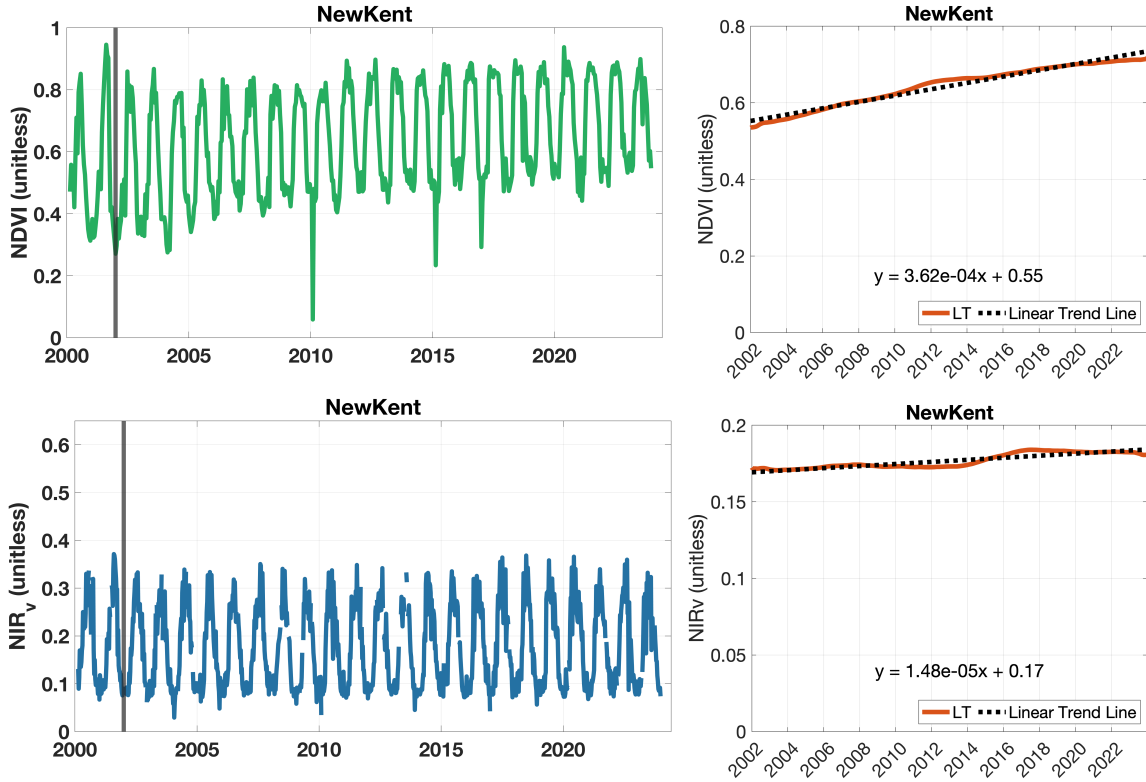


**Figure 3.6.11** Time series (left) and the long-term trends (LT, right) of NDVI (top) and NIR<sub>v</sub> (bottom) at the New Kent Mitigation Bank. Note the time series plot data before and after the restoration and the long-term trend plots are only from data after the restoration. The vertical line on the time series marks the year of the bank’s restoration.

### **3.4 Chapter Conclusions**

This chapter aimed to determine how well mitigation banking has conserved wetland acreage and function in Virginia. Over the past 30 years of wetland impact permitting, I found mitigation banking has led to a ~15,000-acre net increase in Virginia wetlands. However, the wetland mitigation bank production rate has decreased in the past decade, and it is unclear if the supply of compensation credits can meet demand. The net gain of wetlands was concentrated in a few areas of the state where many mitigation banks are located, but no HUC8 region lost a significant amount of wetland. Long-term trends in vegetation greenness and photosynthesis suggest most mitigation banks have maintained vegetation function for up to 25 years after restoration. Given the large surplus in wetland areas produced by mitigation banking compared to the area of permitted wetland impacts, I conclude that wetland function has been conserved, if not increased, across the state. However, some banks struggled to establish wetland vegetation function on shorter time scales, which may lead to a lag in compensating for wetland impacts. Further, saltwater intrusion and sea level rise may lead to a decline in vegetation function at banks near the coast. Ultimately, I conclude that mitigation banking has achieved no net loss of wetland area and function in Virginia. However, establishing more mitigation banks in uplands is essential to conserving wetland functions in the long term.

## Conclusions and Future Work

Salt marshes play an outsized role in the global carbon cycle, but many individual carbon fluxes are highly uncertain (US Global Change Research Program, 2018). Constraining the salt marsh photosynthetic CO<sub>2</sub> flux and its sensitivity to climate change is essential to improving climate models and implementing successful nature-based solutions (Griscom et al., 2017). Further, photosynthesis is a foundational ecosystem function that underlies many wetland ecosystem services. Improved remote sensing of wetland photosynthesis can be used to evaluate wetland restoration strategies and more effectively implement environmental policy. Although remote sensing of vegetation is an extensive scientific field, wetlands are relatively understudied compared to other ecosystem types, and more wetland-specific studies are needed (Ingalls et al., 2024). This dissertation addresses these challenges by (1) building a comprehensive dataset of salt marsh CO<sub>2</sub> fluxes, (2) describing a previously unreported response of salt marsh vegetation to environmental stress, and (3) evaluating remote sensing approaches to monitor wetland vegetation function for scientific and management applications.

In Chapter 1, I identified midday depression of photosynthesis as a mechanism by which salt marsh vegetation responds to salinity and water stress that can build up during periods of low tides and warmer temperatures. This novel finding is a significant contribution to understanding the climate sensitivity of the salt marsh carbon sink. Because midday depression is uncommon in C<sub>4</sub> vegetation, the ubiquitous nature of the depression is particularly surprising and suggests there is still much to learn about the photosynthetic pathway of *Spartina alterniflora*. Future work should investigate the mechanism of midday depression further with leaf-level measurements. This can determine if the midday depression is primarily driven by stomatal closure, biochemical decreases in photosynthesis, increased photorespiration, or another unknown mechanism. Additionally, understanding the mechanism behind salt marsh midday depression may clarify why remote sensing proxies and GPP flux observations diverged in Chapter 2 and suggest ways to improve remote sensing monitoring approaches.

In Chapter 2, I found NIR<sub>v,Rad</sub> and NIR<sub>v,P</sub> to be strong ground-based proxies for salt marsh GPP. This finding addresses two challenges specific to remote sensing of salt marshes. First, salt marshes occupy a heterogeneous landscape plagued by the mixed

pixel problem, making it challenging to attribute satellite observations to vegetation, water, mudflats, or other land types.  $NIR_v$  is particularly appealing for satellite-based remote sensing of salt marshes because its NDVI term isolates the fraction of signal arising from vegetation and can help address the mixed pixel problem of heterogeneous coastal landscapes (Badgley et al., 2017). Second, combined with previous work in other ecosystems with sparse vegetation, the success of ground-based  $NIR_v$  at tracking salt marsh GPP suggests the NDVI term minimizes the effects of soil background and legacy dead vegetation that often hinder vegetation remote sensing observations (Baldocchi et al., 2020). Overcoming these challenges with ground-based observations suggests  $NIR_v$  is a strong candidate to track salt marsh GPP with satellite observations. Future work should use tower-based GPP to validate satellite-based  $NIR_v$  from sensors with various spatial and spectral resolutions. More ground-based observations of  $NIR_v$  in salt marshes of different elevations and latitudes are also needed to further understand and constrain the  $NIR_v$ -GPP relationship. Future work should also examine if more recently developed  $NIR_v$  indices incorporating shortwave infrared reflectance can further reduce the effects of soil background and better track salt marsh GPP (Ranjbar et al., 2024).

Although SIF poorly tracked GPP in this study, future studies should aim to improve SIF retrieval and data processing approaches to generate higher quality SIF data and reexamine the potential of SIF to track salt marsh GPP. SIF has a higher signal-to-noise requirement than  $NIR_v$  because SIF is a small percentage of the total observed surface reflectance, which limited my collection of high-quality SIF data. In theory, SIF is more directly linked to photochemistry than  $NIR_v$ . Thus, SIF may be a better tool to understand the mechanism of midday depression of photosynthesis in *Spartina alterniflora* if the impact of soil background and humidity on signal noise can be better accounted for in its retrieval.

In Chapter 3, I analyzed 30 years of wetland permit data and used  $NIR_v$  and NDVI to monitor vegetation function in wetland mitigation banks for up to 25 years after restoration. I concluded that mitigation banking has achieved no net loss of wetland area and function in Virginia; however, climate change may lead to the degradation of banks in the coming decades. I also observed clear wetland shifts from urban to rural areas, which could have environmental justice implications and alter who benefits from wetland ecosystem services. Future work should investigate this question by integrating finer-

scale permit data (most of my dataset did not include impact site latitude and longitude) and U.S. census data. Incorporating watershed and flood modeling under different wetland location scenarios could also reveal how mitigation banking may alter flooding patterns and help decision-makers ensure that mitigation banking does not increase flooding and other environmental hazards.

My Chapter 3 results highlight the success of academic-stakeholder collaborations extending beyond academia. My initial research questions for this chapter were scientifically interesting but focused too heavily on examining no net loss of wetland on an impact-by-impact basis. Working closely with my collaborator, Dave Davis, who oversees state-level regulations of wetland mitigation banking in Virginia, we identified research questions that would generate results that would be more useful to the needs of stakeholders in his field. In my case, that meant focusing on the trajectory of mitigation banks after passing their performance criteria and examining whether climate change impacts vegetation function. Thus, engaging with stakeholders during a project conceptualization phase and keeping them involved throughout the project is crucial.

# Appendix

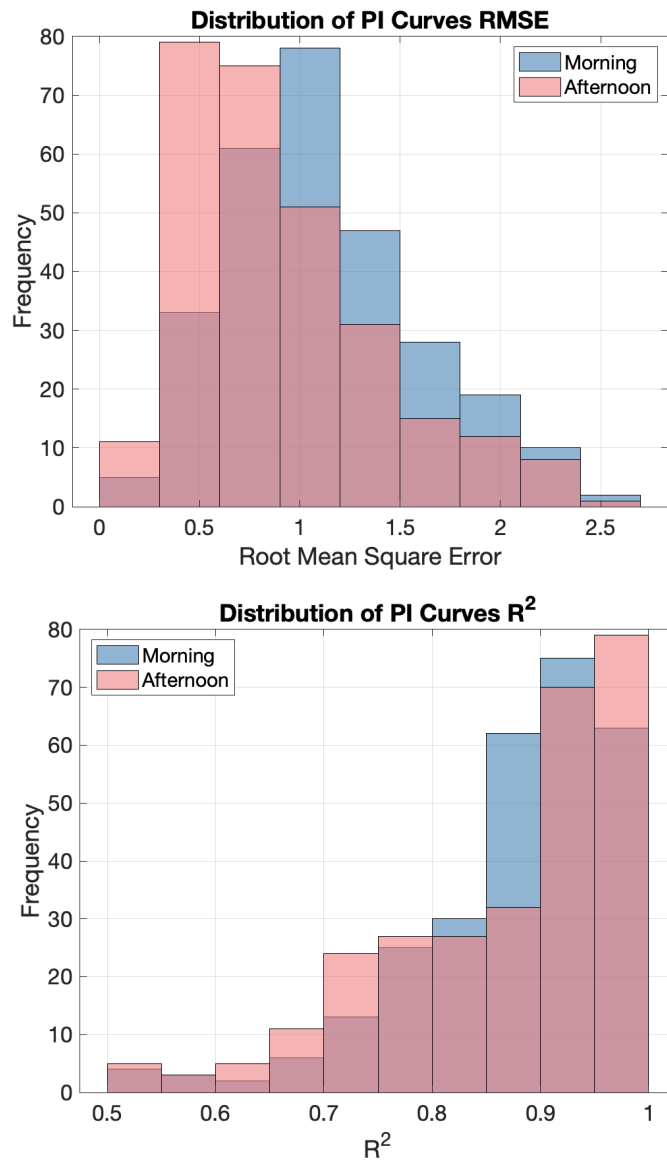


**Figure A1.** Distributions of the root mean square error (RMSE) and R<sup>2</sup> correlation coefficient of morning and afternoon photosynthesis-irradiance curves used in the Chapter 1 data analysis.

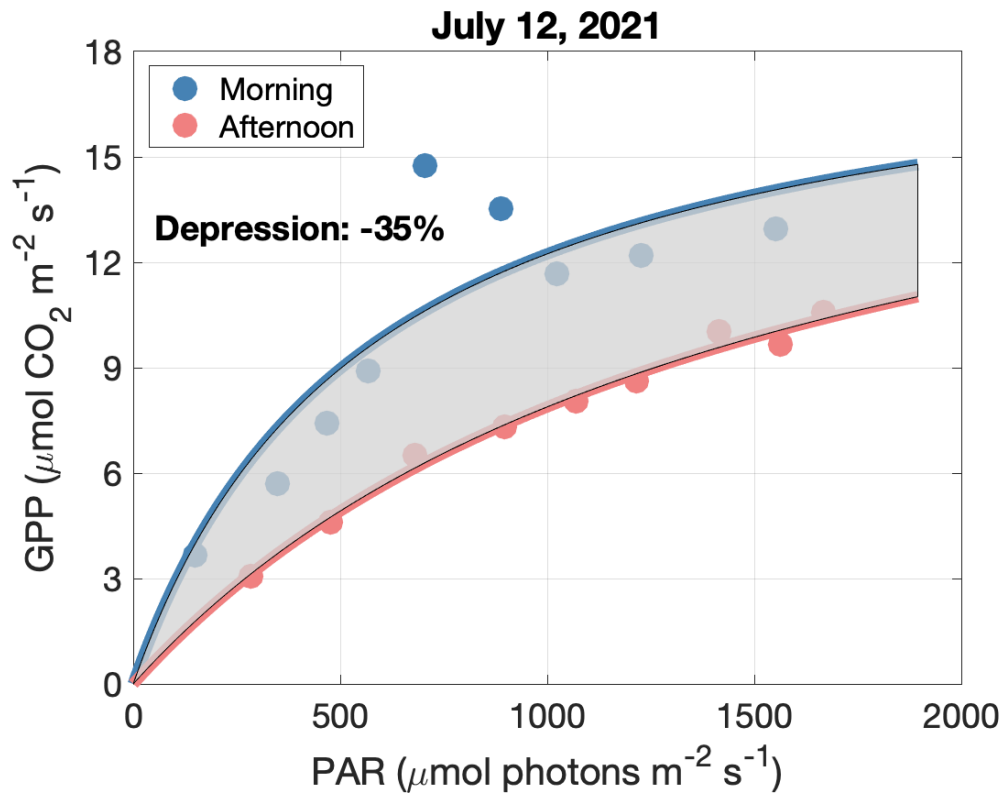


**Figure A2.** Example daily photosynthesis-irradiance curve fitting for July 12, 2021.

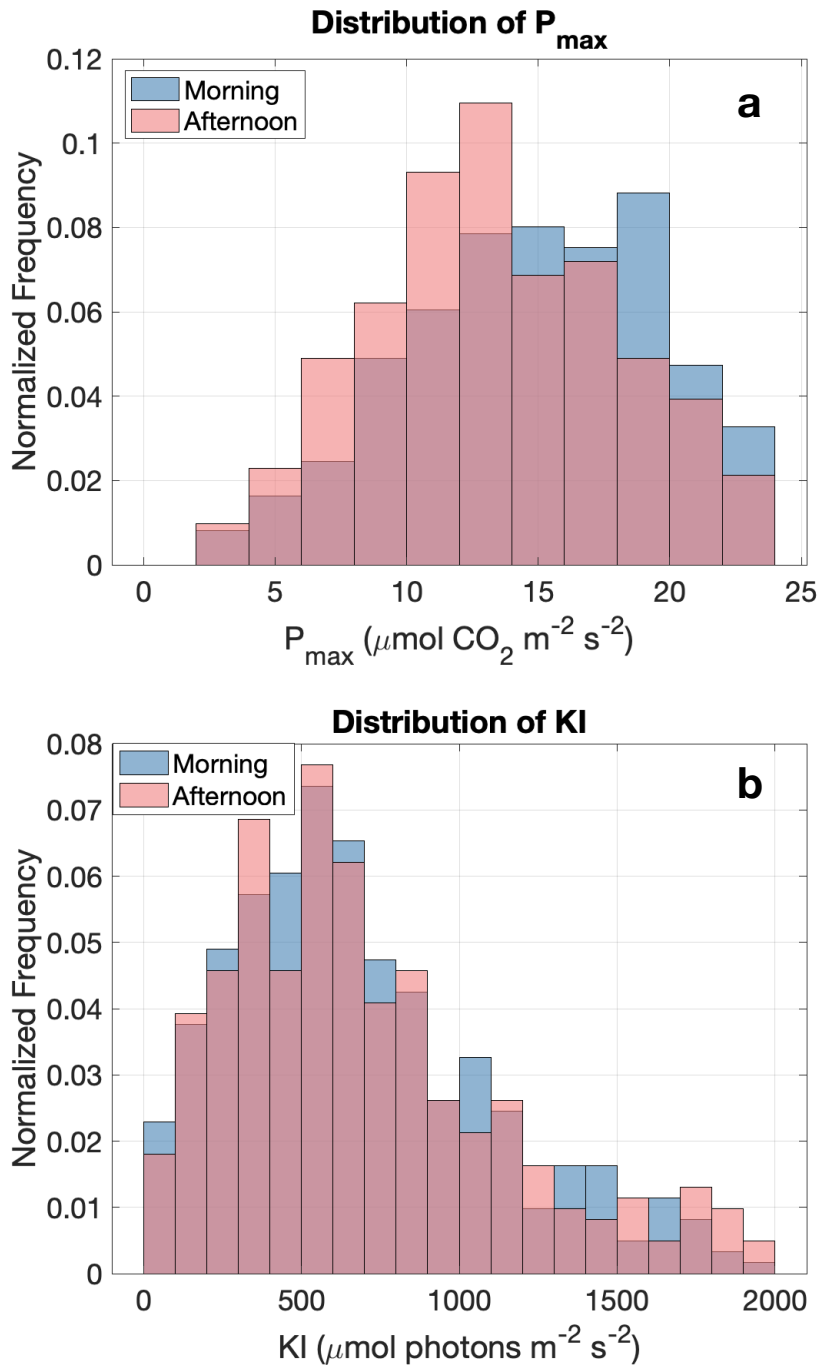


**Figure A3.** Distributions of (a)  $P_{\max}$  and (b) KI coefficients from daily scale morning (blue) and afternoon (red) photosynthesis-irradiance curve fittings.

## References

- 33 USC §1251 et seq. (1972). *The Clean Water Act*.
- 33 USC §1344. (1972). *The Clean Water Act Section 404*.
- Alber, M., Swenson, E. M., Adamowicz, S. C., & Mendelssohn, I. A. (2008). Salt Marsh Dieback: An overview of recent events in the US. *Estuarine, Coastal and Shelf Science*, 80(1), 1–11.
- Alongi, D. M. (2014). Carbon cycling and storage in mangrove forests. *Annual Review of Marine Science*, 6, 195–219.
- Badgley, G., Anderegg, L. D. L., Berry, J. A., & Field, C. B. (2019). Terrestrial gross primary production: Using NIRV to scale from site to globe. *Global Change Biology*, 25(11), 3731–3740.
- Badgley, G., Field, C. B., & Berry, J. A. (2017). Canopy near-infrared reflectance and terrestrial photosynthesis. *Science Advances*, 3(3), e1602244.
- Baker, N. R. (2008). Chlorophyll fluorescence: a probe of photosynthesis in vivo. *Annual Review of Plant Biology*, 59, 89–113.
- Baldocchi, D. D., Hincks, B. B., & Meyers, T. P. (1988). Measuring biosphere-atmosphere exchanges of biologically related gases with micrometeorological methods. *Ecology*, 69(5), 1331–1340.
- Baldocchi, D. D., Ryu, Y., Dechant, B., Eichelmann, E., Hemes, K., Ma, S., Rey Sanchez, C., Shortt, R., Szutu, D., Valach, A., Verfaillie, J., Badgley, G., Zeng, Y., & Berry, J. A. (2020). Outgoing Near Infrared Radiation from Vegetation Scales with Canopy Photosynthesis Across a Spectrum of Function, Structure, Physiological Capacity and Weather. *Journal of Geophysical Research: Biogeosciences*.  
<https://doi.org/10.1029/2019JG005534>
- Barbier, E. B. (2012). Progress and Challenges in Valuing Coastal and Marine Ecosystem Services. *Review of Environmental Economics and Policy*, 6(1), 1–19.
- Barbier, E. B., Koch, E. W., Silliman, B. R., Hacker, S. D., Wolanski, 4. Eric, Primavera, J., Granek, E. F., Polasky, S., Aswani, S., Cramer, 9. Lori A., Stoms, 10 David M., Kennedy, 11 Chris J., Bael, D., Kappel, C. V., & Reed, 13 Denise J. (2008). Coastal Ecosystem–Based Management with Nonlinear Ecological Functions and Values. *Science*, 319. <https://science.sciencemag.org/content/sci/319/5861/321.full.pdf>
- Barnard, P. L., Dugan, J. E., Page, H. M., Wood, N. J., Hart, J. A. F., Cayan, D. R., Erikson, L. H., Hubbard, D. M., Myers, M. R., Melack, J. M., & Iacobellis, S. F. (2021). Multiple climate change-driven tipping points for coastal systems. *Scientific Reports*, 11(1), 15560.
- Bauer, K., & Campbell, B. (2022). *Wetlands in our backyard: A review of wetland types in Virginia State Parks*. <https://doi.org/10.25778/WEW4-QA95>
- BenDor, T., Brozović, N., & Pallathucheril, V. G. (2007). Assessing the Socioeconomic Impacts of Wetland Mitigation in the Chicago Region. *Journal of the American Planning Association*. *American Planning Association*, 73(3), 263–282.
- BenDor, T., & Stewart, A. (2011). Land use planning and social equity in North Carolina’s compensatory wetland and stream mitigation programs. *Environmental Management*, 47(2), 239–253.

- Betzen, B. M., Smart, C. M., Maricle, K. L., & Maricle, B. R. (2019). Effects of increasing salinity on photosynthesis and plant water potential in Kansas salt marsh species. *Transactions of the Kansas Academy of Science*, 122(1–2), 49–58.
- Biçe, K., Schalles, J., Sheldon, J. E., Alber, M., & Meile, C. (2023). Temporal patterns and causal drivers of aboveground plant biomass in a coastal wetland: Insights from time-series analyses. *Frontiers in Marine Science*, 10, 1130958.
- Boretti, A., & Florentine, S. (2019). Atmospheric CO<sub>2</sub> concentration and other limiting factors in the growth of C<sub>3</sub> and C<sub>4</sub> plants. *Plants*, 8(4), 92.
- Bräutigam, A., & Gowik, U. (2016). Photorespiration connects C<sub>3</sub> and C<sub>4</sub> photosynthesis. *Journal of Experimental Botany*, 67(10), 2953–2962.
- Brody, S. D., Kim, H., & Gunn, J. (2013). Examining the Impacts of Development Patterns on Flooding on the Gulf of Mexico Coast. *Urban Studies*, 50(4), 789–806.
- Brody, S. D., Zahran, S., Maghelal, P., Grover, H., & Highfield, W. E. (2007). The Rising Costs of Floods: Examining the Impact of Planning and Development Decisions on Property Damage in Florida. *Journal of the American Planning Association*. *American Planning Association*, 73(3), 330–345.
- Burgos, A. G., Hamlington, B. D., Thompson, P. R., & Ray, R. D. (2018). Future nuisance flooding in Norfolk, VA, from astronomical tides and annual to decadal internal climate variability. *Geophysical Research Letters*, 45(22), 12,432–12,439.
- Campbell, A. D., Fatoyinbo, L., Goldberg, L., & Lagomasino, D. (2022). Global hotspots of salt marsh change and carbon emissions. *Nature*, 1–6.
- Campbell, A. D., Fatoyinbo, T., Charles, S. P., Bourgeau-Chavez, L. L., Goes, J., Gomes, H., Halabisky, M., Holmquist, J., Lohrenz, S., Mitchell, C., Monika Moskal, L., Poulter, B., Qiu, H., De Sousa, C. H. R., Sayers, M., Simard, M., Stewart, A. J., Singh, D., Trettin, C., ... Lagomasino, D. (2022). A review of carbon monitoring in wet carbon systems using remote sensing. *Environmental Research Letters: ERL*, 17(2), 025009.
- Cavender-Bares, J., & A. Bazzaz, F. (2004). From Leaves to Ecosystems: Using Chlorophyll Fluorescence to Assess Photosynthesis and Plant function in Ecological Studies. In G. C. Papageorgiou & Govindjee (Eds.), *Chlorophyll a Fluorescence: A Signature of Photosynthesis* (pp. 737–755). Springer Netherlands.
- Charles, H., & Dukes, J. S. (2009). Effects of warming and altered precipitation on plant and nutrient dynamics of a New England salt marsh. *Ecological Applications: A Publication of the Ecological Society of America*, 19(7), 1758–1773.
- Chen, Siru, Zhao, W., Zhang, R., Sun, X., Zhou, Y., & Liu, L. (2023). Higher sensitivity of NIRv,Rad in detecting net primary productivity of C<sub>4</sub> than that of C<sub>3</sub>: Evidence from ground measurements of wheat and maize. *Remote Sensing*, 15(4), 1133.
- Chen, Siyuan, Sui, L., Liu, L., Liu, X., Li, J., Huang, L., Li, X., & Qian, X. (2023). NIRP as a remote sensing proxy for measuring gross primary production across different biomes and climate zones: Performance and limitations. *International Journal of Applied Earth Observation and Geoinformation: ITC Journal*, 122(103437), 103437.
- Chen, Y., & Kirwan, M. L. (2022). Climate-driven decoupling of wetland and upland biomass trends on the mid-Atlantic coast. *Nature Geoscience*, 15(11), 913–918.

- Chmura, G. L., Anisfeld, S. C., Cahoon, D. R., & Lynch, J. C. (2003). Global carbon sequestration in tidal, saline wetland soils. *Global Biogeochemical Cycles*, 17(4). <https://doi.org/10.1029/2002gb001917>
- Coops, H., Geilen, N., Verheij, H. J., Boeters, R., & van der Velde, G. (1996). Interactions between waves, bank erosion and emergent vegetation: an experimental study in a wave tank. *Aquatic Botany*, 53(3), 187–198.
- Costanza, R., Anderson, S. J., Sutton, P., Mulder, K., Mulder, O., Kubiszewski, I., Wang, X., Liu, X., Pérez-Maqueo, O., Luisa Martinez, M., Jarvis, D., & Dee, G. (2021). The global value of coastal wetlands for storm protection. *Global Environmental Change: Human and Policy Dimensions*, 70, 102328.
- Dahl, T. E. (1990). *Wetlands Losses in the United States, 1780's to 1980's*. U.S. Department of the Interior, Fish and Wildlife Service.
- De Leeuw, J., Olf, H., & Bakker, J. P. (1990). Year-to-year variation in salt marsh production as related to inundation and rainfall deficit. *Aquatic Botany*.
- Dechant, B., Ryu, Y., Badgley, G., Köhler, P., Rascher, U., Migliavacca, M., Zhang, Y., Tagliabue, G., Guan, K., Rossini, M., Goulas, Y., Zeng, Y., Frankenberg, C., & Berry, J. A. (2022). NIRVP: A robust structural proxy for sun-induced chlorophyll fluorescence and photosynthesis across scales. *Remote Sensing of Environment*, 268(112763), 112763.
- Dechant, B., Ryu, Y., Badgley, G., Zeng, Y., Berry, J. A., Zhang, Y., Goulas, Y., Li, Z., Zhang, Q., Kang, M., Li, J., & Moya, I. (2020). Canopy structure explains the relationship between photosynthesis and sun-induced chlorophyll fluorescence in crops. *Remote Sensing of Environment*, 241, 111733.
- DeLaune, R. D., & Pezeshki, S. R. (1994). The influence of subsidence and saltwater intrusion on coastal marsh stability: Louisiana Gulf Coast, U.S.A. *Journal of Coastal Research*, 77–89.
- Dernoga, M. A., Wilson, S., Jiang, C., & Tutman, F. (2015). Environmental justice disparities in Maryland's watershed restoration programs. *Environmental Science & Policy*, 45, 67–78.
- Duarte, C. M. (2017). Reviews and syntheses: Hidden forests, the role of vegetated coastal habitats in the ocean carbon budget. *Biogeosciences*, 14(2), 301–310.
- Duarte, C. M., Losada, I. J., Hendriks, I. E., Mazarrasa, I., & Marbà, N. (2013). The role of coastal plant communities for climate change mitigation and adaptation. *Nature Climate Change*, 3(11), 961–968.
- Dunton, K. H., Hardegree, B., & Whitledge, T. E. (2001). Response of estuarine marsh vegetation to interannual variations in precipitation. *Estuaries*, 24(6), 851.
- Dusenge, M. E., Duarte, A. G., & Way, D. A. (2019). Plant carbon metabolism and climate change: elevated CO<sub>2</sub> and temperature impacts on photosynthesis, photorespiration and respiration. *The New Phytologist*, 221(1), 32–49.
- Feagin, R. A., Forbrich, I., Huff, T. P., Barr, J. G., Ruiz-Plancarte, J., Fuentes, J. D., Najjar, R. G., Vargas, R., Vázquez-Lule, A., Windham-Myers, L., Kroeger, K. D., Ward, E. J., Moore, G. W., Leclerc, M., Krauss, K. W., Stagg, C. L., Alber, M., Knox, S. H., Schäfer, K. V. R., ... Miao, G. (2020). Tidal wetland gross primary production across the continental United States, 2000–2019. *Global Biogeochemical Cycles*, 34(2). <https://doi.org/10.1029/2019gb006349>
- Fluet-Chouinard, E., Stocker, B. D., Zhang, Z., Malhotra, A., Melton, J. R., Poulter, B., Kaplan, J. O., Goldewijk, K. K., Siebert, S., Minayeva, T., Hugelius, G., Joosten,

- H., Barthelmes, A., Prigent, C., Aires, F., Hoyt, A. M., Davidson, N., Finlayson, C. M., Lehner, B., ... McIntyre, P. B. (2023). Extensive global wetland loss over the past three centuries. *Nature*, *614*(7947), 281–286.
- Foken, T., Göockede, M., Mauder, M., Mahrt, L., Amiro, B., & Munger, W. (2005). Post-Field Data Quality Control. In X. Lee, W. Massman, & B. Law (Eds.), *Handbook of Micrometeorology: A Guide for Surface Flux Measurement and Analysis* (pp. 181–208). Springer Netherlands.
- Forbrich, I., Giblin, A. E., & Hopkinson, C. S. (2018). Constraining marsh carbon budgets using long-term C burial and contemporary atmospheric CO<sub>2</sub> fluxes. *Journal of Geophysical Research. Biogeosciences*, *123*(3), 867–878.
- Forbrich, Inke, & Giblin, A. E. (2015). Marsh-atmosphere CO<sub>2</sub> exchange in a New England salt marsh. *Journal of Geophysical Research. Biogeosciences*, *120*(9), 1825–1838.
- Franco, A., & Lüttge, U. (2002). Midday depression in savanna trees: coordinated adjustments in photochemical efficiency, photorespiration, CO<sub>2</sub> assimilation and water use efficiency. *Oecologia*, *131*(3), 356–365.
- Frankenberg, C., & Berry, J. (2018). *Solar Induced Chlorophyll Fluorescence: Origins, Relation to Photosynthesis and Retrieval* (Vols. 1–9, pp. 143–162). Elsevier.
- Frankenberg, Christian, Fisher, J. B., Worden, J., Badgley, G., Saatchi, S. S., Lee, J.-E., Toon, G. C., Butz, A., Jung, M., Kuze, A., & Yokota, T. (2011). New global observations of the terrestrial carbon cycle from GOSAT: Patterns of plant fluorescence with gross primary productivity. *Geophysical Research Letters*, *38*(17). <https://doi.org/10.1029/2011glo48738>
- Friess, D. A., Yando, E. S., Alemu, J. B., Wong, L. W., Soto, S. D., & H., B. (2021). Ecosystem Services and Disservices of Mangrove Forests and Salt Marshes. In *Oceanography and Marine Biology*. CRC Press.
- Ge, Z.-M., Zhang, L.-Q., Yuan, L., & Zhang, C. (2014). Effects of salinity on temperature-dependent photosynthetic parameters of a native C<sub>3</sub> and a non-native C<sub>4</sub> marsh grass in the Yangtze Estuary, China. *Photosynthetica*, *52*(4), 484–492.
- Giurgevich, J. R., & Dunn, E. L. (1979). Seasonal patterns of CO<sub>2</sub> and water vapor exchange of the tall and short height forms of *Spartina alterniflora* Loisel in a Georgia salt marsh. *Oecologia*, *43*(2), 139–156.
- Goulden, M. L., Miller, S. D., da Rocha, H. R., Menton, M. C., de Freitas, H. C., e Silva Figueira, A. M., & de Sousa, C. A. D. (2004). DIEL AND SEASONAL PATTERNS OF TROPICAL FOREST CO<sub>2</sub> EXCHANGE. *Ecological Applications: A Publication of the Ecological Society of America*, *14*(sp4), 42–54.
- Gourevitch, J. D., Diehl, R. M., Wemple, B. C., & Ricketts, T. H. (2022). Inequities in the distribution of flood risk under floodplain restoration and climate change scenarios. *People and Nature (Hoboken, N.J.)*, *4*(2), 415–427.
- Griffin, R. K., & Dahl, T. E. (2016). Restoration Outcomes and Reporting: An Assessment of Wetland Area Gains in Wisconsin, USA. *Ecological Restoration*, *34*(3), 191–199.
- Griscom, B. W., Adams, J., Ellis, P. W., Houghton, R. A., Lomax, G., Miteva, D. A., Schlesinger, W. H., Shoch, D., Siikamäki, J. V., Smith, P., Woodbury, P., Zganjar, C., Blackman, A., Campari, J., Conant, R. T., Delgado, C., Elias, P., Gopalakrishna, T., Hamsik, M. R., ... Fargione, J. (2017). Natural climate

- solutions. *Proceedings of the National Academy of Sciences of the United States of America*, 114(44), 11645–11650.
- Grossiord, C., Buckley, T. N., Cernusak, L. A., Novick, K. A., Poulter, B., Siegwolf, R. T. W., Sperry, J. S., & McDowell, N. G. (2020). Plant responses to rising vapor pressure deficit. *The New Phytologist*, 226(6), 1550–1566.
- Gutrich, J. J., Taylor, K. J., & Fennessy, M. S. (2009). Restoration of vegetation communities of created depressional marshes in Ohio and Colorado (USA): The importance of initial effort for mitigation success. *Ecological Engineering*, 35(3), 351–368.
- Hardy, R. D., Milligan, R. A., & Heynen, N. (2017). Racial coastal formation: The environmental injustice of colorblind adaptation planning for sea-level rise. *Geoforum; Journal of Physical, Human, and Regional Geosciences*, 87, 62–72.
- Haverd, V., Smith, B., Canadell, J. G., Cuntz, M., Mikaloff-Fletcher, S., Farquhar, G., Woodgate, W., Briggs, P. R., & Trudinger, C. M. (2020). Higher than expected CO<sub>2</sub> fertilization inferred from leaf to global observations. *Global Change Biology*, 26(4), 2390–2402.
- Hawman, P. A., Cotten, D. L., & Mishra, D. R. (2024). Canopy heterogeneity and environmental variability drive annual budgets of net ecosystem carbon exchange in a tidal marsh. *Journal of Geophysical Research. Biogeosciences*, 129(4), e2023JG007866.
- Hawman, Peter A., Mishra, D. R., & O’Connell, J. L. (2023). Dynamic emergent leaf area in tidal wetlands: Implications for satellite-derived regional and global blue carbon estimates. *Remote Sensing of Environment*, 290(113553), 113553.
- He, L., Magney, T., Dutta, D., Yin, Y., Köhler, P., Grossmann, K., Stutz, J., Dold, C., Hatfield, J., Guan, K., Peng, B., & Frankenberg, C. (2020). From the ground to space: Using solar-induced chlorophyll fluorescence to estimate crop productivity. *Geophysical Research Letters*, 47(7), e2020GL087474.
- Herbert, E. R., Boon, P., Burgin, A. J., Neubauer, S. C., Franklin, R. B., Ardón, M., Hopfensperger, K. N., Lamers, L. P. M., & Gell, P. (2015). A global perspective on wetland salinization: ecological consequences of a growing threat to freshwater wetlands. *Ecosphere (Washington, D.C)*, 6(10), art206.
- Hessini, K., Jeddi, K., Siddique, K. H. M., & Cruz, C. (2021). Drought and salinity: A comparison of their effects on the ammonium-preferring species *Spartina alterniflora*. *Physiologia Plantarum*, 172(2), 431–440.
- Hill, A. C., Vázquez-Lule, A., & Vargas, R. (2021). Linking vegetation spectral reflectance with ecosystem carbon phenology in a temperate salt marsh. *Agricultural and Forest Meteorology*, 307, 108481.
- Holmquist, J. R., Windham-Myers, L., Bernal, B., Byrd, K. B., Crooks, S., Gonnee, M. E., Herold, N., Knox, S. H., Kroeger, K. D., McCombs, J., Megonigal, J. P., Lu, M., Morris, J. T., Sutton-Grier, A. E., Troxler, T. G., & Weller, D. E. (2018). Uncertainty in United States coastal wetland greenhouse gas inventorying. *Environmental Research Letters*, 13(11), 115005.
- Hopkinson, C. S., Cai, W.-J., & Hu, X. (2012). Carbon sequestration in wetland dominated coastal systems—a global sink of rapidly diminishing magnitude. *Current Opinion in Environmental Sustainability*, 4(2), 186–194.
- Hopple, A., & Craft, C. (2013). Managed disturbance enhances biodiversity of restored wetlands in the agricultural Midwest. *Ecological Engineering*, 61, 505–510.

- Hough, P., & Harrington, R. (2019). Ten years of the compensatory mitigation rule: reflections on progress and opportunities. *Envtl. L. Rep. News & Analysis*, 10018. [https://heinonline.org/hol-cgi-bin/get\\_pdf.cgi?handle=hein.journals/elrna49&section=7](https://heinonline.org/hol-cgi-bin/get_pdf.cgi?handle=hein.journals/elrna49&section=7)
- Howard, J., Hoyt, S., Isensee, K., Telszewski, M., & Pidgeon, E. (2014). *Coastal blue carbon: methods for assessing carbon stocks and emissions factors in mangroves, tidal salt marshes, and seagrasses*. <https://www.cifor.org/knowledge/publication/5095/>
- Huang, Y., Zhou, C., Du, M., Wu, P., Yuan, L., & Tang, J. (2022). Tidal influence on the relationship between solar-induced chlorophyll fluorescence and canopy photosynthesis in a coastal salt marsh. *Remote Sensing of Environment*, 270, 112865.
- Hughes, A. L. H., Wilson, A. M., & Morris, J. T. (2012). Hydrologic variability in a salt marsh: Assessing the links between drought and acute marsh dieback. *Estuarine, Coastal and Shelf Science*, 111, 95–106.
- Hwang, Y.-H., & Morris, J. T. (1994). Whole-plant gas exchange responses of *Spartina alterniflora* (Poaceae) to a range of constant and transient salinities. *American Journal of Botany*, 81(6), 659–665.
- Ingalls, T. C., Li, J., Sawall, Y., Martin, R. E., Thompson, D. R., & Asner, G. P. (2024). Imaging spectroscopy investigations in wet carbon ecosystems: A review of the literature from 1995 to 2022 and future directions. *Remote Sensing of Environment*, 305, 114051.
- Jacob, J., Pandian, K., Lopez, R., & Biggs, H. (2014). *Houston-area freshwater wetland loss, 1992-2010*. <https://repository.library.noaa.gov/view/noaa/43588>
- Jeong, S., Ryu, Y., Dechant, B., Li, X., Kong, J., Choi, W., Kang, M., Yeom, J., Lim, J., Jang, K., & Chun, J. (2023). Tracking diurnal to seasonal variations of gross primary productivity using a geostationary satellite, GK-2A advanced meteorological imager. *Remote Sensing of Environment*, 284, 113365.
- Jones, S. F., Stagg, C. L., Krauss, K. W., & Hester, M. W. (2018). Flooding alters plant-mediated carbon cycling independently of elevated atmospheric CO<sub>2</sub> concentrations. *Journal of Geophysical Research. Biogeosciences*, 123(6), 1976–1987.
- Jordan, D. B., & Ogren, W. L. (1984). The CO<sub>2</sub>/O<sub>2</sub> specificity of ribulose 1,5-bisphosphate carboxylase/oxygenase : Dependence on ribulosebisphosphate concentration, pH and temperature. *Planta*, 161(4), 308–313.
- Kathilankal, J. C., Mozdzer, T. J., Fuentes, J. D., D’Odorico, P., McGlathery, K. J., & Zieman, J. C. (2008). Tidal influences on carbon assimilation by a salt marsh. *Environmental Research Letters: ERL*, 3(4), 044010.
- Kathilankal, J. C., Mozdzer, T. J., Fuentes, J. D., McGlathery, K. J., D’Odorico, P., & Zieman, J. C. (2011). Physiological responses of *Spartina alterniflora* to varying environmental conditions in Virginia marshes. *Hydrobiologia*, 669(1), 167–181.
- Khan, A. M., Stoy, P. C., Joiner, J., Baldocchi, D., Verfaillie, J., Chen, M., & Otkin, J. A. (2022). The diurnal dynamics of gross primary productivity using observations from the advanced baseline imager on the geostationary operational environmental satellite-R series at an oak Savanna ecosystem. *Journal of Geophysical Research. Biogeosciences*, 127(3). <https://doi.org/10.1029/2021jg006701>

- Kirwan, M. L., Guntenspergen, G. R., & Morris, J. T. (2009). Latitudinal trends in *Spartina alterniflora* productivity and the response of coastal marshes to global change. *Global Change Biology*, *15*(8), 1982–1989.
- Knox, S. H., Windham-Myers, L., Anderson, F., Sturtevant, C., & Bergamaschi, B. (2018). Direct and indirect effects of tides on ecosystem-scale CO<sub>2</sub> Exchange in a brackish tidal marsh in northern California. *Journal of Geophysical Research. Biogeosciences*, *123*(3), 787–806.
- Knyazikhin, Y., Schull, M. A., Stenberg, P., Möttus, M., Rautiainen, M., Yang, Y., Marshak, A., Latorre Carmona, P., Kaufmann, R. K., Lewis, P., Disney, M. I., Vanderbilt, V., Davis, A. B., Baret, F., Jacquemoud, S., Lyapustin, A., & Myneni, R. B. (2013). Hyperspectral remote sensing of foliar nitrogen content. *Proceedings of the National Academy of Sciences*, *110*(3), E185–E192.
- Koch, E. W., Barbier, E. B., Silliman, B. R., Reed, D. J., Perillo, G. M. E., Hacker, S. D., Granek, E. F., Primavera, J. H., Muthiga, N., Polasky, S., Halpern, B. S., Kennedy, C. J., Kappel, C. V., & Wolanski, E. (2009). Non-linearity in ecosystem services: temporal and spatial variability in coastal protection. *Frontiers in Ecology and the Environment*, *7*(1), 29–37.
- Kong, J., Ryu, Y., Liu, J., Dechant, B., Rey-Sanchez, C., Shortt, R., Szutu, D., Verfaillie, J., Houborg, R., & Baldocchi, D. D. (2022). Matching high resolution satellite data and flux tower footprints improves their agreement in photosynthesis estimates. *Agricultural and Forest Meteorology*, *316*, 108878.
- Ku, S. B., & Edwards, G. E. (1977a). Oxygen Inhibition of Photosynthesis: I. Temperature Dependence and Relation to O<sub>2</sub>/CO<sub>2</sub> Solubility Ratio. *Plant Physiology*, *59*(5), 986–990.
- Ku, S. B., & Edwards, G. E. (1977b). Oxygen Inhibition of Photosynthesis: II. Kinetic Characteristics as Affected by Temperature. *Plant Physiology*, *59*(5), 991–999.
- Lamers, L. P. M., Govers, L. L., Janssen, I. C. J. M., Geurts, J. J. M., Van der Welle, M. E. W., Van Katwijk, M. M., Van der Heide, T., Roelofs, J. G. M., & Smolders, A. J. P. (2013). Sulfide as a soil phytotoxin—a review. *Frontiers in Plant Science*, *4*, 268.
- Lara, M. V., & Andreo, C. S. (2011). C<sub>4</sub> plants adaptation to high levels of CO<sub>2</sub> and to drought environments. *Abiotic Stress in Plants—Mechanisms and Adaptations*, 415–428.
- Lasslop, G., Reichstein, M., Detto, M., Richardson, A. D., & Baldocchi, D. D. (2010). Comment on Vickers et al.: Self-correlation between assimilation and respiration resulting from flux partitioning of eddy-covariance CO<sub>2</sub> fluxes. *Agricultural and Forest Meteorology*, *150*(2), 312–314.
- Levrel, H., Scemama, P., & Vaissière, A.-C. (2017). Should We Be Wary of Mitigation Banking? Evidence Regarding the Risks Associated with this Wetland Offset Arrangement in Florida. *Ecological Economics: The Journal of the International Society for Ecological Economics*, *135*, 136–149.
- Li, H., Wang, C., Yu, Q., & Smith, E. (2022). Spatiotemporal assessment of potential drivers of salt marsh dieback in the North Inlet-Winyah Bay estuary, South Carolina (1990–2019). *Journal of Environmental Management*, *313*, 114907.
- Li, X., Xiao, J., Fisher, J. B., & Baldocchi, D. D. (2021). ECOSTRESS estimates gross primary production with fine spatial resolution for different times of day from the International Space Station. *Remote Sensing of Environment*, *258*, 112360.

- Li, Xing, Ryu, Y., Xiao, J., Dechant, B., Liu, J., Li, B., Jeong, S., & Gentine, P. (2023). New-generation geostationary satellite reveals widespread midday depression in dryland photosynthesis during 2020 western U.S. heatwave. *Science Advances*, 9(31), eadio775.
- Li, Xing, & Xiao, J. (2022). TROPOMI observations allow for robust exploration of the relationship between solar-induced chlorophyll fluorescence and terrestrial gross primary production. *Remote Sensing of Environment*, 268, 112748.
- Li, Xing, Xiao, J., He, B., Altaf Arain, M., Beringer, J., Desai, A. R., Emmel, C., Hollinger, D. Y., Krasnova, A., Mammarella, I., Noe, S. M., Ortiz, P. S., Rey-Sanchez, A. C., Rocha, A. V., & Varlagin, A. (2018). Solar-induced chlorophyll fluorescence is strongly correlated with terrestrial photosynthesis for a wide variety of biomes: First global analysis based on OCO-2 and flux tower observations. *Global Change Biology*, 24(9), 3990–4008.
- LI-COR. (2020). EddyPro software instruction manual. *LI-COR Inc., Lincoln, Nebraska, USA*, 7.
- Lin, C., Gentine, P., Frankenberg, C., Zhou, S., Kennedy, D., & Li, X. (2019). Evaluation and mechanism exploration of the diurnal hysteresis of ecosystem fluxes. *Agricultural and Forest Meteorology*, 278, 107642.
- Liu, L., Guan, L., & Liu, X. (2017). Directly estimating diurnal changes in GPP for C3 and C4 crops using far-red sun-induced chlorophyll fluorescence. *Agricultural and Forest Meteorology*, 232, 1–9.
- Liu, L., Liu, X., Chen, J., Du, S., Ma, Y., Qian, X., Chen, S., & Peng, D. (2020). Estimating maize GPP using near-infrared radiance of vegetation. *Science of Remote Sensing*, 2(100009), 100009.
- Liu, X., Liu, L., Bacour, C., Guanter, L., Chen, J., Ma, Y., Chen, R., & Du, S. (2023). A simple approach to enhance the TROPOMI solar-induced chlorophyll fluorescence product by combining with canopy reflected radiation at near-infrared band. *Remote Sensing of Environment*, 284(113341), 113341.
- Liu, Z., Fagherazzi, S., She, X., Ma, X., Xie, C., & Cui, B. (2020). Efficient tidal channel networks alleviate the drought-induced die-off of salt marshes: Implications for coastal restoration and management. *The Science of the Total Environment*, 749, 141493.
- Lo Iacono, C., Mateo, M. A., Gràcia, E., Guasch, L., Carbonell, R., Serrano, L., Serrano, O., & Dañobeitia, J. (2008). Very high-resolution seismo-acoustic imaging of seagrass meadows (Mediterranean Sea): Implications for carbon sink estimates. *Geophysical Research Letters*, 35(18). <https://doi.org/10.1029/2008GL034773>
- Lovelock, C. E., Atwood, T., Baldock, J., Duarte, C. M., Hickey, S., Lavery, P. S., Masque, P., Macreadie, P. I., Ricart, A. M., Serrano, O., & Steven, A. (2017). Assessing the risk of carbon dioxide emissions from blue carbon ecosystems. *Frontiers in Ecology and the Environment*, 15(5), 257–265.
- Lovelock, C. E., & Reef, R. (2020). Variable Impacts of Climate Change on Blue Carbon. *One Earth*, 3(2), 195–211.
- Lu, Y. (2017). Hurricane Flooding and Environmental Inequality: Do Disadvantaged Neighborhoods Have Lower Elevations? *Socius*, 3, 2378023117740700.
- Mack, J. J., & Micacchion, M. (2006). An ecological assessment of Ohio mitigation banks: Vegetation, amphibians, hydrology, and soils. *Columbus, OH, Ohio EPA*.

- Macreadie, P. I., Costa, M. D. P., Atwood, T. B., Friess, D. A., Kelleway, J. J., Kennedy, H., Lovelock, C. E., Serrano, O., & Duarte, C. M. (2021). Blue carbon as a natural climate solution. *Nature Reviews. Earth & Environment*, 2(12), 826–839.
- Mao, L., Mishra, D. R., Hawman, P. A., Narron, C. R., O’Connell, J. L., & Cotten, D. L. (2023). Photosynthetic performance of tidally flooded *Spartina alterniflora* salt marshes. *Journal of Geophysical Research. Biogeosciences*, 128(3), e2022JG007161.
- Maricle, B. R., Cobos, D. R., & Campbell, C. S. (2007). Biophysical and morphological leaf adaptations to drought and salinity in salt marsh grasses. *Environmental and Experimental Botany*, 60(3), 458–467.
- Maricle, B. R., & Lee, R. W. (2006). Effects of environmental salinity on carbon isotope discrimination and stomatal conductance in *Spartina* grasses. *Marine Ecology Progress Series*, 313, 305–310.
- Maricle, B. R., Lee, R. W., Hellquist, C. E., Kiirats, O., & Edwards, G. E. (2007). Effects of salinity on chlorophyll fluorescence and CO<sub>2</sub> fixation in C<sub>4</sub> estuarine grasses. *Photosynthetica*, 45(3), 433–440.
- MATLAB. (n.d.). *The MathWorks Inc. (2022). MATLAB version: 9.13.0 (R2022b), Natick, Massachusetts: The MathWorks Inc.* <https://www.mathworks.com>.
- Matthews, J. W. (2015). Group-based modeling of ecological trajectories in restored wetlands. *Ecological Applications: A Publication of the Ecological Society of America*, 25(2), 481–491.
- Matthews, J. W., Spyreas, G., & Endress, A. G. (2009). Trajectories of vegetation-based indicators used to assess wetland restoration progress. *Ecological Applications: A Publication of the Ecological Society of America*, 19(8), 2093–2107.
- McKee, K. L., Mendelssohn, I. A., & Materne. (2004). Acute salt marsh dieback in the Mississippi River deltaic plain: a drought-induced phenomenon? *Global Ecology and Biogeography*, 13, 65–74.
- McKee, Karen L., Cahoon, D. R., & Feller, I. C. (2007). Caribbean mangroves adjust to rising sea level through biotic controls on change in soil elevation. *Global Ecology and Biogeography: A Journal of Macroecology*, 16(5), 545–556.
- McLeod, E., Chmura, G. L., Bouillon, S., Salm, R., Björk, M., Duarte, C. M., Lovelock, C. E., Schlesinger, W. H., & Silliman, B. R. (2011). *A blueprint for blue carbon: toward an improved understanding of the role of vegetated coastal habitats in sequestering CO<sub>2</sub>*. <https://doi.org/10.1890/110004>
- Mcowen, C. J., Weatherdon, L. V., Van Bochove, J.-W., Sullivan, E., Blyth, S., Zockler, C., Stanwell-Smith, D., Kingston, N., Martin, C. S., Spalding, M., & Fletcher, S. (2017). A global map of saltmarshes. *Biodiversity Data Journal*, 5, e11764.
- Meroni, M., Rossini, M., Guanter, L., Alonso, L., Rascher, U., Colombo, R., & Moreno, J. (2009). Remote sensing of solar-induced chlorophyll fluorescence: Review of methods and applications. *Remote Sensing of Environment*, 113(10), 2037–2051.
- Merrick, T., Pau, S., Detto, M., Broadbent, E. N., Bohlman, S. A., Still, C. J., & Almeyda Zambrano, A. M. (2021). Unveiling spatial and temporal heterogeneity of a tropical forest canopy using high-resolution NIRv, FCVI, and NIRvrad from UAS observations. *Biogeosciences*, 18(22), 6077–6091.
- Mitsch, W. J., Bernal, B., & Hernandez, M. E. (2015). Ecosystem services of wetlands. *International Journal of Biodiversity Science, Ecosystems Services & Management*, 11(1), 1–4.

- Mitsch, W. J., & Gosselink, J. G. (2015). *Wetlands, 5th edition*. John Wiley & Sons, Inc.
- Möller, I. (2006). Quantifying saltmarsh vegetation and its effect on wave height dissipation: Results from a UK East coast saltmarsh. *Estuarine, Coastal and Shelf Science*, 69(3), 337–351.
- Moncrieff, Clement, R., Finnigan, J., & Meyers, T. (2005). Averaging, Detrending, and Filtering of Eddy Covariance Time Series. In X. Lee, W. Massman, & B. Law (Eds.), *Handbook of Micrometeorology: A Guide for Surface Flux Measurement and Analysis* (pp. 7–31). Springer Netherlands.
- Moncrieff, Massheder, J. M., de Bruin, H., Elbers, J., Friborg, T., Heusinkveld, B., Kabat, P., Scott, S., Soegaard, H., & Verhoef, A. (1997). A system to measure surface fluxes of momentum, sensible heat, water vapour and carbon dioxide. *Journal of Hydrology*, 188–189, 589–611.
- Moreno-Mateos, D., Power, M. E., Comín, F. A., & Yockteng, R. (2012). Structural and functional loss in restored wetland ecosystems. *PLoS Biology*, 10(1), e1001247.
- Murray, B. C., Pendleton, L., Aaron Jenkins, W., & Sifleet, S. (2011). Economic Incentives for Protecting Threatened Coastal Habitats. *Nicholas Institute for Environmental Policy Solutions, Duke University*.  
<https://nicholasinstitute.duke.edu/environment/publications/naturalresources/blue-carbon-report>
- Nahrawi, H., Leclerc, M. Y., Pennings, S., Zhang, G., Singh, N., & Pahari, R. (2020). Impact of tidal inundation on the net ecosystem exchange in daytime conditions in a salt marsh. *Agricultural and Forest Meteorology*, 294, 108133.
- National Research Council, Division on Earth and Life Studies, Water Science and Technology Board, Board on Environmental Studies and Toxicology, & Committee on Mitigating Wetland Losses. (2001). *Compensating for Wetland Losses Under the Clean Water Act*. National Academies Press.
- Nellemann, C., & Corcoran, E. (2009). *Blue Carbon: The Role of Healthy Oceans in Binding Carbon : a Rapid Response Assessment*. UNEP/Earthprint.
- O'Donnell, K. L., Bernhardt, E. S., Yang, X., Emanuel, R. E., Ardón, M., Lerdaun, M. T., Manda, A. K., Braswell, A. E., BenDor, T. K., Edwards, E. C., Frankenberg, E., Helton, A. M., Kominoski, J. S., Lesen, A. E., Naylor, L., Noe, G., Tully, K. L., White, E., & Wright, J. P. (2024). Saltwater Intrusion and Sea Level Rise threatens U.S. rural coastal landscapes and communities. *Anthropocene*, 100427.
- Odum, W. E. (1988). COMPARATIVE ECOLOGY OF TIDAL FRESHWATER AND SALT MARSHES. *Annual Review of Ecology and Systematics*, 19(1), 147–176.
- Ollinger, S. V., Richardson, A. D., Martin, M. E., Hollinger, D. Y., Frolking, S. E., Reich, P. B., Plourde, L. C., Katul, G. G., Munger, J. W., Oren, R., Smith, M.-L., Paw U, K. T., Bolstad, P. V., Cook, B. D., Day, M. C., Martin, T. A., Monson, R. K., & Schmid, H. P. (2008). Canopy nitrogen, carbon assimilation, and albedo in temperate and boreal forests: Functional relations and potential climate feedbacks. *Proceedings of the National Academy of Sciences of the United States of America*, 105(49), 19336–19341.
- ORNL DAAC. (2024). [Data set]. In *Terrestrial Ecology Subsetting & Visualization Services (TESViS) Global Subsets Tool*. ORNL DAAC, Oak Ridge, Tennessee, USA. <https://doi.org/10.3334/ORNLDAAC/1379>
- Ouyang, X., & Lee, S. Y. (2014). Updated estimates of carbon accumulation rates in coastal marsh sediments. *Biogeosciences*, 11(18), 5057–5071.

- Papale, D., Reichstein, M., Aubinet, M., Canfora, E., Bernhofer, C., Kutsch, W., Longdoz, B., Rambal, S., Valentini, R., Vesala, T., & Yakir, D. (2006). Towards a standardized processing of Net Ecosystem Exchange measured with eddy covariance technique: algorithms and uncertainty estimation. *Biogeosciences*, 3(4), 571–583.
- Pardo, J., & VanBuren, R. (2021). Evolutionary innovations driving abiotic stress tolerance in C4 grasses and cereals. *The Plant Cell*, 33(11), 3391–3401.
- Pastorello, G., Trotta, C., Canfora, E., Chu, H., Christianson, D., Cheah, Y.-W., Poindexter, C., Chen, J., Elbashandy, A., Humphrey, M., Isaac, P., Polidori, D., Reichstein, M., Ribeca, A., van Ingen, C., Vuichard, N., Zhang, L., Amiro, B., Ammann, C., ... Papale, D. (2020). The FLUXNET2015 dataset and the ONEFlux processing pipeline for eddy covariance data. *Scientific Data*, 7(1), 225.
- Pathre, U., Sinha, A. K., Shirke, P. A., & Sane, P. V. (1998). Factors determining the midday depression of photosynthesis in trees under monsoon climate. *Trees*, 12(8), 472–481.
- Paul-Limoges, E., Damm, A., Hueni, A., Liebisch, F., Eugster, W., Schaepman, M. E., & Buchmann, N. (2018). Effect of environmental conditions on sun-induced fluorescence in a mixed forest and a cropland. *Remote Sensing of Environment*, 219, 310–323.
- Pearcy, R. W., & Ustin, S. L. (1984). Effects of salinity on growth and photosynthesis of three California tidal marsh species. *Oecologia*, 62(1), 68–73.
- Peterson, P. M., Romaschenko, K., Arrieta, Y. H., & Saarela, J. M. (2014a). (2332) Proposal to conserve the name *Sporobolus* against *Spartina*, *Crypsis*, *Poncoletia*, and *Heleochloa* (Poaceae: Chloridoideae: Sporobolinae). *Taxon*, 63(6), 1373–1374.
- Peterson, P. M., Romaschenko, K., Arrieta, Y. H., & Saarela, J. M. (2014b). A molecular phylogeny and new subgeneric classification of *Sporobolus* (Poaceae: Chloridoideae: Sporobolinae). *Taxon*, 63(6), 1212–1243.
- Pinto, F., Celesti, M., Acebron, K., Alberti, G., Cogliati, S., Colombo, R., Juszczak, R., Matsubara, S., Miglietta, F., Palombo, A., Panigada, C., Pignatti, S., Rossini, M., Sakowska, K., Schickling, A., Schüttemeyer, D., Stróżecki, M., Tudoroiu, M., & Rascher, U. (2020). Dynamics of sun-induced chlorophyll fluorescence and reflectance to detect stress-induced variations in canopy photosynthesis. *Plant, Cell & Environment*, 43(7), 1637–1654.
- Pons, T. L., & Welschen, R. A. M. (2003). Midday depression of net photosynthesis in the tropical rainforest tree *Eperua grandiflora*: contributions of stomatal and internal conductances, respiration and Rubisco functioning. *Tree Physiology*, 23(14), 937–947.
- Poppe, K. L., & Rybczyk, J. M. (2021). Climatic Impacts on Salt Marsh Vegetation. In *Salt Marshes: Function, Dynamics, and Stresses* (pp. 337–366). Cambridge University Press.
- Porcar-Castell, A., Tyystjärvi, E., Atherton, J., Van Der Tol, C., Flexas, J., Pfündel, E. E., Moreno, J., Frankenberg, C., & Berry, J. A. (2014). Linking chlorophyll a fluorescence to photosynthesis for remote sensing applications: Mechanisms and challenges. *Journal of Experimental Botany*, 65(15), 4065–4095.
- Porter, J., Krovetz, D., Nuttle, W., & Spitler, J. (2023). *Hourly meteorological data for the Virginia Coast Reserve LTER 1989-present*.

- Ranjbar, S., Losos, D., Dechant, B., Hoffman, S., Başakın, E. E., & Stoy, P. C. (2024). Harnessing information from shortwave infrared reflectance bands to enhance satellite-based estimates of gross primary productivity. *Journal of Geophysical Research. Biogeosciences*, 129(11), e2024JG008240.
- Raschke, K., & Resemann, A. (1986). The midday depression of CO<sub>2</sub> assimilation in leaves of *Arbutus unedo* L.: diurnal changes in photosynthetic capacity related to changes in temperature and humidity. *Planta*, 168(4), 546–558.
- RIBITS. (n.d.). Regulatory In-Lieu Fee and Bank Information Tracking System. Retrieved July 1, 2024, from <https://ribits.ops.usace.army.mil/>
- Rolando, J. L., Hodges, M., Garcia, K. D., Krueger, G., Williams, N., Carr, J., Jr, Robinson, J., George, A., Morris, J., & Kostka, J. E. (2023). Restoration and resilience to sea level rise of a salt marsh affected by dieback events. *Ecosphere*, 14(4). <https://doi.org/10.1002/ecs2.4467>
- Rosentreter, J. A., Laruelle, G. G., Bange, H. W., Bianchi, T. S., Busecke, J. J. M., Cai, W.-J., Eyre, B. D., Forbrich, I., Kwon, E. Y., Maavara, T., Moosdorf, N., Najjar, R. G., Sarma, V. V. S. S., Van Dam, B., & Regnier, P. (2023). Coastal vegetation and estuaries are collectively a greenhouse gas sink. *Nature Climate Change*, 13(6), 579–587.
- Rossini, M., Meroni, M., Celesti, M., Cogliati, S., Julitta, T., Panigada, C., Rascher, U., Van der Tol, C., & Colombo, R. (2016). Analysis of Red and Far-Red Sun-Induced Chlorophyll Fluorescence and Their Ratio in Different Canopies Based on Observed and Modeled Data. *Remote Sensing*, 8(5), 412.
- Ruhl, J. B., & Salzman, J. E. (2006). *The Effects of Wetland Mitigation Banking on People*. <https://papers.ssrn.com/abstract=878331>
- Rupprecht, F., Möller, I., Paul, M., Kudella, M., Spencer, T., van Wesenbeeck, B. K., Wolters, G., Jensen, K., Bouma, T. J., Miranda-Lange, M., & Schimmels, S. (2017). Vegetation-wave interactions in salt marshes under storm surge conditions. *Ecological Engineering*, 100, 301–315.
- Russell, S. J., Windham-Myers, L., Stuart-Haëntjens, E. J., Bergamaschi, B. A., Anderson, F., Oikawa, P., & Knox, S. H. (2023). Increased salinity decreases annual gross primary productivity at a Northern California brackish tidal marsh. *Environmental Research Letters: ERL [Web Site]*, 18(3), 034045.
- Sage, R. F., Sage, T. L., & Kocacinar, F. (2012). Photorespiration and the evolution of C<sub>4</sub> photosynthesis. *Annual Review of Plant Biology*, 63, 19–47.
- Saintilan, N., Horton, B., Törnqvist, T. E., Ashe, E. L., Khan, N. S., Schuerch, M., Perry, C., Kopp, R. E., Garner, G. G., Murray, N., Rogers, K., Albert, S., Kelleway, J., Shaw, T. A., Woodroffe, C. D., Lovelock, C. E., Goddard, M. M., Hutley, L. B., Kovalenko, K., ... Guntenspergen, G. (2023). Widespread retreat of coastal habitat is likely at warming levels above 1.5 °C. *Nature*, 621(7977), 112–119.
- Seddon, N., Daniels, E., Davis, R., Chausson, A., Harris, R., Hou-Jones, X., Huq, S., Kapos, V., Mace, G. M., Rizvi, A. R., Reid, H., Roe, D., Turner, B., & Wicander, S. (2020). Global recognition of the importance of nature-based solutions to the impacts of climate change. *Global Sustainability*, 3(e15), e15.
- Sellers, P. J. (1987). Canopy reflectance, photosynthesis, and transpiration, II. The role of biophysics in the linearity of their interdependence. *Remote Sensing of Environment*, 21(2), 143–183.

- Sellers, P. J., Berry, J. A., Collatz, G. J., Field, C. B., & Hall, F. G. (1992). Canopy reflectance, photosynthesis, and transpiration. III. A reanalysis using improved leaf models and a new canopy integration scheme. *Remote Sensing of Environment*, 42(3), 187–216.
- Shea, M. L. (1977). *Spartina photosynthesis and photorespiration* [Ph.D.]. Yale University.
- Shea, M. L., Warren, R. S., & Niering, W. A. (1975). Biochemical and transplantation studies of the growth form of *Spartina alterniflora* on Connecticut salt marshes. *Ecology*, 56(2), 461–466.
- Shen C., Zhang C., Xin P., Kong J, Li L. (2018). Salt dynamics in coastal marshes: formation of hypersaline zones. *Water Resources Research*, 54(5), 3259–3276.
- Shen, Y., Tahvildari, N., Morsy, M. M., Huxley, C., Chen, T. D., & Goodall, J. L. (2022). Dynamic modeling of inland flooding and storm surge on coastal cities under climate change scenarios: Transportation infrastructure impacts in Norfolk, Virginia USA as a case study. *Geosciences*, 12(6), 224.
- Spieles, D. J. (2005). Vegetation development in created, restored, and enhanced mitigation wetland banks of the United States. *Wetlands*, 25(1), 51–63.
- Spieles, D. J., Coneybeer, M., & Horn, J. (2006). Community structure and quality after 10 years in two central Ohio mitigation bank wetlands. *Environmental Management*, 38(5), 837–852.
- Stagg, C. L., Osland, M. J., Moon, J. A., Feher, L. C., Laurenzano, C., Lane, T. C., Jones, W. R., & Hartley, S. B. (2021). Extreme Precipitation and Flooding Contribute to Sudden Vegetation Dieback in a Coastal Salt Marsh. *Plants*, 10(9).  
<https://doi.org/10.3390/plants10091841>
- Stefanik, K. C., & Mitsch, W. J. (2012). Structural and functional vegetation development in created and restored wetland mitigation banks of different ages. *Ecological Engineering*, 39, 104–112.
- Sulliván, S. M. P., & Gardner, R. C. (2023). US Supreme Court opinion harms watersheds. *Science*, 381(6656), 385.
- Sun, Y., Frankenberg, C., Wood, J. D., Schimel, D. S., Jung, M., Guanter, L., Drewry, D. T., Verma, M., Porcar-Castell, A., Griffis, T. J., Gu, L., Magney, T. S., Köhler, P., Evans, B., & Yuen, K. (2017). OCO-2 advances photosynthesis observation from space via solar-induced chlorophyll fluorescence. *Science*, 358(6360).  
<https://doi.org/10.1126/science.aam5747>
- Tang, Y., Leon, A. S., & Kavvas, M. L. (2020). Impact of size and location of wetlands on watershed-scale flood control. *Water Resources Management*, 34(5), 1693–1707.
- Teal, J. M. (2001). Salt Marshes And Mud Flats. In J. H. Steele (Ed.), *Encyclopedia of Ocean Sciences* (pp. 2490–2495). Academic Press.
- Tenhunen, J. D., Lange, O. L., Gebel, J., Beyschlag, W., & Weber, J. A. (1984). Changes in photosynthetic capacity, carboxylation efficiency, and CO<sub>2</sub> compensation point associated with midday stomatal closure and midday depression of net CO<sub>2</sub> exchange of leaves of *Quercus suber*. *Planta*, 162(3), 193–203.
- Tillman, S. C., & Matthews, J. W. (2023). Evaluating the ability of wetland mitigation banks to replace plant species lost from destroyed wetlands. *The Journal of Applied Ecology*, 60(6), 990–998.
- Tillman, S. C., Spyreas, G., Olnas, A., & Matthews, J. W. (2022). Plant communities in wetland mitigation banks surpass the quality of those in the most degraded,

- naturally occurring wetlands, but fall short of high-quality wetlands. *Ecological Engineering*, 176, 106526.
- Trabjerg, L., & Højerslev, N. K. (1996). Temperature influence on light absorption by fresh water and seawater in the visible and near-infrared spectrum. *Applied Optics*, 35(15), 2653–2658.
- Turner, N. C., & Burch, G. J. (1983). The role of water in plants. In *Crop Water Relations* (pp. 73–126). unknown.
- US Army Corps of Engineers, & Environmental Protection Agency. (2008). Compensatory mitigation for losses of aquatic resources. *Federal Register*, 73, 19594–19705.
- US Environmental Protection Agency. (1990). *Memorandum of Agreement regarding Mitigation under CWA Section 404(b)(1) Guidelines (Text)*.  
<https://www.epa.gov/cwa-404/memorandum-agreement-regarding-mitigation-under-cwa-section-404b1-guidelines-text>
- US Global Change Research Program. (2018). *Second State of the Carbon Cycle Report*.  
[https://nca2018.globalchange.gov/downloads/NCA2018\\_FullReport.pdf](https://nca2018.globalchange.gov/downloads/NCA2018_FullReport.pdf)
- Va Code § 62.1-44.15:20. (2001). *Virginia Water Protection Permit*.  
<https://law.lis.virginia.gov/vacode/title62.1/chapter3.1/section62.1-44.15:20/>
- VA Dept. of Environmental Quality. (n.d.). *Compensatory Mitigation*. Retrieved December 30, 2024, from  
<https://www.deq.virginia.gov/permits/water/compensatory-mitigation>
- Valentini, R., Epron, D., de Angelis, P., Matteucci, G., & Dreyer, E. (1995). *In situ* estimation of net CO<sub>2</sub> assimilation, photosynthetic electron flow and photorespiration in Turkey oak (*Q. cerris* L.) leaves: diurnal cycles under different levels of water supply. *Plant, Cell & Environment*, 18(6), 631–640.
- Van Coppenolle, R., & Temmerman, S. (2020). Identifying global hotspots where coastal wetland conservation can contribute to nature-based mitigation of coastal flood risks. *Global and Planetary Change*, 187(103125), 103125.
- Van den Bosch, K., & Matthews, J. W. (2017). An Assessment of Long-Term Compliance with Performance Standards in Compensatory Mitigation Wetlands. *Environmental Management*, 59(4), 546–556.
- van Maasakkers, M. (2021). What role does planning have in the creation of ecosystem service markets? Evidence from two cases in Oregon. *Journal of Planning Education and Research*, 41(1), 18–31.
- Vázquez-González, C., Moreno-Casasola, P., Peralta Peláez, L. A., Monroy, R., & Espejel, I. (2019). The value of coastal wetland flood prevention lost to urbanization on the coastal plain of the Gulf of Mexico: An analysis of flood damage by hurricane impacts. *International Journal of Disaster Risk Reduction*, 37, 101180.
- Vázquez-Lule, A., & Vargas, R. (2023). Proximal remote sensing and gross primary productivity in a temperate salt marsh. *Agricultural and Forest Meteorology*, 341, 109639.
- Vickers, D., & Mahrt, L. (1997). Quality Control and Flux Sampling Problems for Tower and Aircraft Data. *Journal of Atmospheric and Oceanic Technology*, 14(3), 512–526.
- Voss, I., Sunil, B., Scheibe, R., & Raghavendra, A. S. (2013). Emerging concept for the role of photorespiration as an important part of abiotic stress response. *Plant Biology*, 15(4), 713–722.

- Wall, C. B., & Stevens, K. J. (2015). Assessing wetland mitigation efforts using standing vegetation and seed bank community structure in neighboring natural and compensatory wetlands in north-central Texas. *Wetlands Ecology and Management*, 23(2), 149–166.
- Wang, H., Krauss, K. W., Noe, G. B., Dai, Z., & Trettin, C. C. (2023). Soil salinity and water level interact to generate tipping points in low salinity tidal wetlands responding to climate change. *Estuaries and Coasts: Journal of the Estuarine Research Federation*, 46(7), 1808–1828.
- Wang, S., Zhang, Y., Ju, W., Qiu, B., & Zhang, Z. (2021). Tracking the seasonal and inter-annual variations of global gross primary production during last four decades using satellite near-infrared reflectance data. *The Science of the Total Environment*, 755(Pt 2), 142569.
- Webb, E. K., Pearman, G. I., & Leuning, R. (1980). Correction of flux measurements for density effects due to heat and water vapour transfer. *Quarterly Journal of the Royal Meteorological Society*, 106(447), 85–100.
- Więski, K., & Pennings, S. C. (2014). Climate Drivers of *Spartina alterniflora* Saltmarsh Production in Georgia, USA. *Ecosystems (New York, N.Y.)*, 17(3), 473–484.
- Wilczak, J. M., Oncley, S. P., & Stage, S. A. (2001). Sonic Anemometer Tilt Correction Algorithms. *Boundary-Layer Meteorology*, 99(1), 127–150.
- Wilson, K. B., Baldocci, D., Falge, E., Aubinet, M., Berbigier, P., Bernhofer, C., Dolman, H., Field, C., Goldstein, A., Granier, A., Hollinger, D., Katul, G., Law, B. E., Meyers, T., Moncrieff, J., Monson, R., Tenhunen, J., Valentini, R., Verma, S., & Wofsy, S. (2003). Diurnal centroid of ecosystem energy and carbon fluxes at FLUXNET sites. *JGR Atmo*. <https://doi.org/10.1029/2001JD001349>
- Windham-Myers, L., Cai, W.-J., Alin, S., Andersson, A., Crosswell, J., Dunton, K. H., Hernandez-Ayon, J. M., Herrmann, M., Hinson, A. L., Hopkinson, C. S., Howard, J., Hu, X., Knox, S. H., Kroeger, K., Lagomasino, D., Megonigal, P., Najjar, R., Paulsen, M.-L., Peteet, D., ... Watson, E. B. (2018). *Chapter 15: Tidal wetlands and estuaries. Second state of the carbon cycle report* (N. Cavallaro, G. Shrestha, R. Birdse, M. A. Mayes, R. Najjar, S. Reed, P. Romero-Lankao, & Z. Zhu, Eds.). U.S. Global Change Research Program. <https://doi.org/10.7930/soccr2.2018.ch15>
- Wohlfahrt, G., & Gu, L. (2015). The many meanings of gross photosynthesis and their implication for photosynthesis research from leaf to globe. *Plant, Cell & Environment*, 38(12), 2500–2507.
- Wu, G., Guan, K., Jiang, C., Peng, B., Kimm, H., Chen, M., Yang, X., Wang, S., Suyker, A. E., Bernacchi, C. J., & Others. (2020). Radiance-based NIRv as a proxy for GPP of corn and soybean. *Environmental Research Letters: ERL*, 15(3), 034009.
- Wutzler, T., Lucas-Moffat, A., Migliavacca, M., Knauer, J., Sickel, K., Šigut, L., Menzer, O., & Reichstein, M. (2018). Basic and extensible post-processing of eddy covariance flux data with REddyProc. *Biogeosciences*, 15(16), 5015–5030.
- Xin, P., Li, L., & Barry, D. A. (2013). Tidal influence on soil conditions in an intertidal creek-marsh system. *Water Resources Research*, 49(1), 137–150.
- Xin, P., Zhou, T., Lu, C., Shen, C., Zhang, C., D'Alpaos, A., & Li, L. (2017). Combined effects of tides, evaporation and rainfall on the soil conditions in an intertidal creek-marsh system. *Advances in Water Resources*, 103, 1–15.

- Xu, D.-Q., & Shen, Y.-K. (1996). Midday depression of photosynthesis. *Handbook of Photosynthesis*, 451–459.
- Xu, H., Xiao, J., & Zhang, Z. (2020). Heatwave effects on gross primary production of northern mid-latitude ecosystems. *Environmental Research Letters: ERL [Web Site]*, 15(7), 074027.
- Xu, X., Xin, P., & Yu, X. (2024). Interactions of macropores with tides, evaporation and rainfall and their effects on pore-water salinity in salt marshes. *Journal of Hydrology*, 130740.
- Yamori, W., Hikosaka, K., & Way, D. A. (2014). Temperature response of photosynthesis in C<sub>3</sub>, C<sub>4</sub>, and CAM plants: temperature acclimation and temperature adaptation. *Photosynthesis Research*, 119(1–2), 101–117.
- Yang, X., Li, R., Jablonski, A., Stovall, A., Kim, J., Yi, K., Ma, Y., Beverly, D., Phillips, R., Novick, K., Xu, X., & Lerda, M. (2023). Leaf angle as a leaf and canopy trait: Rejuvenating its role in ecology with new technology. *Ecology Letters*, 26(6), 1005–1020.
- Yang, X., Shi, H., Stovall, A., Guan, K., Miao, G., Zhang, Y., Zhang, Y., Xiao, X., Ryu, Y., & Lee, J.-E. (2018). FluoSpec 2—An Automated Field Spectroscopy System to Monitor Canopy Solar-Induced Fluorescence. *Sensors*, 18(7), 2063.
- Yang, X., Tang, J., Mustard, J. F., Lee, J.-E., Rossini, M., Joiner, J., Munger, J. W., Kornfeld, A., & Richardson, A. D. (2015). Solar-induced chlorophyll fluorescence that correlates with canopy photosynthesis on diurnal and seasonal scales in a temperate deciduous forest. *Geophysical Research Letters*, 42(8), 2977–2987.
- Yang, Z., Huang, Y., Duan, Z., & Tang, J. (2023). Capturing the spatiotemporal variations in the gross primary productivity in coastal wetlands by integrating eddy covariance, Landsat, and MODIS satellite data: A case study in the Yangtze Estuary, China. *Ecological Indicators*, 149, 110154.
- Zeng, Y., Badgley, G., Dechant, B., Ryu, Y., Chen, M., & Berry, J. A. (2019). A practical approach for estimating the escape ratio of near-infrared solar-induced chlorophyll fluorescence. *Remote Sensing of Environment*, 232, 111209.
- Zeng, Y., Hao, D., Badgley, G., Damm, A., Rascher, U., Ryu, Y., Johnson, J., Krieger, V., Wu, S., Qiu, H., Liu, Y., Berry, J. A., & Chen, M. (2021). Estimating near-infrared reflectance of vegetation from hyperspectral data. *Remote Sensing of Environment*, 267, 112723.
- Zhang, W., Villarini, G., Vecchi, G. A., & Smith, J. A. (2018). Urbanization exacerbated the rainfall and flooding caused by hurricane Harvey in Houston. *Nature*, 563(7731), 384–388.
- Zhang, Y., Fang, J., Smith, W. K., Wang, X., Gentine, P., Russell, S., Migliavacca, M., Jeong, S., Litvak, M., & Zhou, S. (2023). Satellite solar-induced chlorophyll fluorescence tracks physiological drought stress development during 2020 southwest US drought. *Global Change Biology*, n/a(n/a). <https://doi.org/10.1111/gcb.16683>
- Zhang, Z., Cescatti, A., Wang, Y.-P., Gentine, P., Xiao, J., Guanter, L., Huete, A. R., Wu, J., Chen, J. M., Ju, W., Peñuelas, J., & Zhang, Y. (2023). Large diurnal compensatory effects mitigate the response of Amazonian forests to atmospheric warming and drying. *Science Advances*, 9(21), eabq4974.

Zhao, W., Wu, J., Shen, Q., Liu, L., Lin, J., & Yang, J. (2022). Estimation of the net primary productivity of winter wheat based on the near-infrared radiance of vegetation. *The Science of the Total Environment*, 838(Pt 2), 156090.